CHARACTERIZATION OF WOOD-PLASTIC COMPOSITES BY DISSIPATED ENERGY

By

MATTHEW M ZAWLOCKI

A thesis submitted in partial fulfillment of
the requirements for the degree of

MASTER OF SCIENCE IN CIVIL ENGINEERING

WASHINGTON STATE UNIVERSITY
Department of Civil and Environmental Engineering

May 2003

To the Faculty of Washington State University:

The members of the Committee appointed to examine the thesis of MATTHEW M ZAWLOCKI find it satisfactory and recommend that it be accepted.

_____
Chair

_____

_____

ACKNOWLEDGEMENT

This research was sponsored by the Office of Naval Research (contract N00014-00-C-0488). I would like to thank all the people who donated their time and effort (and money) to help me achieve my educational goals, and apologize to all the people who I should've thanked, but didn't.

Planning to go back to school was not easy. From the beginning of this adventure, I have enjoyed the support of wife, Barbara, and my two daughters, Kristina and Madeleine. To my wife, I love you. Thanks for being there through it all, I told you things would get better. To my daughters, I hope one day that you will remember these days fondly. Just prior to graduation, my wife and I were blessed with a beautiful son, Trey. Thank you Trey, you helped me stay focused.

Thank you Mom and Dad, you have always given me whatever you had, whether it was time, money or just a hug. Thanks.

Thank you to all my friends at school. This includes my advisor, Dr. John Hermanson. I told you that I needed a kick in the butt, and you were there to give it to me. I appreciate your effort. I also appreciate the effort put forth by my committee members Dr. William Cofer and Dr. Michael Wolcott. Someday I will send you another draft to edit.

I would like to say thank you to all the staff at the WMEL. It was great working with you.

CHARACTERIZATION OF WOOD-PLASTIC COMPOSITES BY DISSIPATED ENERGY

Abstract

By Matthew M Zawlocki, M.S.
Washington State University
May 2003

Chair: John Hermanson

Dissipated energy is a method of characterizing non-linear materials based on the difference between the total energy and the recoverable energy in a material system. Wood-plastic composites with high wood-fiber content are an example of a material that exhibits a non-linear load-displacement behavior. High-density polyethylene, high-density polyethylene with an ethylene-maleic anhydride polymer additive, and poly-vinyl chloride are three wood-plastic formulations chosen to be characterized using dissipated energy. Tension and biaxial (axial and shear) tests were used to create dissipated energy density functions for each of the three formulations. The dissipated energy density functions obtained were then used with beam bending theory to predict the total energy dissipated by test coupons in 3-point bending.

The nonlinear behavior of wood-plastics means that there is no distinct point that marks the onset of material damage as in metals. As an alternative means to assign design strengths, not based on a distinct yield point, the maximum curvature in the dissipated energy function was used to define an allowable design strength. The

maximum curvature in the dissipated energy function provides allowable design strengths in a range where damage accumulation rates are kept relatively low.

Because the strength of wood is traditionally based on a statistical analysis of the 5% parametric tolerance limit (PTL), the 5% PTL for the three wood-plastic formulations was also calculated. The 5% PTL stresses and strains were higher than the stresses and strains at maximum DE curvature. The 5% PTL strengths provided no consistent rate of damage accumulation. A small change in 5% PTL strengths has a large effect on the rate of damage accumulation.

Failure criteria (maximum stress, maximum strain, maximum shear stress, Tsai-Wu and Yeh-Stratton) were evaluated to determine their accuracy in predicting failure of the three wood-plastic composites. An envelope for each wood-plastic formulation based on 1) the maximum curvature of the dissipated energy function, 2) the 5% PTL and 3) the ultimate strength was created for each criterion. Biaxial test results on HDPE and HDPE with MAPE materials revealed shear failures which were accurately predicted by the maximum shear stress criterion.

TABLE OF CONTENTS

LIST OF FIGURES

LIST OF TABLES

CHAPTER ONE: INTRODUCTION

Background

Wood-plastic composites (WPC) with high wood-fiber content have started to gain an increased presence in the building industry due to the availability for use in applications such as doorframes, window moldings and residential decking, but there is an increasing interest in using these wood-plastic composites in heavy structural applications. Many mechanical tests have been performed and these tests indicate that wood-plastic composites are anisotropic and have a non-linear constitutive behavior. Characterization of the observed non-linearity is a first step toward structural design of wood-plastic composite members.

The Composite Materials & Structures (CMS) division at the Naval Research Laboratory in Washington DC has been conducting research into anisotropic and non-linear materials which exhibit continuous damage accumulation through micro-cracking. CMS researchers proposed using dissipated energy as a measure of damage accumulation in materials. This thesis investigates using dissipated energy to characterize wood-plastic composites, which are also believed to accumulate damage through micro-cracking.

Objectives

The purpose of this thesis is to characterize wood-plastic composites by dissipated energy. It is hypothesized that dissipated energy can be used as a material characteristic to describe damage accumulation of wood-plastic composites with high wood-fiber

content. This research will lay the foundation for a design methodology using dissipated energy by also examining the consequences of using dissipated energy to define allowable WPC design stresses and strains. In accomplishing this goal, some other specific objectives will be met. They are the following:

1) Characterize dissipated energy functions for an arbitrary combination of shear and normal loads for HDPE (High-Density Polyethylene), HDPE with MAPE, and PVC (Polyvinyl Chloride) formulations of wood-plastic composites using tension tests, v-notch shear tests, flexure tests and combined axial and torsion tests.
2) Compare a design strength based on the maximum curvature in the dissipated energy function to design strengths defined by ultimate strength, and 5% parametric tolerance limit strength.
3) Define failure envelopes for wood-plastic composites using the maximum stress, maximum strain, maximum shear stress, the Tsai-Wu, and the Yeh-Stratton failure criteria, and compare them to test data.

These three objectives will collectively show the ability of dissipated energy to characterize wood-plastic composites, investigate the possibility of using dissipated energy for finding allowable structural design strengths and provide an initial comparison with failure criteria.

CHAPTER TWO: LITERATURE REVIEW

Dissipated Energy

Strain energy is the net work done by external forces in causing deformation [23], and can be found using the area under a load-displacement curve. A load-displacement curve can also be used to define a stress-strain curve in a particular test. Integration of the area under a stress-strain curve yields a scalar quantity called strain energy density. Strain energy density is a useful quantity since it is independent of the size of the specimen being loaded. Strain energy density (U_o) is mathematically represented by Equation 1.

$$U_o = \int \sigma_{ij} d\varepsilon_{ij} \qquad \text{[Equation 1]}$$

Ugural and Fenster [23] show the strain energy density equation as in Equation 2. The strain energy density equation is commonly presented as in Equation 2, but this equation is only valid for linear elastic materials.

$$U_0 = \int E_{ij}\varepsilon_{ij} d\varepsilon_{ij} = \frac{1}{2} E_{ij}\varepsilon_{ij}^2 \qquad \text{[Equation 2]}$$

Some materials are non-linear because of damage accumulation during loading. For this class of nonlinear materials, there is a difference between the energy put into the material upon loading and the energy that can be recovered upon unloading. One such non-linear material is fiber-reinforced epoxy composites. Mast et al, at the U.S. Naval Research Laboratory [15, 16, and 17] have used the energy dissipation density to characterize damage in fiber-reinforced, fiberglass-epoxy composite specimens. The

model used by Mast et al assumes that the material has no damage before loading and that some portion of the material immediately accumulates damage upon loading.

The main mode of damage accumulation observed by Mast et al in their fiber-reinforced composite specimens was through the evolution of micro-cracks. The tiny cracks are initiating and propagating as the load on the material increases. Upon unloading of the material, the cracks close and the material returns linearly to a state of zero stress and zero strain. Energy is recovered in the undamaged portion of the material. The recoverable strain energy density is represented by a triangular area under the stress-strain plot (see Figure 1). Observations of this damage evolution agree with other observations by Mast et al. [15, 16, 17] that the quantity of energy dissipated is independent of loading path.

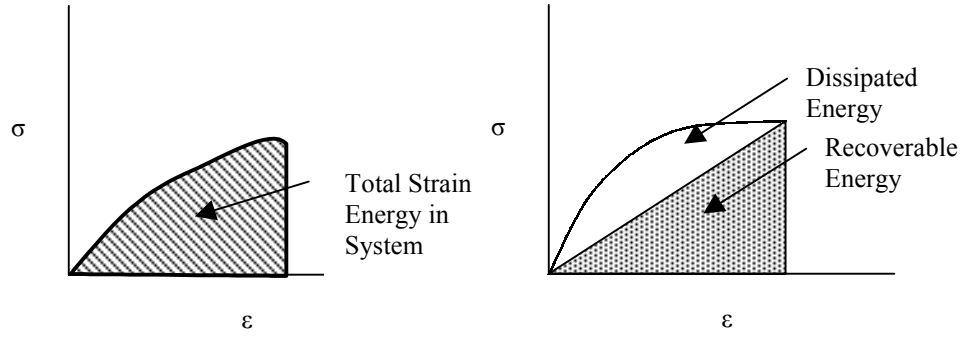

Figure 1: Total, recoverable and dissipated strain energy density.

The assumption that a material will linearly return to a state of zero strain upon unloading is common in damage mechanics. For example, Biegler and Mehrabadi [2] use this assumption in their presentation of an energy-based constitutive damage model for aniotropic solids. They assume that once damage has occurred, the load can be removed from that specimen and as long as the reapplied load does not exceed the prior

load, no additional damage will occur. The assumption is used to develop the stiffness term in their constitutive model, which contains an undamaged portion and a damaged portion. The damage portion reduces the undamaged stiffness as loads are increased. The damaged portion of stiffness is not added back into the total stiffness when the material is unloaded because the material cannot heal itself.

In the development of dissipated energy functions by Mast et al, there is an assumption that if a material is loaded and unloaded, there will be no residual strain. This assumption was verified for the fiber-reinforced epoxy materials used in their research. Cyclic testing of the fiber reinforced epoxy material showed negligible residual strains. Rangaraj [22] performed cyclic tension fatigue tests on a Maple/HDPE wood-plastic formulation. He observed that when the HDPE wood-plastic composite was loaded and then unloaded, residual strains were less than 5% of the test strain. He also noted that because the thermoplastic is viscoelastic, the residual strains would be further reduced if no loads were reapplied. Using the research by Rangaraj, it appears that the assumptions used by Mast to develop dissipated energy functions for fiber-reinforced composites can also be used to develop dissipated energy functions for wood-plastic composites.

Equation 3 uses the functional form of the observed constitutive relationship to mathematically represent the quantity of dissipated energy density shown in Figure 1. The equation is the general form of the dissipated energy density equation used by Mast et al [15].

$$\Phi(\varepsilon) = U_{Total} - U_{\text{Recoverable}} = \int \sigma(\varepsilon) d\varepsilon - \frac{1}{2}\sigma(\varepsilon)\varepsilon \qquad \text{[Equation 3]}$$

Since the stress in Equation 3 is written as a function of strain, the dissipated energy function is also a function of strain, $\Phi(\varepsilon)$. The integral in Equation 3 represents

the total energy in the system, and the "½ σ ε" represents the recoverable energy (See Figure 1).

Mast et al has not attempted to describe all the methods of energy dissipation. The methods may consist of more than micro cracking. Micro buckling of fibers or even heat generation may also contribute to material damage. All of the damage mechanisms can be lumped into one function known as the dissipated energy function (*Φ)*.

In the method of characterizing a material's dissipated energy used by Mast et al, an in-plane loader is used to take test specimens to 125 different states of plane strain and the corresponding dissipated energy density is calculated. From these test results, a known set of 125 dissipated energy values corresponding to 125 states of strain is developed [15]. The 125 states of strain become a set of basis functions for the dissipated energy function. The basis function can be represented (using plane stress assumptions) by setting up a grid with 5 points in each of the strain directions, ε_x, ε_y, and ε_{xy}. Figure 2 shows a strain space representation of the basis functions defining dissipated energy where the vectors o, p and q are indices for the plane stress quantities ε_{xx}, ε_{yy}, and ε_{xy}.

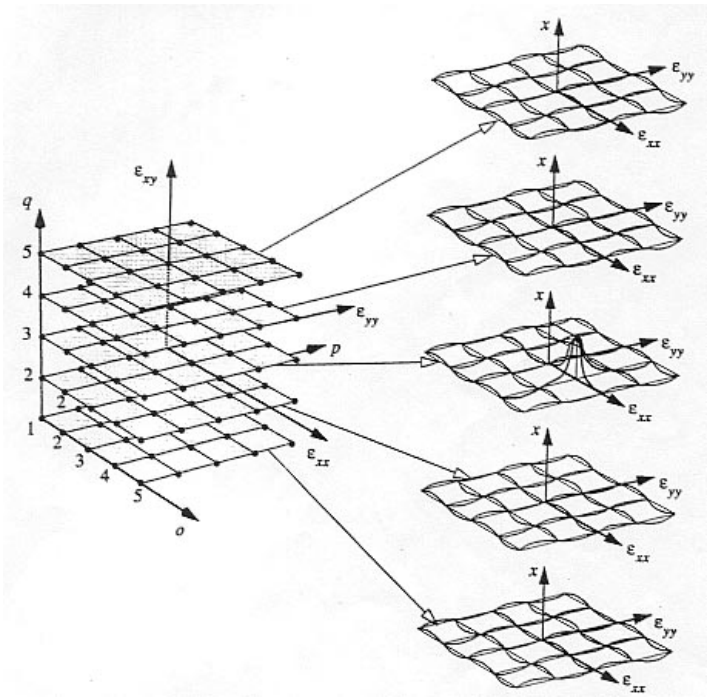

Figure 2: Strain Space Representation of Dissipated Energy Basis Functions (taken from [15])

A Lagrange interpolation function is used to find the dissipated energy at any state of strain in-between the known 125 data points. Lagrange interpolation uses a set of Lagrange polynomials, N_i, which are functions of strain space coordinates. The resulting interpolation function is a summation of each Lagrange polynomial multiplied by the value of dissipated energy at that strain state. The form of the dissipated energy function is shown in Equation 4.

$$\Phi(\varepsilon_1, \varepsilon_2, \varepsilon_{12}) = \sum_{i=1}^{125} N_i(\varepsilon_1, \varepsilon_2, \varepsilon_{12})\phi_i \qquad \text{[Equation 4]}$$

In Equation 4, N_i is the value of the Lagrange polynomial for a particular node (written as a function of strain) and ϕ_i is the quantity of dissipated energy at that node.

Further discussion of Lagrange polynomials can be found in many textbooks on finite element analysis (see Cook [7]).

While Equation 4 gives a form for dissipated energy as a function of strain, it is only a polynomial form of the tensor Equation 3. Equation 4 should be considered as a relationship between a scalar value and a tensor. Because the quantity of energy dissipated is assumed to be path independent, it is possible for a given scalar value of dissipated energy to be given by an infinite number of different strain tensors. The strain tensors for a particular quantity of dissipated energy can be plotted as closed loops in strain space. Plotting many different quantities of dissipated energy will reveal a map, which is analogous to a topographic map. Each contour represents the state of strain required to produce a given level of dissipated energy. From this contour map, a researcher can easily assess what type of load is most damaging to the material.

Design Strength

The yield point of certain metals is often used in calculating allowable design strengths. The yield point would be a distinct change in the stress-strain relationship due to an abrupt change in material behavior. Wood-plastic composites do not exhibit an abrupt change in material behavior, instead, they are constantly accumulating damage, giving wood-plastic composites a non-linear stress-strain relationship described by Murphy [18] using a hyperbolic tangent function. The constantly changing slope of the WPC stress-strain relationships does not exhibit a distinct point at which a material transition can be defined; design strengths for WPC's must be based on something else.

Allowable design strengths for wood are published by American Forest & Paper Association (AF&PA). The allowable stresses are based on a statistical analysis of the ultimate strength for many wood specimens per ASTM 2917. The equation from ASTM2917 used to calculate the 5% PTL (x_{95}) is shown in Equation 5.

$$x_{95} = \overline{X} - k \cdot \hat{s} \qquad \text{[Equation 5]}$$

In Equation 5, $\overline{X}$ is the average strength and $\hat{s}$ is the standard deviation. The k value is chosen from Table 3 in ASTM2917 to provide the appropriate confidence level for the appropriate number of test specimens. AF&PA publish the 5% parametric tolerance limit (PTL) at 75% confidence as the basis for the design strengths.

Failure Theories

Failure theories for composite materials have traditionally attempted to describe the overall material behavior in terms of a distinct point at which failure is defined. The failure theories below all try to connect distinct test strengths into a continuous design envelope. The equations defining a design envelope could be based on observations of material ductility, on material toughness, or on ultimate strength. Failure criteria usually take the form of the absolute value of some limiting stress or a linear (or quadratic) combination of limiting stresses.

The maximum stress criterion is a macro failure theory for composite materials. It is an extension of the maximum normal stress criterion (for isotropic materials) in which different strengths in tension and compression can be accounted for in any principal material direction. The criterion states failure will occur when the maximum

allowable stress in any principal material direction is exceeded. Gibson [8] presents the criterion in plane stress conditions in Equations 6, 7 and 8.

$$-\sigma_{1\,\max}^{(-)} \le \sigma_1 \le \sigma_{1\,\max}^{(+)} \qquad \text{[Equation 6]}$$

$$-\sigma_{2\,\max}^{(-)} \le \sigma_2 \le \sigma_{2\,\max}^{(+)} \qquad \text{[Equation 7]}$$

$$\tau_{12} \le \tau_{\max} \qquad \text{[Equation 8]}$$

The ultimate stresses (σ_{1max} and σ_{2max}) in Equations 6, and 7 are the strength of the composite in material directions 1 and 2 respectively. The plus *(+)* and minus *(-)* signs in Equations 6 and 7 distinguish between the ultimate stress in tension or compression, respectively. Equation 8 assumes that shear failure along the principal material axes is independent of the sign of the shear stress. Thus, only the magnitude of τ_{12} is important.

The maximum stress criterion predicts that there is no interaction between any stresses in the principal material directions. Therefore, the failure surfaces in σ_1-σ_2, σ_1-τ_{12}, and σ_2-τ_{12} plane stress spaces are all rectangular.

The maximum strain criterion is a macro failure theory popular in the field of fiber-reinforced composites because it is easy to apply. The criterion states failure will occur when the maximum allowable strain in any direction is exceeded. Gibson [8] presents the criterion in plane stress conditions in Equations 9, 10 and 11.

$$-\varepsilon_{\max}^{(-)} \le \varepsilon_1 \le \varepsilon_{\max}^{(+)} \qquad \text{[Equation 9]}$$

$$-\varepsilon_{\max}^{(-)} \le \varepsilon_2 \le \varepsilon_{\max}^{(+)} \qquad \text{[Equation 10]}$$

$$\gamma_{12} \le \gamma_{\max} \qquad \text{[Equation 11]}$$

The ultimate strains (ε_{max} and γ_{max}) in Equations 9, 10 and 11 are determined by uniaxial tension, compression and shear tests. The plus *(+)* and minus *(-)* signs in Equations 9 and 10 distinguish between the ultimate strain in tension or compression, respectively. Because the ultimate strains are developed directly from uniaxial test data, Gibson [8] noted that the maximum strain criterion accurately predicts failure in uniaxial strain but cannot predict biaxial failure strains for graphite-epoxy fiber-reinforced composites.

The maximum shear stress criterion is often used to predict yielding of ductile materials. Yielding in ductile materials is usually caused by slippage along the crystal plane along the maximum shear surface. Therefore, a material is considered safe as long as the maximum shear stress within a material stays below the yield stress (σ_y). The criterion is presented in plane stress by as shown in Equations 12, 13 and 14.

$$\left|\sigma_1\right| \le \sigma_y \qquad \text{[Equation 12]}$$

$$\left|\sigma_2\right| \le \sigma_y \qquad \text{[Equation 13]}$$

$$\left|\sigma_1 - \sigma_2\right| \le \sigma_y \qquad \text{[Equation 14]}$$

The yield stress can be determined by uniaxial tests. Tension tests are often used if the tension test coupons exhibit a ductile failure surface.

The Tsai-Wu failure criterion is perhaps the most widely accepted failure criterion for fiber-reinforced composite materials [6]. The criterion is a quadratic equation that expands on the Tsai-Hill criterion using an increased number of terms in its prediction equation. Comparisons of test data and experimental data confirm that this criterion does a better job of predicting the failure envelope than the Tsai-Hill criterion for brittle fiber-reinforced composite materials.

The Tsai-Wu criterion is often shown in indicial form for simplicity as in Equation 15.

$$F_i\sigma_i + F_{ij}\sigma_{ij} = 1 \quad \text{[Equation 15]}$$

Hyer [12] presents a general formula for the plane stress Tsai-Wu criterion. He notes that since the sign of the shear stress is assumed to have no effect on the failure, the linear shear stress terms (F_6 and F_{16}) should be zero. Then, under plane stress conditions, the criterion reduces to Equation 16.

$$F_1\sigma_1 + F_2\sigma_2 + F_{11}\sigma_1^2 + F_{22}\sigma_2^2 + F_{66}\tau_{12}^2 + F_{12}\sigma_1\sigma_2 = 1 \quad \text{[Equation 16]}$$

The subscripts in Equation 16 indicate directions in the material coordinate system. To determine the constants in the Tsai-Wu criterion, uniaxial tests are used, because a uniaxial test in the "1" direction reduces the criterion to the following;

$$F_1\sigma_1 + F_{11}\sigma_1^2 = 1 \quad \text{[Equation 17]}$$

Separate applications of only tension and compression stresses in the "1" direction are then used to obtain two equations (18 and 19) and two unknowns (F_1 and F_{11}).

$$F_1\sigma_T + F_{11}\sigma_T^2 = 1 \quad \text{[Equation 18]}$$

$$F_1\sigma_C + F_{11}\sigma_C^2 = 1 \quad \text{[Equation 19]}$$

Simultaneously solving equations 18 and 19, the F_1 and F_{11} constants to be written as Equations 20 and 21, respectively.

$$F_1 = \frac{1}{\sigma_T} - \frac{1}{\sigma_C} \quad \text{[Equation 20]}$$

$$F_{11} = \frac{1}{\sigma_C \cdot \sigma_T} \qquad \text{[Equation 21]}$$

The values σ_C and σ_T are typically the maximum compressive and tensile stresses respectively in the direction corresponding to material direction 1. The constants F_2 and F_{22} are determined in a similar fashion using uniaxial tests in the material "2" direction.

By application of only a shear load, several terms in the Tsai-Wu criterion drop out. The reduced criterion can be rearranged to determine the shear constant, F_{66}, (Equation 22).

$$F_{66} = \left(\frac{1}{\tau_{\max}} \right)^2 \qquad \text{[Equation 22]}$$

The F_{12} factor is an interaction term between the normal stresses and should be determined using biaxial tests. In fact, Gibson [8] notes that it has been suggested that the F_{12} factor can have four different values since there are four different failure pairs of σ_1 and σ_2. Because biaxial test equipment is not as accessible as uniaxial test equipment, theoretical values for F_{12} are often determined. One theoretical value (see Equation 23) yields interesting results.

$$F_{12} = -\frac{1}{2}\sqrt{F_{11}F_{22}} \qquad \text{[Equation 23]}$$

Using Equation 21 above, with isotropic materials, forces the Tsai-Wu criterion (Equation 16) to take on the exact same form as the von Mises criterion, a predecessor of the Tsai-Hill and Tsai-Wu criteria. Since the von Mises failure criterion works reasonably well to predict failure in metals, the value of F_{12} given by Equation 21 is often published as the interaction constant for all materials. However, an investigation by Lui

[14] indicated that there is no interaction between the normal stresses in wood and found the F_{12} value is approximately zero for wood.

Other theories have been examined for composite materials such as the Yeh-Stratton failure theory. Yeh and Lee [24] published an analysis of the Yeh-Stratton criterion on composite materials. They claim that while the Tsai-Wu criterion has been shown valid for brittle composites, the Yeh-Stratton criterion is valid for both brittle and ductile fiber-reinforced composites. Equation 24 presents the criterion for composite materials in indicial form.

$$f = A_i\sigma_i + A_j\sigma_j + B_{ij}\sigma_i\sigma_j + C_{ij}\tau_{ij}^2 = 1 \qquad \text{[Equation 24]}$$

In Equation 24, i, j=1,2,3 (repeated index is not summed) where A_i, A_j, B_{ij}, and C_{ij} are experimental constants. Here again, the sign of the shear stress should not affect the failure prediction, so no linear shear stress terms have been included in the criterion.

The Yeh-Stratton criterion provides a system of equations each describing a piece-wise continuous failure surface. Yeh and Lee [24] state, "The Y-S criterion for the anisotropic materials utilizes different equations for in each stress space quadrant." The use of different equations in each quadrant of stress space addresses some of the issues that the Tsai-Wu equation has with determination of theoretical values for the biaxial constant F_{12}.

Under plane stress conditions, the criterion is written out as the following:

$$A_1\sigma_1 + A_2\sigma_2 + B_{12}\sigma_1\sigma_2 + C_{12}\tau_{12}^2 = 1 \quad \text{[Equation 25]}$$

$$A_1\sigma_1 = 1 \quad \text{[Equation 26]}$$

$$A_2\sigma_2 = 1 \quad \text{[Equation 27]}$$

It is Equation 25 that provides a lower bound on the failure criterion [Yeh and Lee, 1995]. Coefficients in Equation 25 must be determined for each quadrant of plane-stress space. While uniaxial tests can be used to determine A_1, A_2, and C_{12} (as shown Equations 28, 29, and 30), the constant B_{12} must be determined using biaxial tests.

$$A_1 = \left(\frac{1}{\sigma_{1\max}}\right) \quad \text{[Equation 28]}$$

$$A_2 = \left(\frac{1}{\sigma_{2\max}}\right) \quad \text{[Equation 29]}$$

$$C_{12} = \left(\frac{1}{\tau_{\max}}\right)^2 \quad \text{[Equation 30]}$$

Yeh and Lee go on to conclude that "compared to failure criteria developed from the macro mechanics point of view, the Y-S criterion gives very accurate theoretical failure predictions. With results compared between the Y-S criterion and a failure theory derived from micromechanics, this study has shown that the Y-S criterion offers good and conservative strength predictions for both angle crack problems and tensile loading tests. In summary, the Y-S criterion is among the most accurate and reliable."

CHAPTER THREE: MATERIALS and METHODS

Materials

For the purposes of investigating both brittle and ductile behaviors in wood-plastic composites (WPC), three WPC formulations were characterized by dissipated energy. One formulation consisted of maple flour and high-density polyethylene (HDPE). The second formulation was maple flour and HDPE with an ethylene-maleic anhydride polymer (MAPE) additive. Finally, the third formulation consisted of ponderosa pine flour and polyvinyl chloride (PVC) compound. The wood flour and plastics were dry blended in a 4-ft diameter drum. Table 1 shows the percentages (by weight) of wood, plastic and additive in each of the formulations.

Table 1: Wood-Plastic Composite Formulations

% Wood	Wood	% Plastic	Plastic	% Additives
67.5	Maple (American Wood Fiber #4010)	32.5	HDPE (Equistar LB0010 00)	None
67.5	Maple (American Wood Fiber #4010)	31	HDPE (Equistar LB0010 00)	1.5% MAPE (Honeywell AC 575A)
50	Pine (American Wood Fiber #4020)	50	PVC (Georgia Gulf 3014B000-3 3014NAT)	None

All three formulations were extruded at the Washington State University Wood Materials and Engineering Laboratory using a conical twin-screw extruder (Cincinnati-Milacron E55) and a stranding die. A box-cylinder cross-section (see Figure 3) was chosen as the extruded shape for all three wood-plastic formulations in order to provide the necessary raw materials for producing test specimens. The flat sides of the box-

cylinder provided bending, tension, and v-notch test specimens (see Figure 3). The cylinder section was removed for axial/torsion test specimens (also shown in Figure 3)

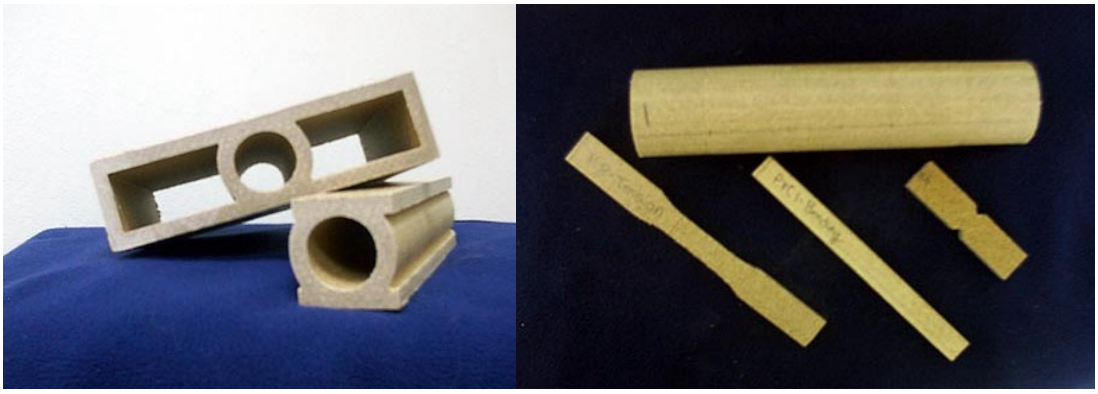

Figure 3: Extrusion Cross-Section and Test Coupons

The extrusion process is presumed to be responsible for the transversely isotropic nature of the WPC. For notation purposes, a coordinate system will be used for the rest of this thesis. Stresses and strains in the "one" direction will indicate a stress or strain parallel to the extrusion direction of the WPC. Stresses and strains in the "two" and "three" directions are mutually perpendicular to the extrusion direction.

Testing

Data from uniaxial and biaxial tests were utilized to create dissipated energy functions for the three wood-plastic formulations. ASTM standards developed for testing plastic coupons were used to determine loading rates. The load rates for all tests were chosen to provide strain rates of 1% per minute. Table 2 shows the test matrix, including type of test performed and number of specimens for each test. The table only includes

the quantity of specimens successfully tested. Biaxial test specimens that failed as a result of gripping the specimens were not included in Table 2. Note: the HDPE v-notch specimens were not tested because of the lack of availability of the v-notch test fixture.

Table 2: Number of Specimens Successfully Tested for Each Type of Test

Test Performed	Number of Specimens		
	HDPE Formulation	HDPE w/ MAPE	PVC Formulation
Tension	10	10	8
V-Notch Beam Shear	0	10	9
3-point Bending	10	10	10
Combined Axial and Torsion	12	11	5

Tension Tests

Tension tests per ASTM D638 were conducted to characterize dissipated energy in material direction 1. Rectangular specimens ½" wide were narrowed in the middle to give the specimens a "dog bone" shape. The nominal dimensions of each test coupon are given in ASTM D638 (Specimen Type I). The exact specimen length and cross-section dimensions (in the narrowed location) are shown in Table 3.

Table 3: Tension Test Specimen Dimensions

	HDPE			**HDPE with MAPE**			**PVC**		
#	Length (in.)	Width (in.)	Depth (in.)	Length (in.)	Width (in.)	Depth (in.)	Length (in.)	Width (in.)	Depth (in.)
1	6.5	0.473	0.310	6.5	0.480	0.296	6.5	0.493	0.316
2	6.5	0.496	0.309	6.5	0.475	0.299	6.5	0.492	0.296
3	6.5	0.465	0.300	6.5	0.469	0.299	6.5	0.506	0.298
4	6.5	0.477	0.307	6.5	0.472	0.302	6.5	0.505	0.318
5	6.5	0.492	0.307	6.5	0.472	0.303	6.5	0.493	0.317
6	6.5	0.477	0.311	6.5	0.474	0.310	6.5	0.521	0.321
7	6.5	0.480	0.306	6.5	0.471	0.310	6.5	0.509	0.324
8	6.5	0.476	0.321	6.5	0.491	0.300	6.5	0.492	0.301
9	6.5	0.471	0.302	6.5	0.469	0.301	6.5	0.493	0.318
10	6.5	0.485	0.313	6.5	0.502	0.309	6.5	0.496	0.322

An MTS extensometer with a 1-inch gage length measured strain in the narrowed location. A 2-kip Instron screw-driven universal testing machine (model #4466) was used in displacement control to load these specimens. The crosshead displacement rate used for all materials was 0.002 inches per minute.

Loads were obtained from the loading head of the test machine and strains were collected from the strain gage at ½ second intervals. Dissipated energy was found using Equation 3. Integration of the area under the stress-strain plot was accomplished by summation of the trapezoidal area provided by consecutive data points (see Figure 4).

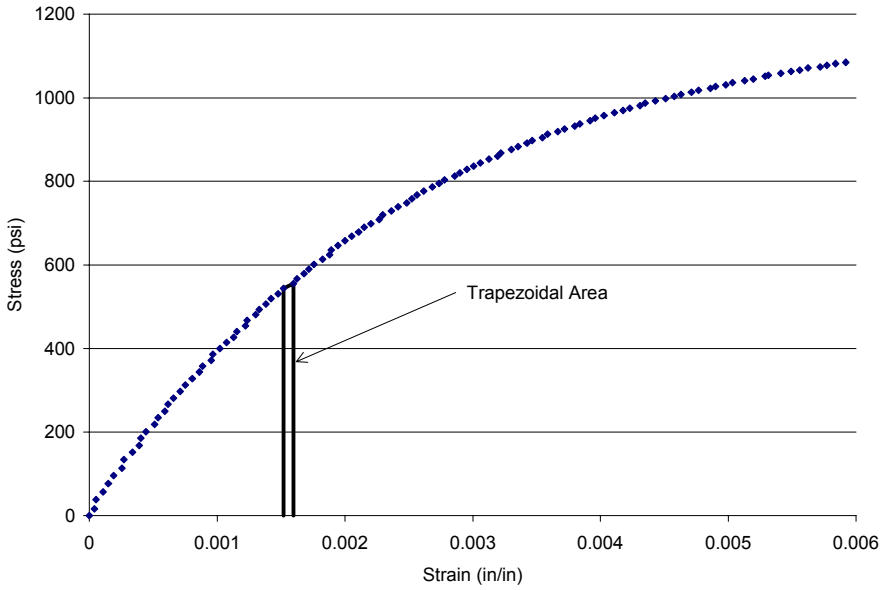

Figure 4: Trapezoidal areas used for integration under a stress-strain plot.

In order to find the maximum curvature of the dissipated energy function, the raw data was "smoothed" by using every fifth dissipated energy value. The slope between every fifth data point provided a smooth first derivative of the dissipated energy function. The slope of the first derivative points was then used to provide a second derivative of the

dissipated energy function. The maximum value of the second derivative was then chosen as the maximum curvature of the original dissipated energy function.

The applied load was then used to calculate the stress in the narrowed location. A 5% parametric tolerance limit at 75% confidence was calculated per ASTM2917 using Equation 5, the average maximum stress, and the maximum-stress standard deviation. A "k" value of 2.104 was selected from Table 3 in ASTM2917 to provide a 75% confidence level for a sample size of 10 specimens.

A statistical "z-test" of each specimen was performed on the tension test data within each material population. Two PVC specimens were determined to be statistically different ($z<0.0001$) from the rest of the population and they were removed from the population (see Table 2). A "k" value of 2.189 was chosen to provide a 75% confidence level for the remaining eight PVC specimens. Once the 5% PTL stress was calculated, the corresponding strain and dissipated energy density could be noted.

V-Notch Shear Tests

Rectangular specimens 3 inches long and 0.75 inches wide were notched on two sides (in the center of the 3-inch side) to a width of 0.5 inches per ASTM D5379. A sketch of the v-notch specimen dimensions is shown in Figure 5.

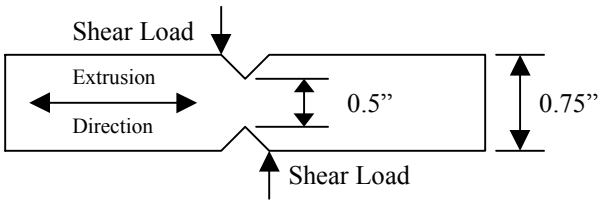

Figure 5: V-Notch Test Specimen Configuration

The overall width, width at the notch, and thickness for each V-notch test coupon are shown in Table 4. PVC Specimen #4 was removed from the test population because a crack in the specimen was discovered prior to testing.

Table 4: V-Notch Test Specimen Dimensions

	HDPE			HDPE with MAPE			PVC		
#	Width (in)	Notch Width (in.)	Thick (in.)	Width (in)	Notch Width (in.)	Thick (in.)	Width (in)	Notch Width (in.)	Thick (in.)
1	0.747	0.488	0.301	0.739	0.487	0.293	0.736	0.476	0.291
2	0.752	0.492	0.301	0.749	0.484	0.291	0.732	0.498	0.291
3	0.747	0.488	0.307	0.729	0.470	0.296	0.752	0.522	0.304
4	0.748	0.488	0.306	0.721	0.458	0.295	N/A	N/A	N/A
5	0.750	0.444	0.299	0.751	0.487	0.298	0.745	0.480	0.293
6	0.749	0.445	0.301	0.751	0.491	0.299	0.731	0.469	0.293
7	0.747	0.484	0.305	0.744	0.466	0.291	0.729	0.466	0.291
8	0.742	0.489	0.304	0.747	0.484	0.299	0.743	0.471	0.290
9	0.745	0.484	0.309	0.740	0.484	0.303	0.735	0.475	0.292
10	0.746	0.493	0.310	0.743	0.479	0.292	0.743	0.479	0.302

A 2-kip Instron screw-driven universal testing machine (model #4466) was also used to test these specimens at a displacement rate of 0.005 inches per minute. Load-displacement data was collected to analyze total energy dissipated under shear loading in the plane perpendicular to extrusion (see Figure 5). These tests also provided a method of examining failure of wood-plastics under pure shear loads.

In the V-notch shear test, only load and crosshead displacements were collected. Total dissipated energy (not dissipated energy density) for each specimen was calculated using the same method of summation of trapezoidal areas under the load-displacement curve, with one adjustment. The shape of the load-displacement curve was not the same as those seen in tension loading. The v-notch load-displacement plot has a linear region in between two portions with opposite curvature (see Figure 6).

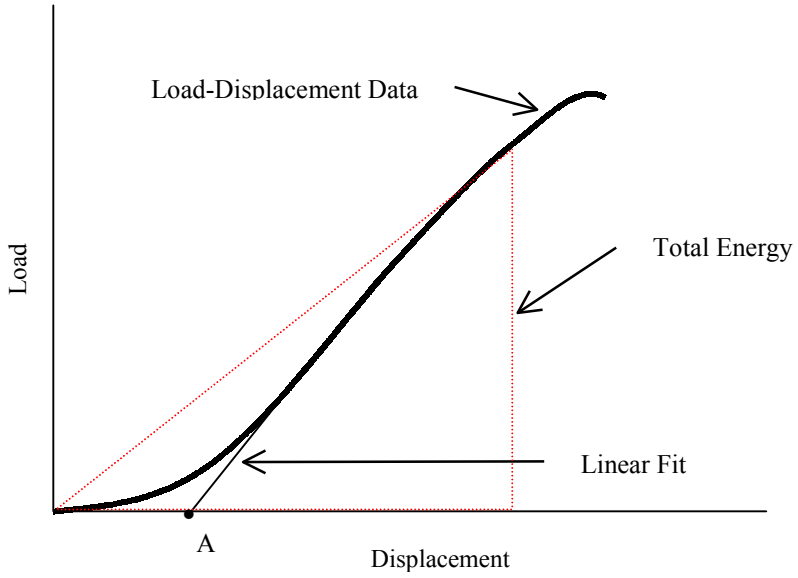

Figure 6: Dissipated Energy from a V-Notch Load-Displacement Plot

Recoverable energy is found using the triangular area in Figure 1, but for the v-notch tests, using a triangular area that goes through the zero load and zero displacement point does not make sense. A portion of the triangular "total energy" area (shown in Figure 6) would be a chord above the load-displacement plot, yielding negative energy. In order to calculate the recoverable energy in the v-notch tests, a "toe compensation" procedure was used similar to ASTM D638. To compensate for the toe, a straight-line approximation of the test data was extrapolated to the point of zero load (Point A in Figure 6). The straight line can be seen in Figure 6 labeled as "linear fit." Point A was then used as the origin of energy dissipation, i.e., the origin of the triangular area representing the recoverable energy.

Biaxial Tests

Cylindrical specimens were prepared for each material formulation by removing the center of box-cylinder cross-sections (see Figure 3). The axis of the cylinders was in the primary material direction (direction 1). The cylinders were 8 inches long in order to provide adequate space for a biaxial extensometer between the machine grips. The specimens were turned on a lathe to an outside diameter of 1.75 inches ± 0.05 inches. The extruded wall thickness of each cylinder was 0.3 inches. The outside diameter dimension was chosen to accommodate the grips of the testing machine. While sixteen specimens were planned to be used for each material, many cylinders cracked while they were being turned to final dimensions or failed upon gripping with the biaxial test machine. The outside diameter and wall thickness for each test specimen is shown in Table 5.

Table 5: Biaxial Test Specimen Dimensions

	HDPE			HDPE with MAPE			PVC		
#	Length (in.)	Thick (in.)	O.D. (in.)	Length (in.)	Thick (in.)	O.D. (in.)	Length (in.)	Thick (in.)	O.D. (in.)
1	8	0.284	1.762				8	0.310	1.779
2	8	0.308	1.752	8	0.308	1.761			
3	8	0.304	1.746	8	0.311	1.752			
4	8	0.296	1.744				8	0.275	1.774
5	8	0.299	1.738	8	0.307	1.764	8	0.296	1.768
6	8	0.285	1.750	8	0.292	1.769			
7	8	0.311	1.776				8	0.309	1.775
8									
9	8	0.295	1.755	8	0.313	1.768	8	0.300	1.780
10				8	0.293	1.756			
11				8	0.307	1.772			
12	8	0.292	1.763	8	0.306	1.779			
13	8	0.282	1.758	8	0.311	1.757			
14				8	0.307	1.764			
15	8	0.278	1.758	8	0.301	1.756			
16	8	0.300	1.759						

Several combinations of shear and axial strains were included in the test plan for each wood-plastic formulation. Pure compression and pure torsion were targeted displacement applications since they provide the needed data for use in failure theories. Other combinations of axial and shear loads were chosen to fill in between the pure compression and pure torsion data. A plot of the planned strain states is shown in Figure 7.

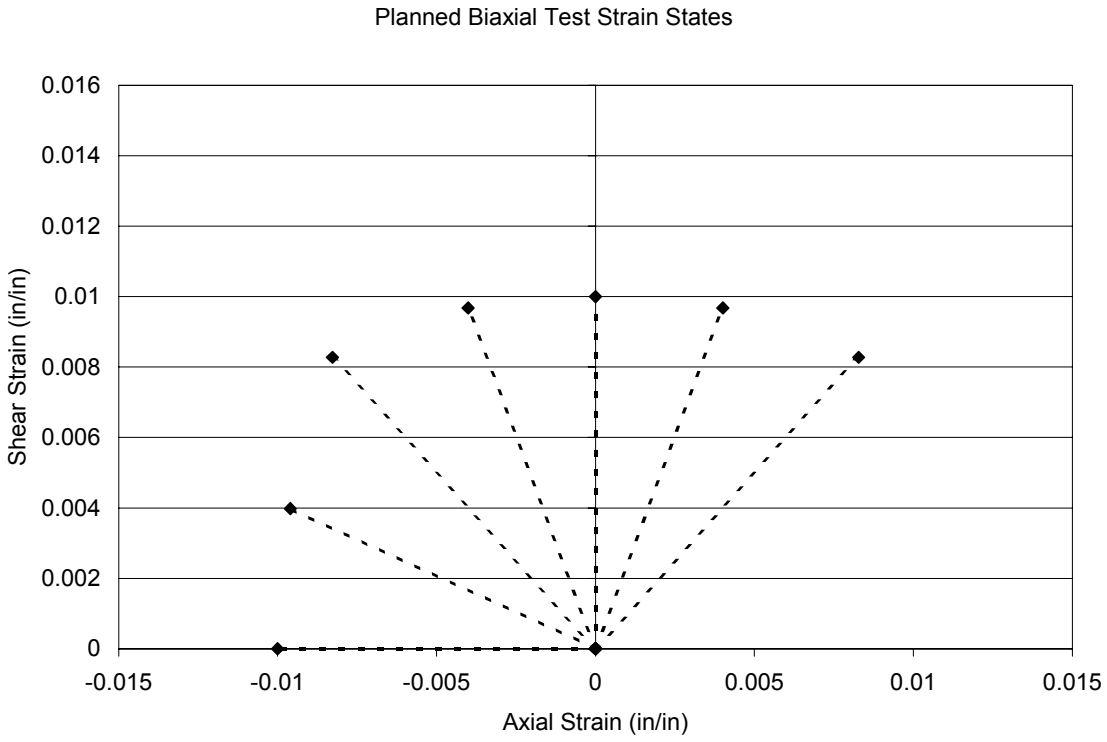

Figure 7: Planned Strain States for Biaxial Test Specimens

The displacement rate was determined based on the principal strain rate as calculated by Equation 31. The target principal strain rate was 1% per minute to coincide with the strain rates used for the tension tests.

$$\varepsilon_1, \varepsilon_2 = \frac{(\varepsilon_x + \varepsilon_y)}{2} \pm \sqrt{\frac{(\varepsilon_x - \varepsilon_y)^2}{4} + \frac{\gamma_{xy}{}^2}{4}} \qquad \text{[Equation 31]}$$

Testing was done on a 55-kip servo-hydraulic testing machine capable of applying axial and torsion loads simultaneously. Prior to loading each specimen in the test machine, a snug fitting, 2-inch long, dowel was inserted into each end. The dowels were intended to limit the probability that the test cylinders would be crushed by the hydraulic grips. The testing machine was capable of holding the test cylinders with 1000-2500 psi, but in order to reduce the chance of crushing the cylinders, a grip pressure of 1150 psi was used. This 1150-psi grip pressure was the lowest pressure that would hold the specimens without allowing them to slip in the grips under torsion loading.

Shear and axial strains were measured using a biaxial extensometer (MTS Multiaxis Extensometer Model #638) while load-displacement data was collected using the testing machine. The extensometer and load gage were "zeroed" after the first hydraulic grip grabbed the cylinder, which allowed measurement of any compressive pre-loads due to closing the grips.

3-Point Bending Tests

Three-point bending tests were conducted for each material on a 2-kip Instron universal testing machine (model #4466) using displacement control following ASTM D790. Rectangular specimens were placed flat-wise on a test span of 4.8 inches in order to provide span-to-depth ratio of approximately 16 (see Haiar [9]). The actual dimensions of each specimen are shown in Table 6.

Table 6: Bending Test Specimen Dimensions

	HDPE			HDPE with MAPE			PVC		
#	Length (in.)	Width (in.)	Depth (in.)	Length (in.)	Width (in.)	Depth (in.)	Length (in.)	Width (in.)	Depth (in.)
1	6	0.520	0.303	6	0.458	0.294	6	0.544	0.306
2	6	0.517	0.303	6	0.51	0.297	6	0.537	0.295
3	6	0.532	0.306	6	0.478	0.295	6	0.556	0.308
4	6	0.527	0.301	6	0.504	0.302	6	0.542	0.294
5	6	0.525	0.302	6	0.483	0.298	6	0.535	0.293
6	6	0.529	0.305	6	0.527	0.301	6	0.541	0.312
7	6	0.517	0.304	6	0.461	0.301	6	0.521	0.295
8	6	0.505	0.305	6	0.505	0.295	6	0.545	0.309
9	6	0.503	0.312	6	0.495	0.294	6	0.540	0.296
10	6	0.521	0.308	6	0.556	0.306	6	0.541	0.312

Load data was taken from the load cell and deflection data was collected using the crosshead motion. Displacement of the crosshead (at 0.002 inches/sec) was used to provide approximately 1% strain per minute in the extreme tension fiber at mid-span. The material 2-3 plane was used as the bending plane, meaning that the pure bending stresses were in the "1" direction. Figure 8 shows the 3-point bending test set-up with respect to the material coordinate system.

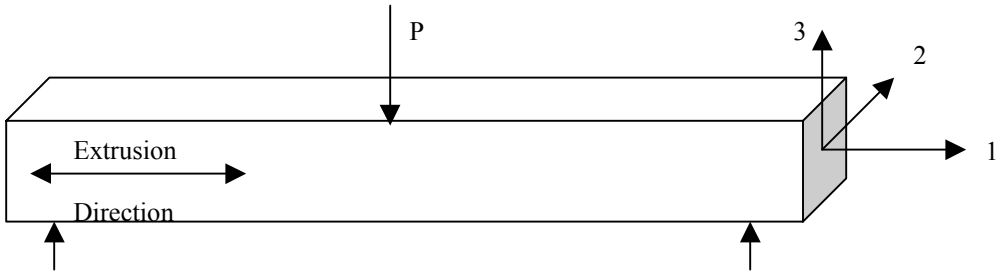

Figure 8: Specimen Orientation During 3-Point Bending Test

Analytical Methods

Dissipated Energy Function

Dissipated energy functions were developed in normal and shear strain-space using tension and biaxial test results. Data from the tension and biaxial tests provided a set of strain states (normal and shear strain), where each state corresponded to a calculated quantity of dissipated energy density. Normal and shear strain data from each test specimen was converted to polar coordinates and written as a strain vector. Each test specimen had only one vector orientation (θ) but several magnitudes (r) that corresponded to different quantities of dissipated energy density. The "r" values and dissipated energy quantities were used to create a Lagrange interpolation function for a particular loading.

In order to plot the dissipated energy contour maps, Mathematica (version 4.1) was used to back-solve the Lagrange dissipated energy function for a strain magnitude (r) that gave specific quantities of dissipated energy. The quantities started at zero in-lbs/in^3 and increased in increments of 0.35 in-lbs/in^3. In cases where multiple test specimens were used under the same strain state (θ), an average value (r) for each increment was found. An interpolation function was then used to connect the magnitude values ("r" value associated with a particular increment of dissipated energy) in the "θ" direction for each increment of dissipated energy. The results provided a smooth contour plot that was presented in normal/shear strain space.

Dissipated Energy during 3-Point Bending Tests

It is proposed that tension and compression dissipated energy density functions (ϕ) can be used to predict the total energy dissipated (Φ) in a 3–point bending test by integrating the dissipated energy density functions over the volume of the beam. Because the dissipated energy density function is a function of strain, the state of strain throughout the entire beam must be found. The first step is to find the strain profile at a particular cross-section.

In beam bending theory, the tensile and compressive strains are assumed linear along the depth of the beam (see Figure 9). For WPC beams, linear strain distribution does not mean a linear stress distribution (see Figure 10), but a hyperbolic tangent distribution [18].

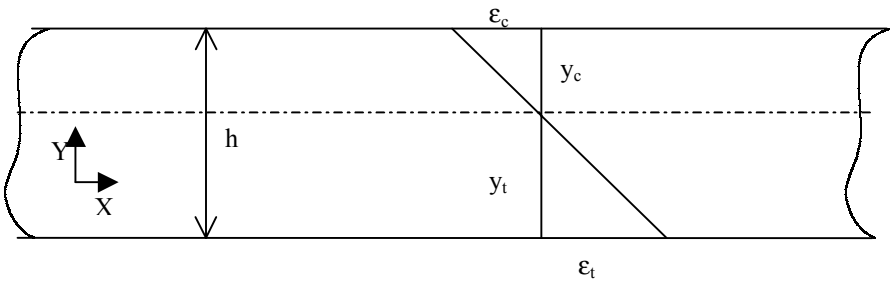

Figure 9: Strain Distribution in Bending of WPC Beams

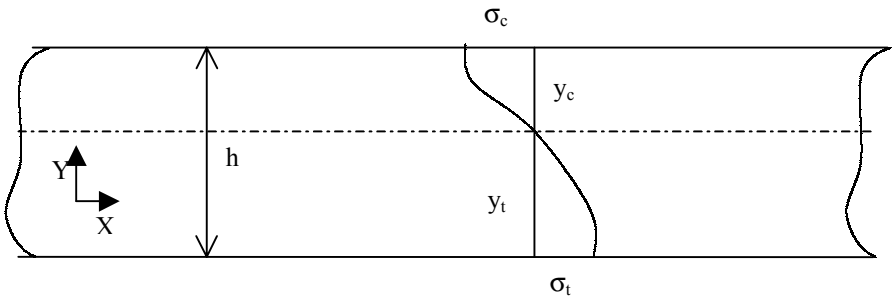

Figure 10: Stress Distribution in Bending of WPC Beams

Wood-plastic beams in bending have a neutral axis that is not located at the mid-height of the beam because the tension and compression stress-strain relationships are different. The location of the neutral axis (denoted in Figure 9 as y_t) was found using the equation of static force equilibrium applied along the axis of the beam. Summation of forces can be done using stresses and strains as shown in Equation 32.

$$\int_{\varepsilon_c}^{\varepsilon_t} \sigma \, \partial \varepsilon = 0 \qquad \text{[Equation 32]}$$

The linear relationship between tension and compression strains can be found using similar triangles (see Figure 9) and represented by Equation 33.

$$\frac{\varepsilon_c}{y_c} = \frac{\varepsilon_t}{y_t} \qquad \text{[Equation 33]}$$

By considering only the magnitude of the tension and compression stresses, Equations 32 and 33 can be used to create a relationship between the neutral axis position (y_t) and the tension strain (ε_t) as shown in Equation 34.

$$\int_0^{\varepsilon_t} \sigma_t \, \partial \varepsilon - \int_0^{(\frac{h}{y_t} - 1)\varepsilon_t} \sigma_c \, \partial \varepsilon = 0 \qquad \text{[Equation 34]}$$

Mathematica version 4.1 was used to solve Equation 34 for position of the neutral axis at a given maximum tensile strain. Now, a relationship that describes the strains over the cross-section of the beam has been developed. For any given tensile strain, the neutral axis height can be calculated, which in turn allows a compressive strain to be calculated. The complete strain distribution over the cross-section of a beam in bending can now be described.

The next step is to describe the strain distribution over the length of the beam. This is done using the internal moment of the beam. In general, the internal moment in a beam is the area integral of the stress (σ) multiplied by its moment arm (y), as shown in Equation 35.

$$Moment = \int y\sigma \partial A \qquad \text{[Equation 35]}$$

Using the linear strain distribution (from Equation 33) and the constant width of the rectangular cross-section (b), the internal moment can be written as shown in Equation 36.

$$Moment = b\int_0^{yt} y\sigma_T(\frac{y}{yt}\varepsilon_T)\partial y + b\int_0^{h-yt} y\sigma_C(\frac{y}{yt}\varepsilon_T)\partial y \qquad \text{[Equation 36]}$$

For the 3–point bending tests, the moment in Equation 36 is a linear function of the position along the length of the beam. For one-half of the beam, the moment is $\frac{Px}{2}$, where P is the applied load and x is the distance from the end of the beam. The equation defining moment can be put into Equation 36 to give Equation 37.

$$\frac{Px}{2} = b\int_0^{yt} y\sigma_T(\frac{y}{yt}\varepsilon_T)\partial y + b\int_0^{h-yt} y\sigma_C(\frac{y}{yt}\varepsilon_T)\partial y \qquad \text{[Equation 37]}$$

Equation 37 will be used to develop the state of strain throughout the volume of a rectangular beam with a single point load at midspan. Once the state of strain is known, the dissipated energy can be integrated over the volume of the beam.

The total dissipated energy can be found by integration of the dissipated energy density function. Equation 38 shows integration of the strain energy density equation for a rectangular beam (of constant width) assuming that the strain distribution is

symmetrical about the mid-span; the strain distribution from x=0 to x=L/2 is the same as the strain distribution from x=L/2 to x=L.

$$\Phi = \int \phi(\varepsilon)\partial V = 2b\int_0^{L/2}\int_0^{h} \phi(\varepsilon)\partial y\partial x \qquad \text{[Equation 38]}$$

If the dissipated energy functions were linear functions of strain, the dissipated energy functions would be linear through the cross-section of the beam. However, the dissipated energy functions in tension and compression are not linear (with respect to strain). The resulting dissipated energy in a beam's cross-section is represented by two non-linear functions (see Figure 11).

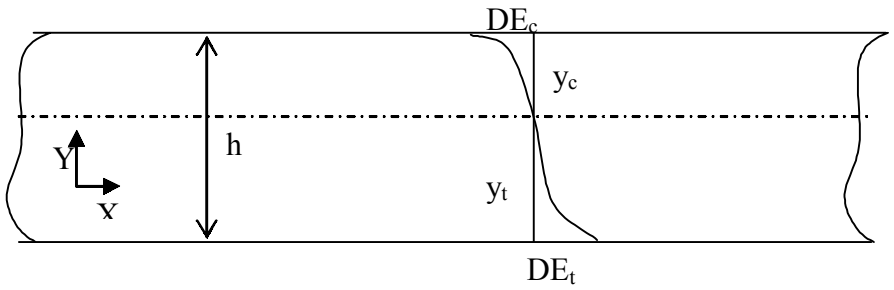

Figure 11: Dissipated Energy Distribution in Bending of WPC Beam

Since the tension and compression dissipated energy functions are not the same, the total quantity of energy dissipated cannot be found by integrating a single dissipated energy density function as in Equation 38. The tension and compression DE density functions must be integrated over the appropriate portion of the cross-section. The compression dissipated energy function was integrated from zero to y_c and the tension dissipated energy function was integrated from zero to y_t.

The total energy dissipated can now be predicted by rearranging Equation 38 into Equation 39.

$$\Phi = 2\int_0^{L/2} b\left[\int_0^{\varepsilon_t} \phi_T \partial\varepsilon + \int_0^{(\frac{h}{yt}-1)\varepsilon_t} \phi_C \partial\varepsilon\right]\partial x \qquad \text{[Equation 39]}$$

In Equation 39, h and y_t are defined in Figure 9, b is the width of the beam, and ϕ_T and ϕ_C are the tension and compression dissipated energy functions, respectively. It is only the ε_t and y_t terms that are variable, but y_t is related to ε_t by solving Equation 33. Using two equations (33 and 39), the total energy dissipated by a rectangular beam in bending can be found. The total energy dissipation predicted by integration of the tension and compression dissipated energy functions over the volume of the beam should be the same as the total energy dissipation under the 3–point bending load-displacement plot.

Comparison with Failure Theories

The average value of maximum dissipated energy curvature was found in the tension and biaxial tests. The strain and stress corresponding to the maximum curvature was noted. The average ultimate stress and standard deviation allowed for calculation of a 5% PTL (see Equation 5) for each of the three wood-plastic formulations under each test condition. A corresponding 5% PTL strain was then found.

Stresses and strains based on the ultimate strength, the strength at maximum curvature in the dissipated energy function and the 5% parametric tolerance limit were compared to each other. Failure envelopes for the maximum stress, maximum strain, maximum shear stress, Tsai-Wu and Yeh-Stratton failure criteria were drawn and compared to the failures observed in the tension and biaxial tests. For each criteria, three

limit states were chosen to define failure. They were ultimate stress, maximum dissipated energy curvature, and 5% PTL.

Maximum Stress Criterion

The average stress at failure (for each wood-plastic formulation) found by tension, torsion and compression tests can be inserted into the failure criterion directly. The values of tension, torsion and compression strains at maximum dissipated energy curvature were also inserted directly into Equations 6, 7, and 8.

Stress values based on the 5% PTL are found using an average ultimate strength and a standard deviation. Tension test results provided an average ultimate stress and standard deviation directly. The 5% PTL compressive and shear stresses were calculated using the ultimate compression stress and ultimate shear stress obtained in biaxial testing and a representative COV of 8%. The 8% COV is based on previous research on wood-plastic composites by Haiar [9] and Lockyear [13].

Maximum Strain Criterion

The average strain at failure (for each wood-plastic formulation) found by tension, torsion and compression tests were inserted into the failure criterion directly. The values of tension, shear and compression strains at maximum dissipated energy curvature were also inserted directly into Equations 9, 10, and 11.

Strain values based on the 5% PTL are found using an average ultimate strength and a standard deviation. Tension test results provided an average ultimate strain and standard deviation directly. The 5% PTL compressive and shear strains were calculated

using the ultimate compression strain and ultimate shear strain obtained in biaxial testing and a representative COV of 8%. The 8% COV is based on previous research on wood-plastic composites by Haiar [9] and Lockyear [13].

Maximum Shear Stress Criterion

The average maximum shear stress values at failure in each combined torsion/compression specimen was inserted into the failure criterion directly. The failure envelope was plotted using the equation below.

$$\sigma_y = \pm\frac{1}{2}\sqrt{(\sigma_1 - \sigma_2)^2 + (2\tau_{12})^2} \qquad \text{[Equation 40]}$$

The average maximum-shear-stress for the HDPE and HDPE with MAPE under combined compression and torsion was used to define the yield strength, because all of the compression/torsion specimens exhibited shear failures. In order to be consistent, the average maximum-shear-stress for the PVC compression/torsion specimens was used to define the PVC yield strength although no shear failures were observed.

Tsai-Wu Criterion

The constants used to plot the Tsai-Wu failure envelope were defined earlier (see Equations 20-22). The only items needed to define these constants were the values of maximum compression stress, σ_C, and maximum tension stress, σ_T, in the primary material direction (direction #1) and the maximum shear stress (material direction 1-2).

Tension test results provided data for the calculation of the maximum tension stress, the 5% PTL stress and the maximum dissipated energy curvature stress. Biaxial

test results were used to calculate the values of maximum compressive and shear stresses, and the maximum DE curvature compressive and shear stresses. For the 5% PTL compression and shear stresses, not enough test specimens were prepared for pure compression and pure torsion. Therefore, the 5% PTL compression and shear stresses were found using a representative COV of 8% based on previous wood-plastic composite research.

Yeh-Stratton Criterion

The Yeh-Stratton criterion, also a stress-based interaction criterion, is similar in form to that of the Tsai-Wu criterion. The three sets of stresses (ultimate, 5% PTL, and maximum dissipated energy curvature) defining failure were directly inserted into Equations 28, 29, and 30 to find the A_1, A_2 and C_{12} constants.

The 5% PTL tension strengths were calculated directly from tension test results. As with the maximum stress, maximum strain, and Tsai-Wu criteria, the 5% PTL compression and shear stresses were based on a representative COV of 8%.

CHAPTER FOUR: RESULTS

Test Results

Tension Test Results

Results of tension tests on the three wood-plastic formulations are represented by a stress-strain plot (see Figure 12) and a dissipated energy plot (see Figure 13). Each figure shows the following three data points for each wood-plastic formulation.

1) The average value of the maximum stress (denoted by an "X")

2) The average value at maximum curvature in the dissipated energy density function (denoted by an "O")

3) The 5% parametric tolerance limit (denoted by a "□").

Table 7 summarizes the noted values in Figure 12 and Figure 13, for each material and provides coefficients of variation (COV). Appendix A contains complete stress-strain and dissipated energy density plots for each of the materials tested.

Table 7: Tension Test Summary

Material	Max Strain (in/in)	Max Stress (psi)	Strain @ Max DE Curvature	Stress @ Max DE Curvature	Strain @ 5% PTL (in/in)	Stress @ 5% PTL (psi)
HDPE	0.0139	1271.5	0.00307	871.3	0.00487	1063.7
COV (%)	13.3%	5.61%	19.5%	11.9%	19.5%	N/A
MAPE	0.00672	2167.6	0.00386	1716.2	0.00403	1755.0
COV (%)	14.3%	6.5%	9.9%	7.75%	7.1%	N/A
PVC	0.00647	3197.5	0.00266	2000.2	0.00401	2647
COV (%)	12.0%	5.4%	13.75%	7.5%	11.25%	N/A

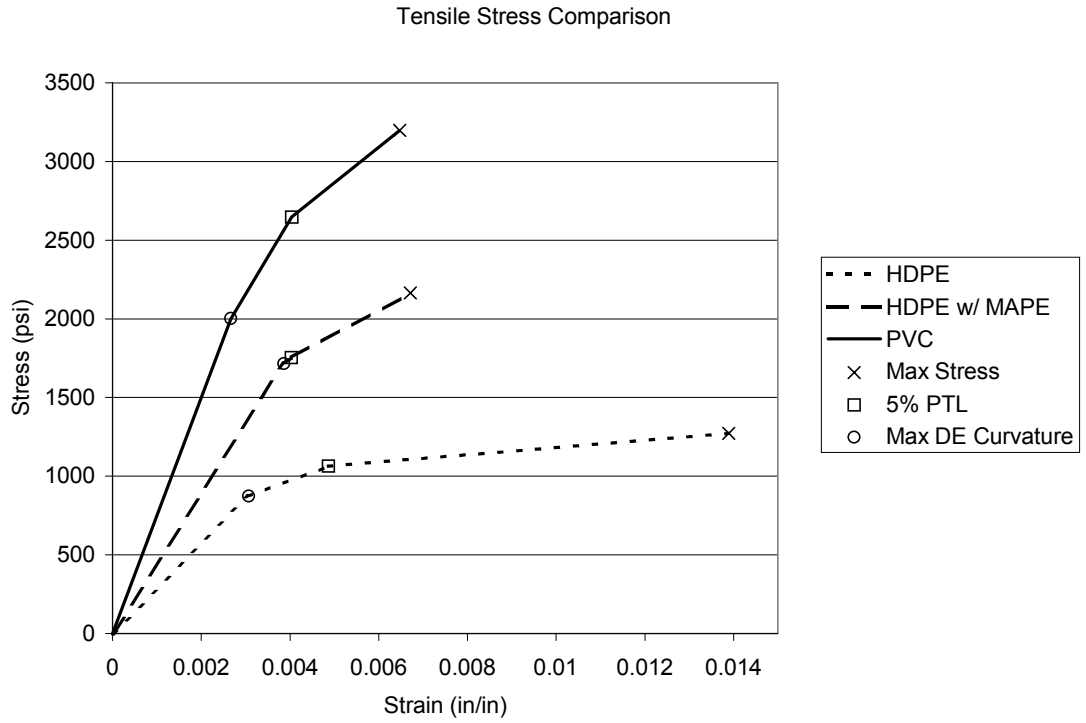

Figure 12: Tension Test Stress-Strain Results

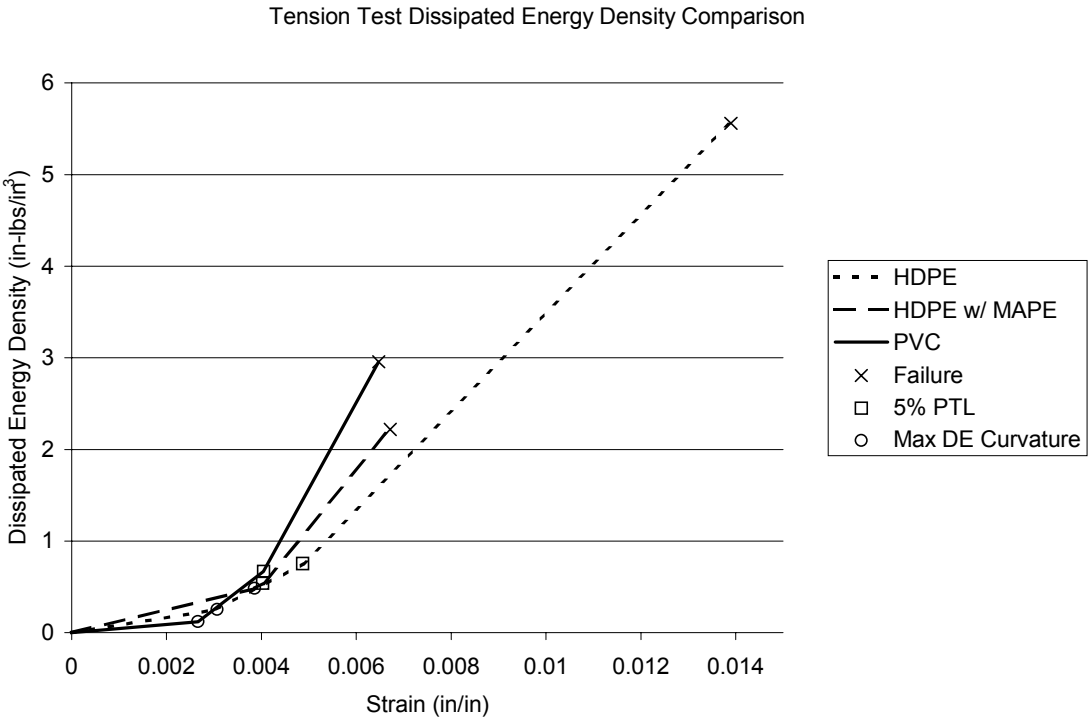

Figure 13: Tension Test Dissipated Energy Results

V-Notch Shear Test Results

In the V-notch shear test, load and crosshead displacements were collected to calculate the total dissipated energy and the maximum curvature. Figure 14 summarizes the load-displacement results for the HDPE with MAPE and PVC wood-plastic formulations. Figure 15 summarizes the dissipated energy results for the HDPE with MAPE and PVC wood-plastic formulation. Appendix B contains load-displacement and dissipated energy plots for the HDPE with MAPE and PVC wood-plastic formulations.

Shear stress calculations in ASTM D5379 are based on the cross-sectional area at the notched location. Stresses are calculated using the applied load divided by the area at the notch. V-notch shear test results are summarized in Table 8. It shows the average value and the coefficient of variation for 1) the ultimate shear stress and displacement, 2) the maximum dissipated energy curvature shear stress and displacement, and 3) the 5% PTL shear stress and displacement.

Table 8: V-Notch Shear Test Results

Material/ Coefficient of Variation	Max Disp (in)	Max Stress (psi)	Disp @ Max DE Curvature (in)	Stress @ Max DE Curvature (psi)	Disp @ 5% PTL (in)	Stress @ 5% PTL (psi)
HDPE*	N/A	N/A	N/A	N/A	N/A	N/A
C.O.V.	N/A	N/A	N/A	N/A	N/A	N/A
MAPE	0.055	2138	0.041	1723	0.044	1863
C.O.V.	11.2%	5.7%	12.4 %	8.1%	10.6%	N/A
PVC	0.056	3525	0.044	2838	0.047	3031
C.O.V.	4.5%	5.0%	11.8 %	9.3%	5.1%	N/A

*HDPE Specimens could not be tested due to unavailability of the V-notch test fixture.

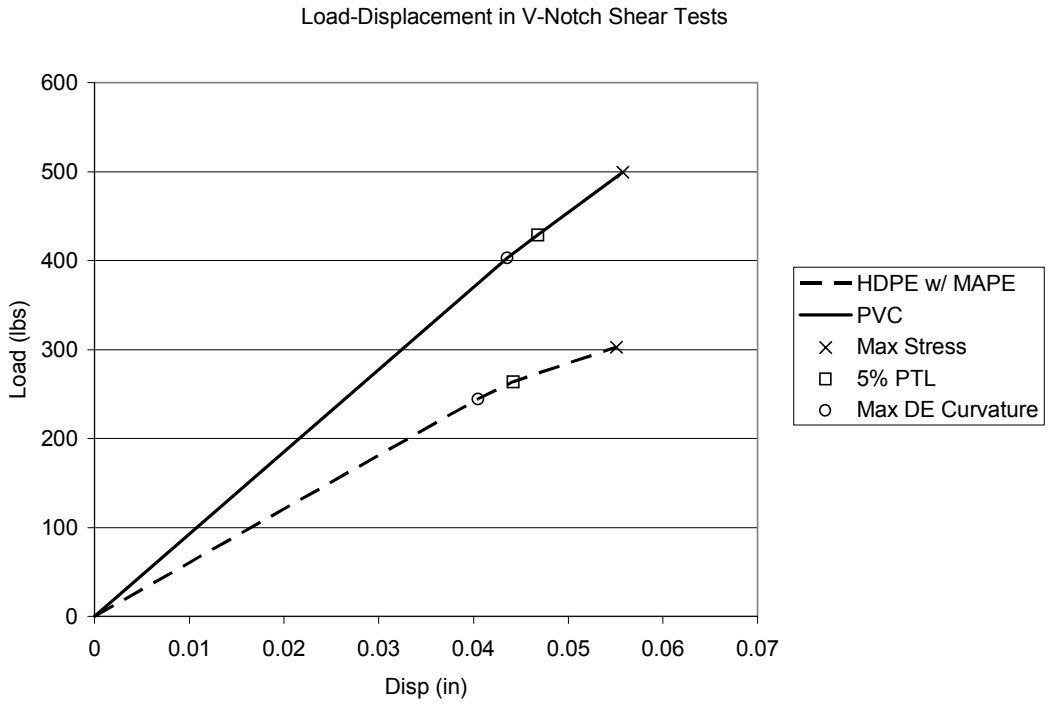

Figure 14: V-Notch Load-Displacement Test Results

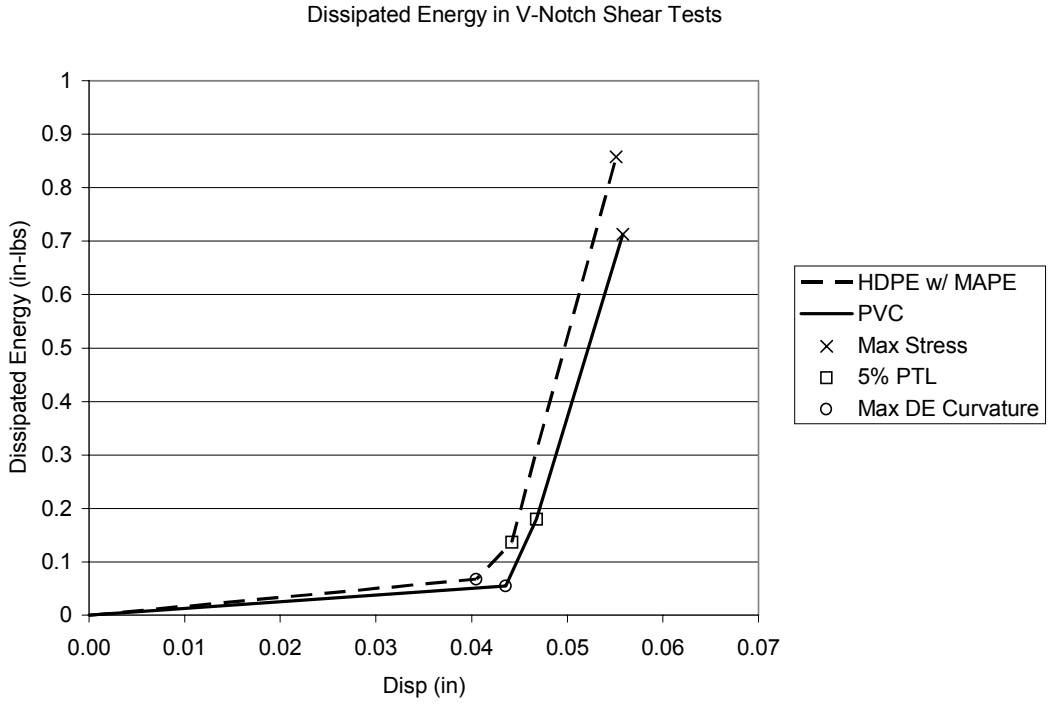

Figure 15: V-Notch Dissipated Energy Test Results

Biaxial Test Results

Errors in programming the test machine displacements resulted in a difference between some of the actual strain states (as shown in Figure 16) and the planned states (see Figure 7). Several different combinations of axial and shear strains were still attained, but some principal strain rates were nearly 2% per minute. Brandt [3] conducted rate-of-load experiments on HDPE, HDPE with MAPE and PVC wood-plastics and found that strain rates of 4% per minute increased modulus of rupture values less than 5% over strain rates of 1% per minute. For this research, a principal strain rate of 1% per minute was targeted, but a principal strain rate of 2% per minute was still acceptable. Actual loading rates for each test specimen are given in Appendix C.

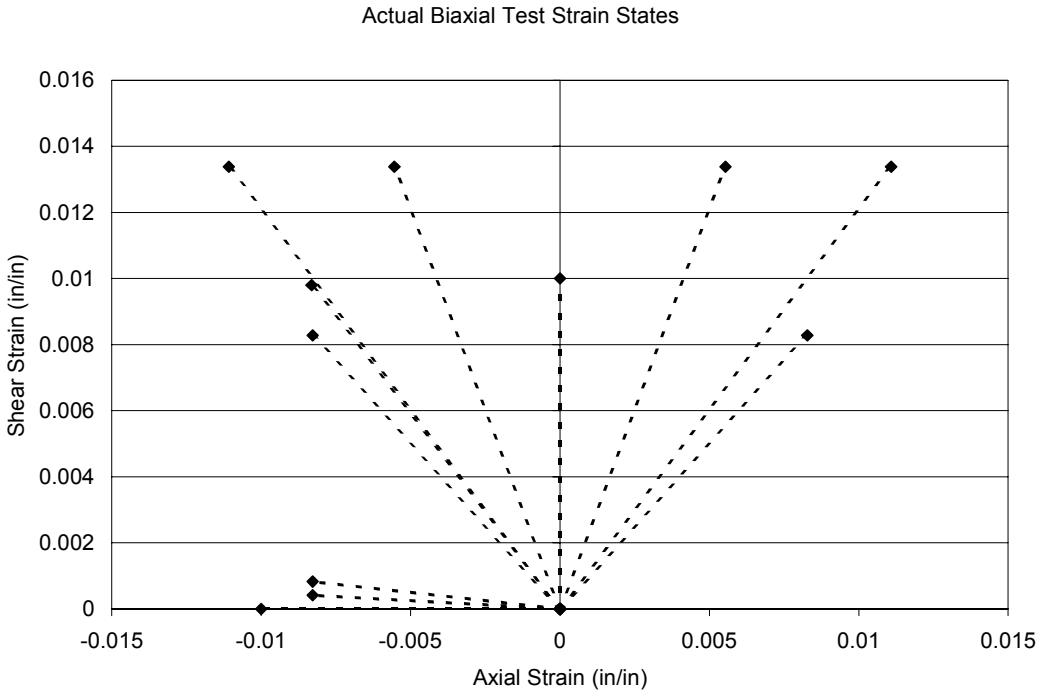

Figure 16: Actual Strain States During Biaxial Testing

The ultimate strain and ultimate stress for each wood-plastic formulation is summarized in Figure 17 and Figure 18 respectively. Dissipated energy plots (DE density versus principal strain) for all biaxial test specimens are shown in Appendix C.

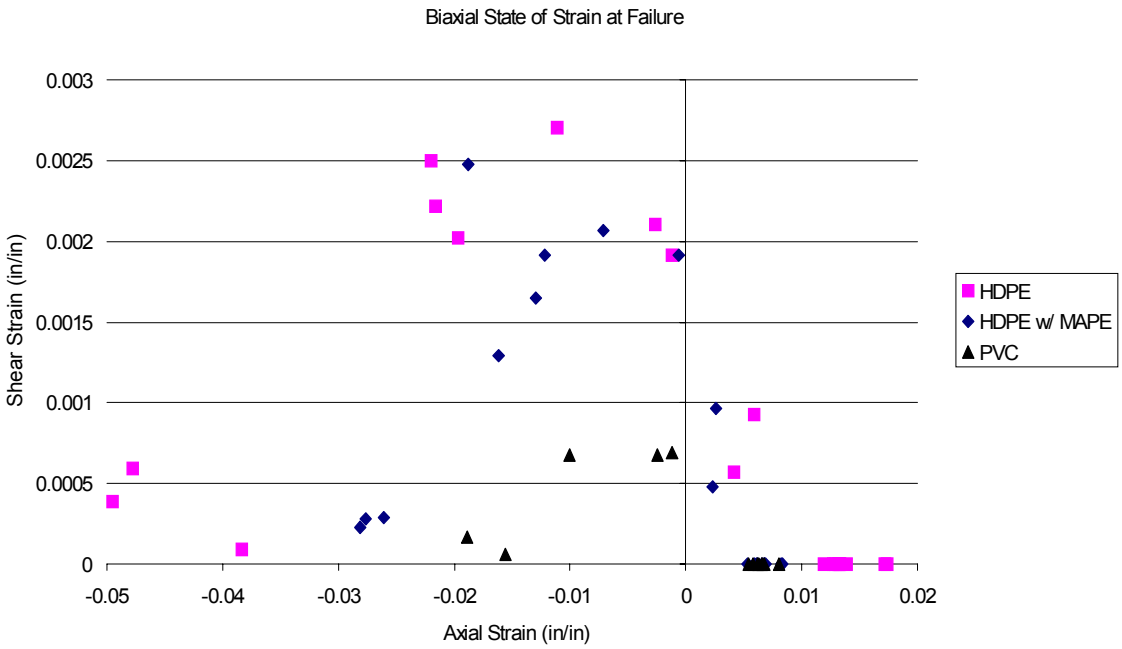

Figure 17: Biaxial Test Results - Strain at Failure

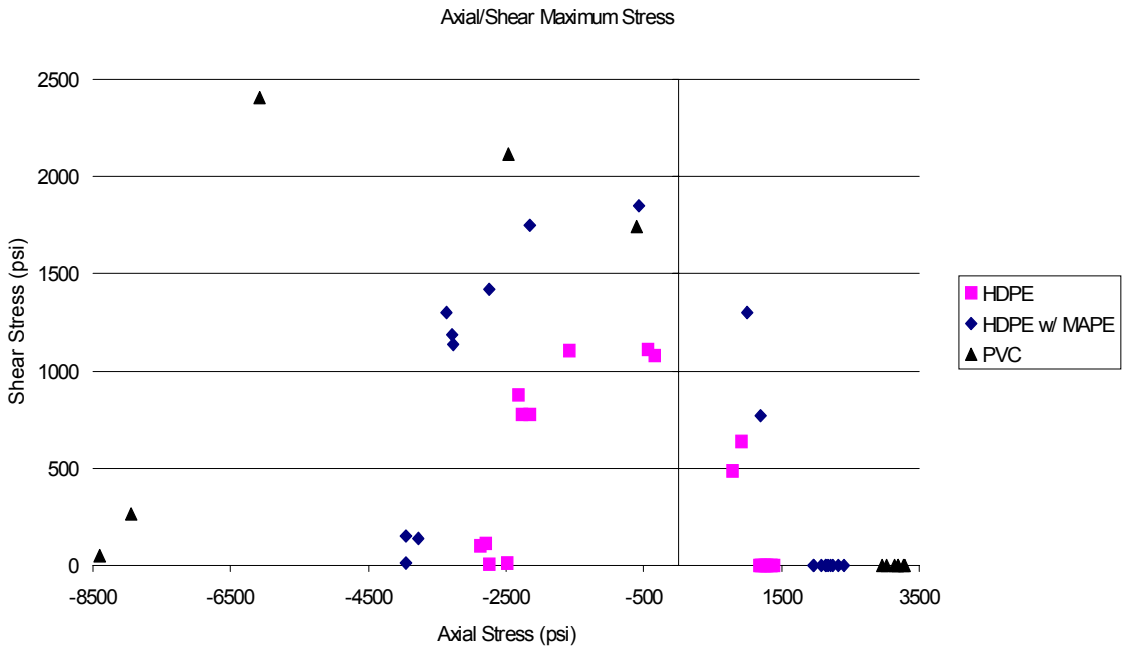

Figure 18: Biaxial Test Results – Stress at Failure

3-Point Bending Test Results

Load and displacement data from 3-point bending tests was collected for all three materials. The 5% PTL load was calculated for each wood-plastic composite formulation using the average maximum load and standard deviation. Total dissipated energy was calculated for each test specimen by integrating the trapezoidal areas under the load-displacement plot. The load and displacement corresponding to maximum curvature in the total dissipated energy function was found. Load and displacement values at 1) failure, 2) maximum curvature in the dissipated energy, and 3) the 5% PTL are summarized in Table 9. Load-Displacement and dissipated energy plots for each wood-plastic formulation are included in Appendix D.

Table 9: 3-Point Bending Test Results

Material / Coefficient of Variation	Max Disp (in)	Max Load (lbs)	Disp @ Max DE Curvature (in)	Load @ Max DE Curvature (lbs)	Disp @ 5% PTL (in)	Load @ 5% PTL (lbs)
HDPE	0.188	17.2	0.084	12.8	0.125	15.5
COV (%)	9.8%	4.5%	7.9%	6.0%	9.3%	N/A
MAPE	0.141	25.5	0.104	22.1	0.108	22.7
COV (%)	7.6%	5.2%	8.2%	7.8%	12.2%	N/A
PVC	0.125	40.2	0.081	30.4	0.087	32.2
COV (%)	9.3%	8.9%	5.6%	13.3%	16.5%	N/A

Analytical Results

Dissipated Energy Function

Strain vectors and dissipated energy density calculations from the tension and biaxial tests were used for development of a dissipated energy function for each wood-plastic composite. Specific increments of dissipated energy density were solved for in order to plot the dissipated energy contours. A contour map of dissipated energy values was created in axial/shear strain space by connecting the dissipated energy increments for each test specimen. Figures 19, 21, and 23 show the increments of dissipated energy (0.35 inch-lbs per in^3 of DE density) from each test specimens.

Some combinations of axial and torsion loads had multiple test specimens. Dissipated energy quantities from specimens that underwent the same combination of axial and torsion loads were averaged. Figure 20 shows the averaged specimen results and connects the increments of dissipated energy into a contour plot for HDPE. Figure 22 and Figure 24 are similar to Figure 20, and show dissipated energy contour plots for HDPE with MAPE and PVC, respectively.

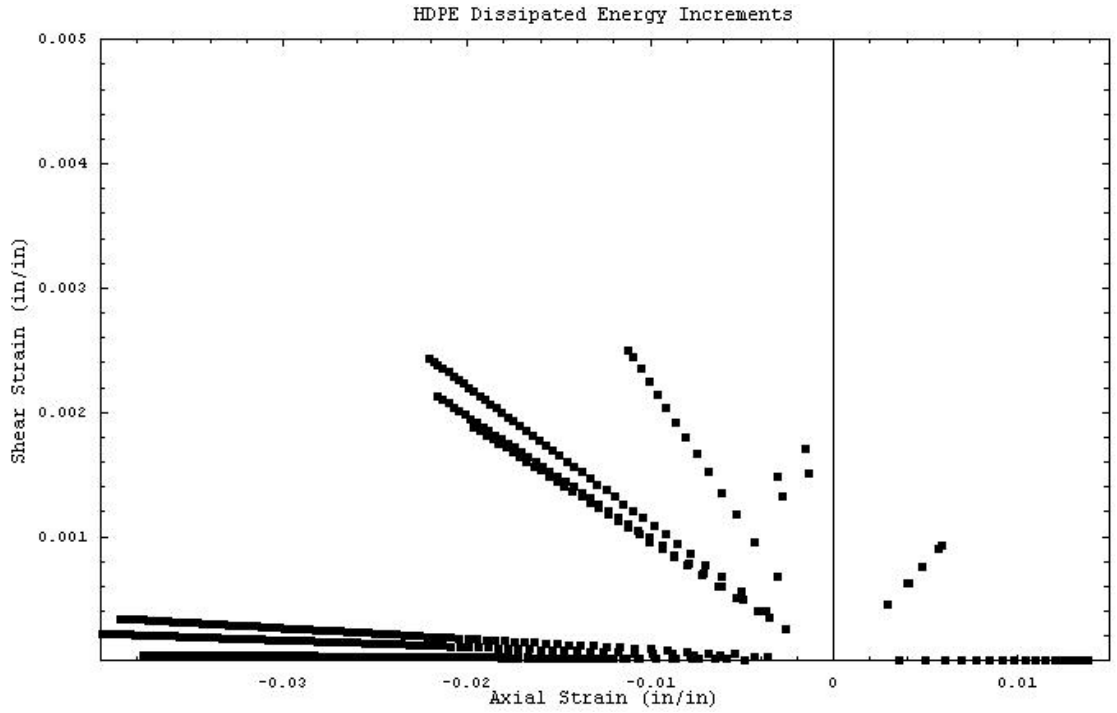

Figure 19: Dissipated Energy Contour Increments of 0.35 inch-lbs per in^3 for Each HDPE Test Specimen

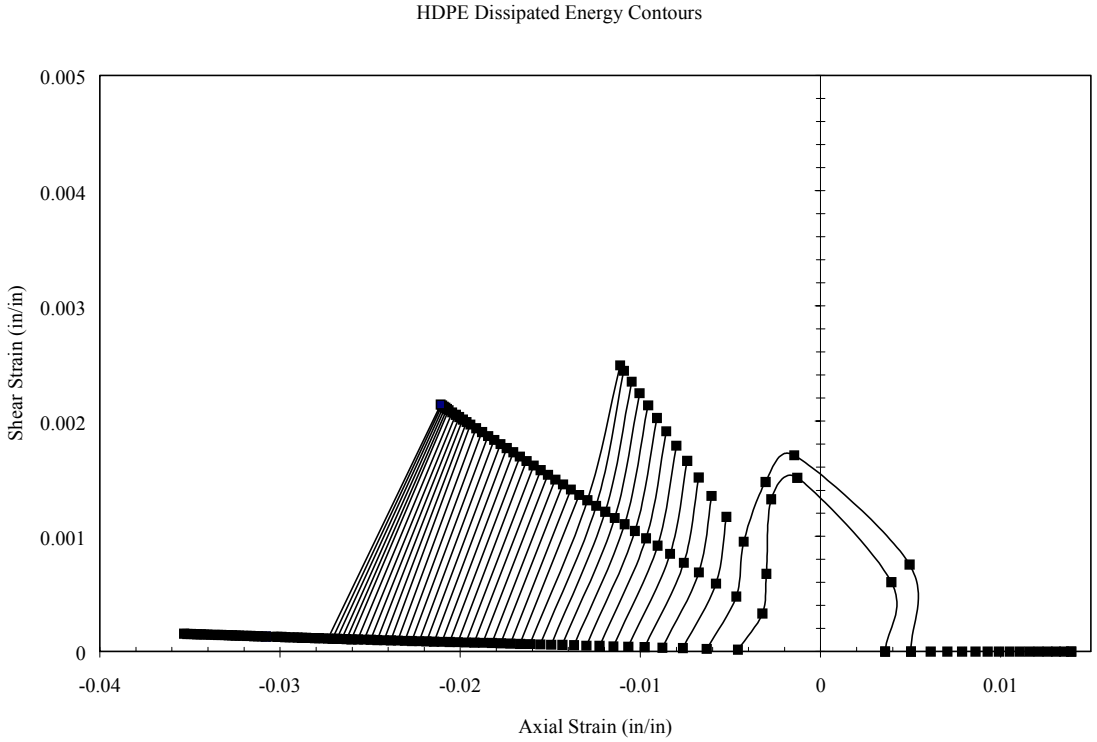

Figure 20: HDPE Dissipated Energy Contour Plot in Axial/Shear Space (0.35 inch-lbs per in^3 increments)

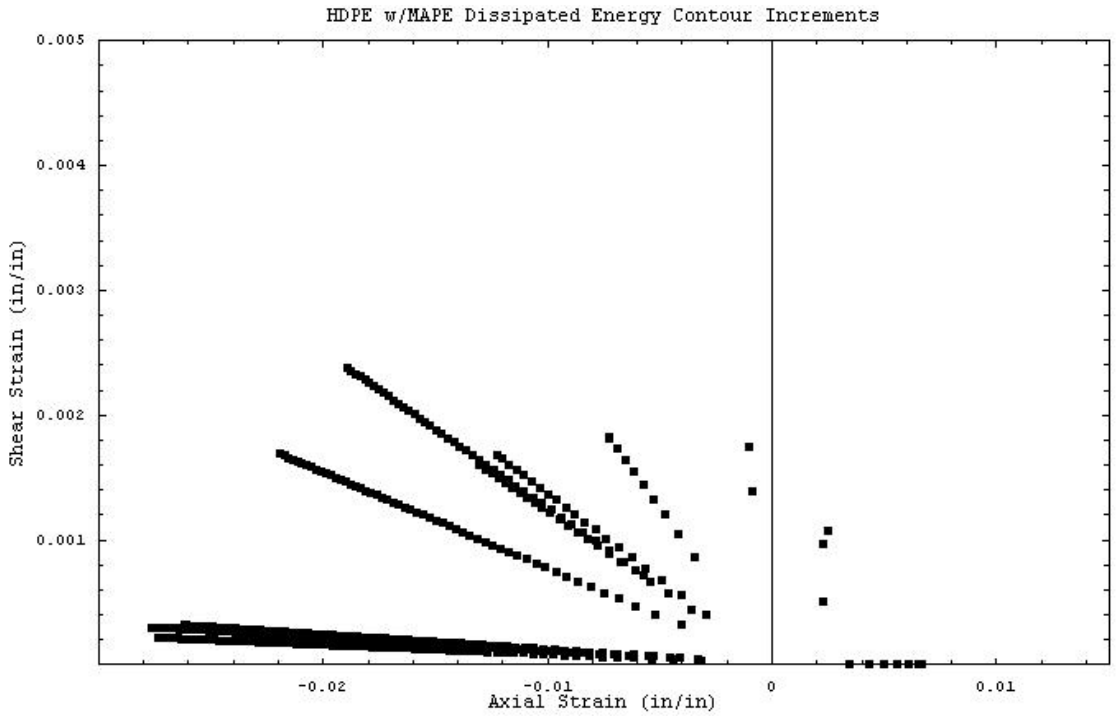

Figure 21: Dissipated Energy Contour Increments of 0.35 inch-lbs per in^3 in Each HDPE w/ MAPE Test Specimen

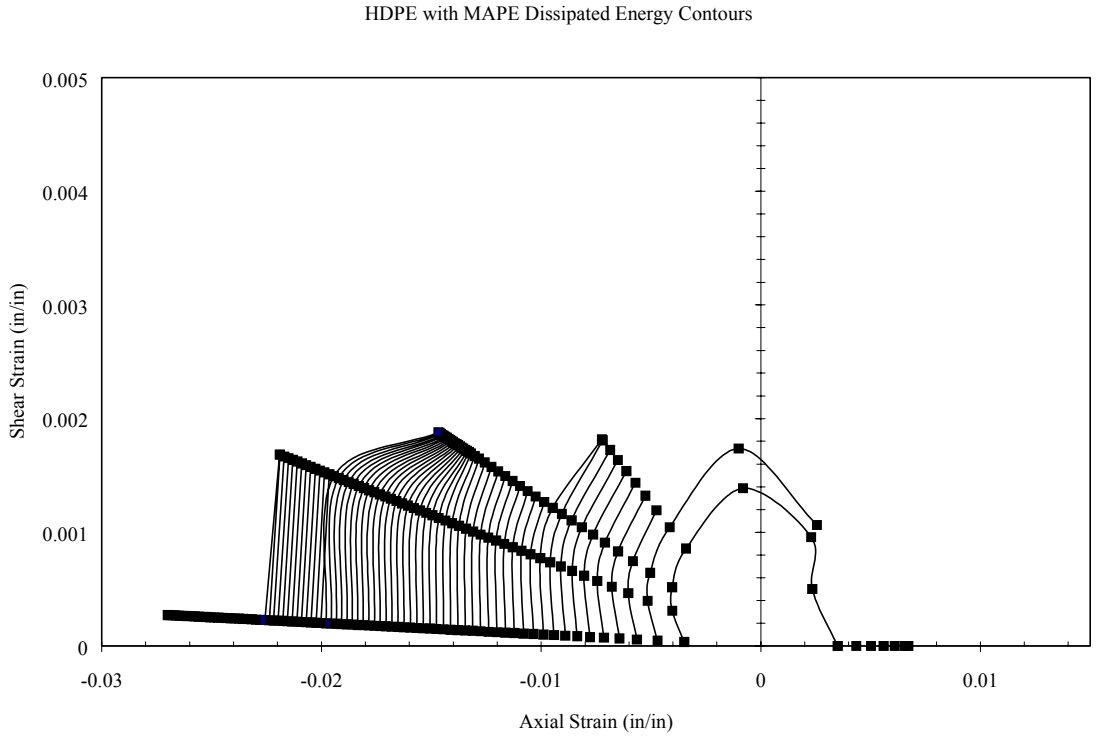

Figure 22: HDPE w/ MAPE Dissipated Energy Contour Plot in Axial/Shear Space (0.35 inch-lbs per in^3 increments)

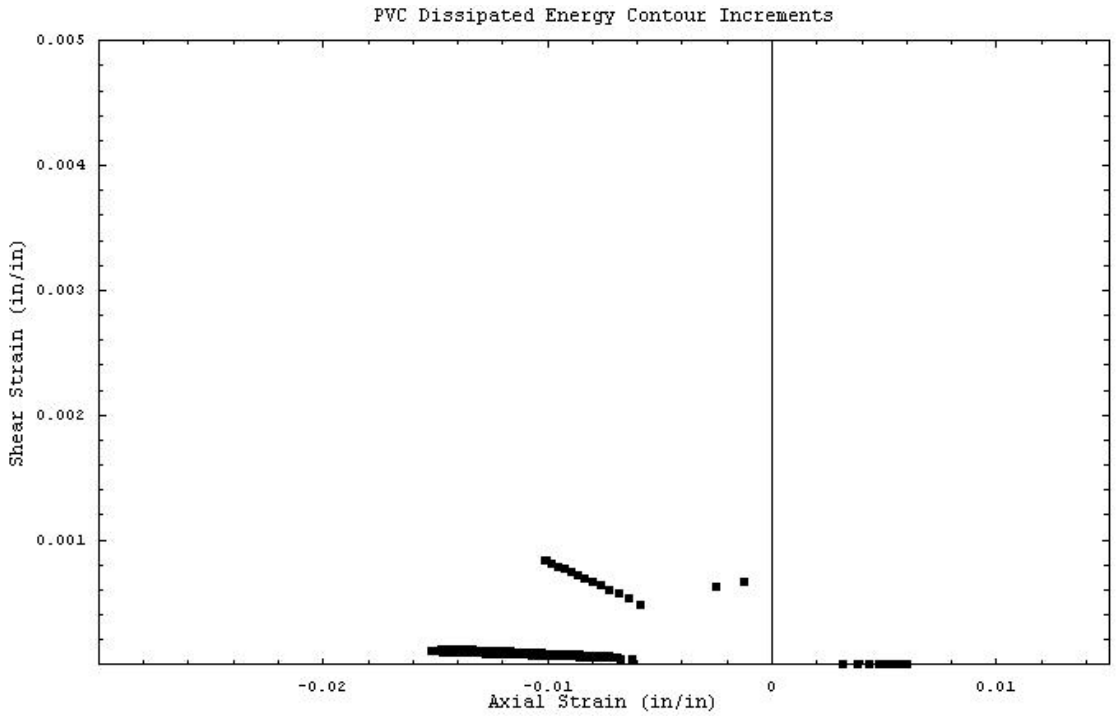

Figure 23: Dissipated Energy Contour Increments of 0.35 inch-lbs per in^3 in Each PVC Test Specimen

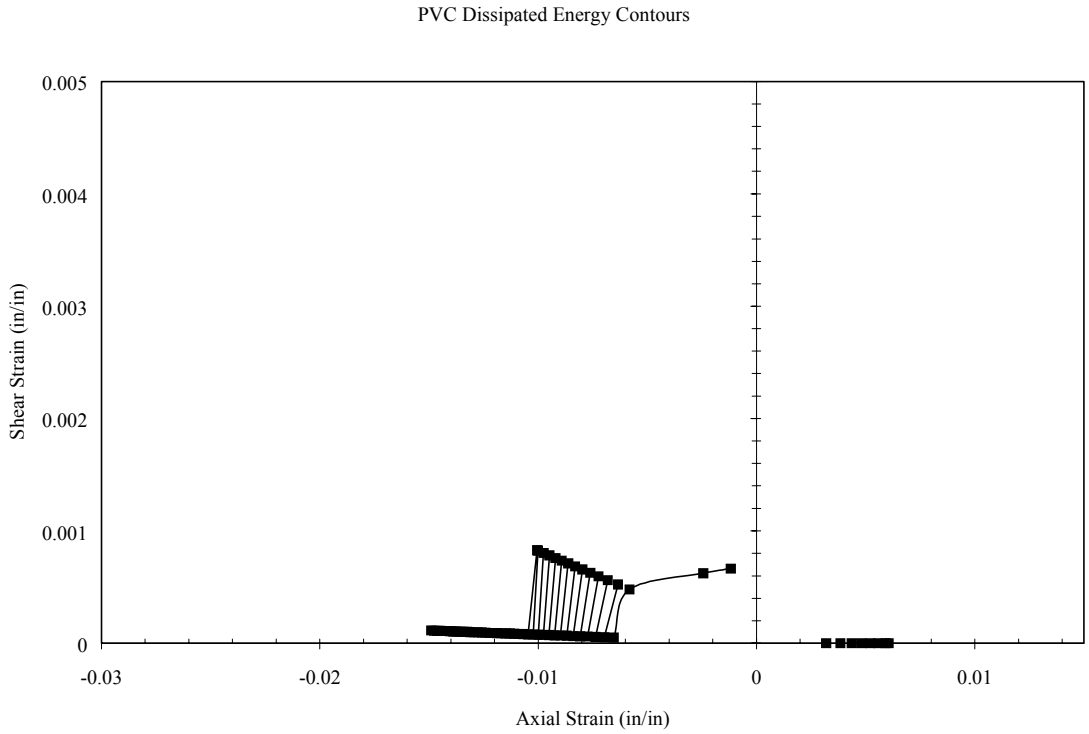

Figure 24: PVC Dissipated Energy Contour Plot in Axial/Shear Space (0.35 inch-lbs per in^3 increments)

Dissipated Energy during 3-Point Bending Tests

Utilizing beam theory, tension and compression strains were calculated throughout the volume of the beam. The strains were used as input into the dissipated energy functions and integrated over the volume of the beam using Equation 39. The total dissipated energy predicted by Equation 39 was compared to test data at six displacements for each material. The six displacements used for comparison were based on the following:

1) no load
2) maximum curvature in the tension test dissipated energy function
3) maximum tension stress
4) maximum curvature in the bending test dissipated energy function
5) 5% PTL in 3-point bending test
6) Ultimate strength in bending

Plots of the total energy dissipated versus mid-span displacement are shown in Figure 25, Figure 26, and Figure 27. In these figures, the total dissipated energy predicted using Equation 39 has been labeled "Prediction."

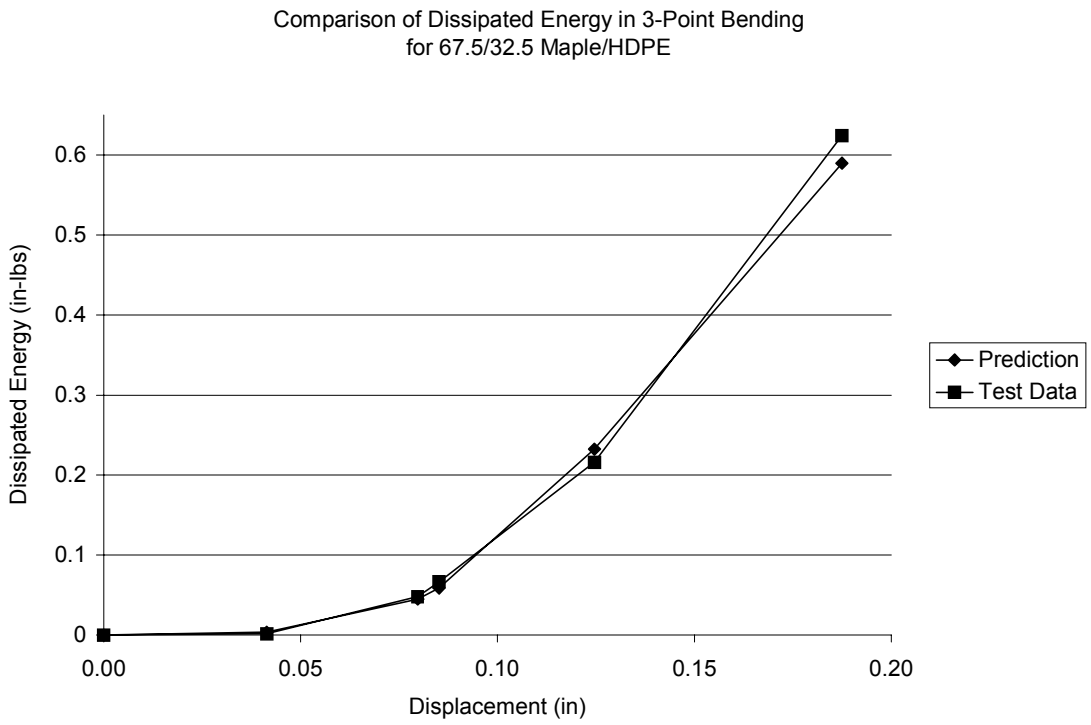

Figure 25: Dissipated Energy of HDPE Coupons in 3-Point Bending

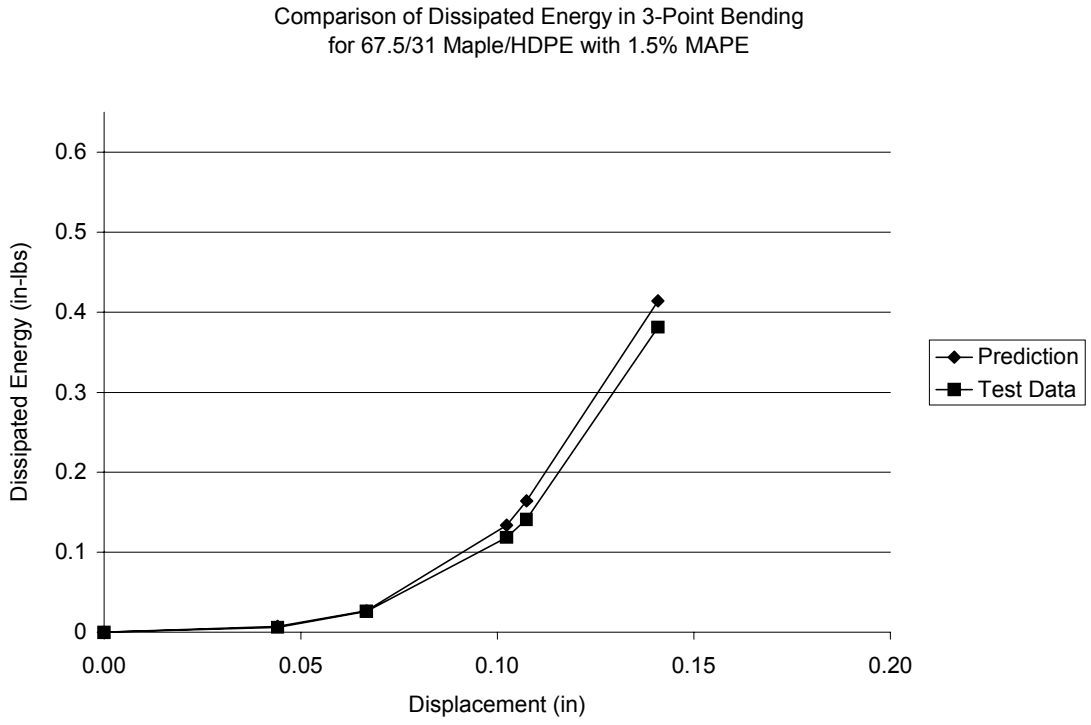

Figure 26: Dissipated Energy of HDPE w/ MAPE Coupons in 3-Point Bending

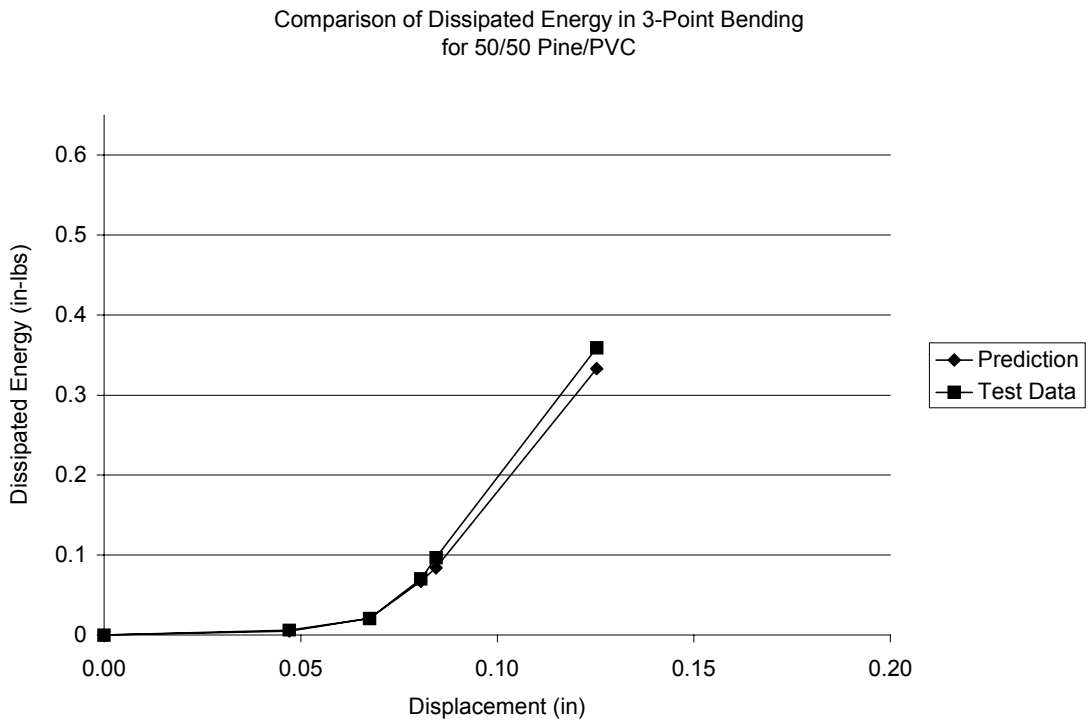

Figure 27: Dissipated Energy of PVC Coupons in 3-Point Bending

Comparison with Failure Theories

Tension test results provided stress/strain data in the "1" direction. Biaxial test results supplied compression stresses and strains in the "1" direction, and shear stresses and strains in the "1-2" direction. Using only these data sets limited the failure envelopes that could be drawn for each failure criterion to a plane stress space.

Each failure criterion is plotted for three different limit states, ultimate strength, maximum dissipated energy curvature and 5% parametric tolerance limit.

Maximum Stress Criterion

Without any stress measured in the "2" direction, the maximum stress criterion is reduced to only Equations 6 and 8. Tension test results provided the average tension stress limits ($\sigma_1^{(+)}$), while biaxial test data provided the compression and shear stress limits ($\sigma_1^{(-)}$ and τ_{MAX}).

Failure envelopes for each wood-plastic formulation were drawn using the ultimate strength, maximum dissipated energy curvature and 5% PTL as failure limits. The envelopes are shown in Figure 28, Figure 29, and Figure 30. For reference, the ultimate strength test data and maximum dissipated energy curvature test data have been included in each figure.

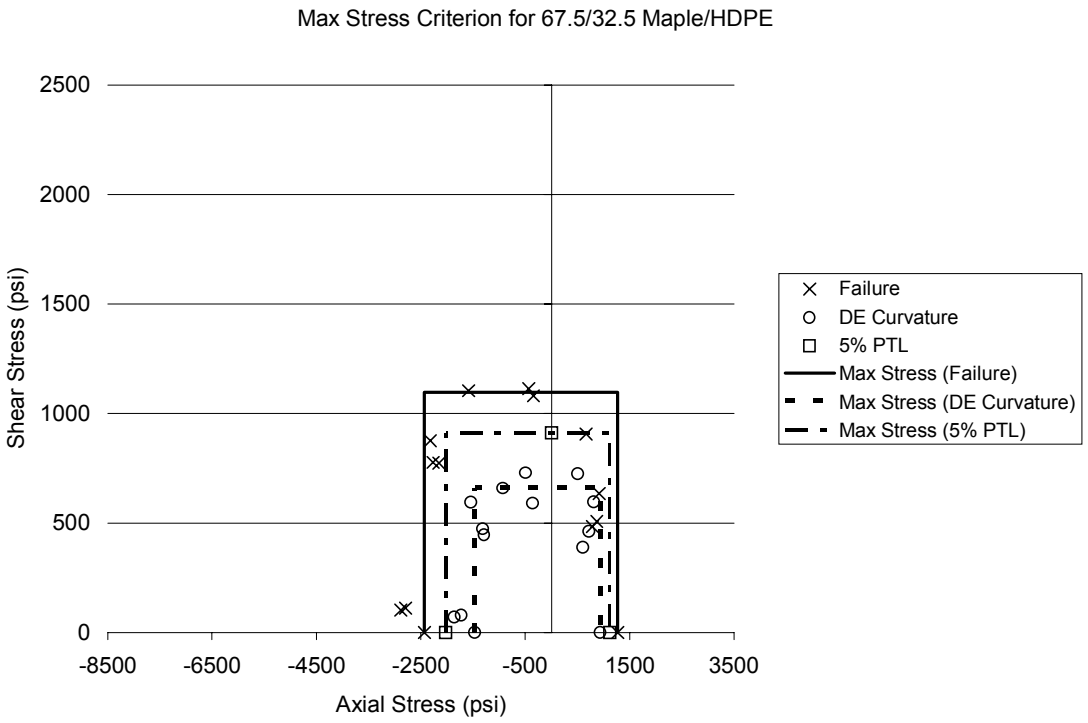

Figure 28: Max Stress Criterion for HDPE

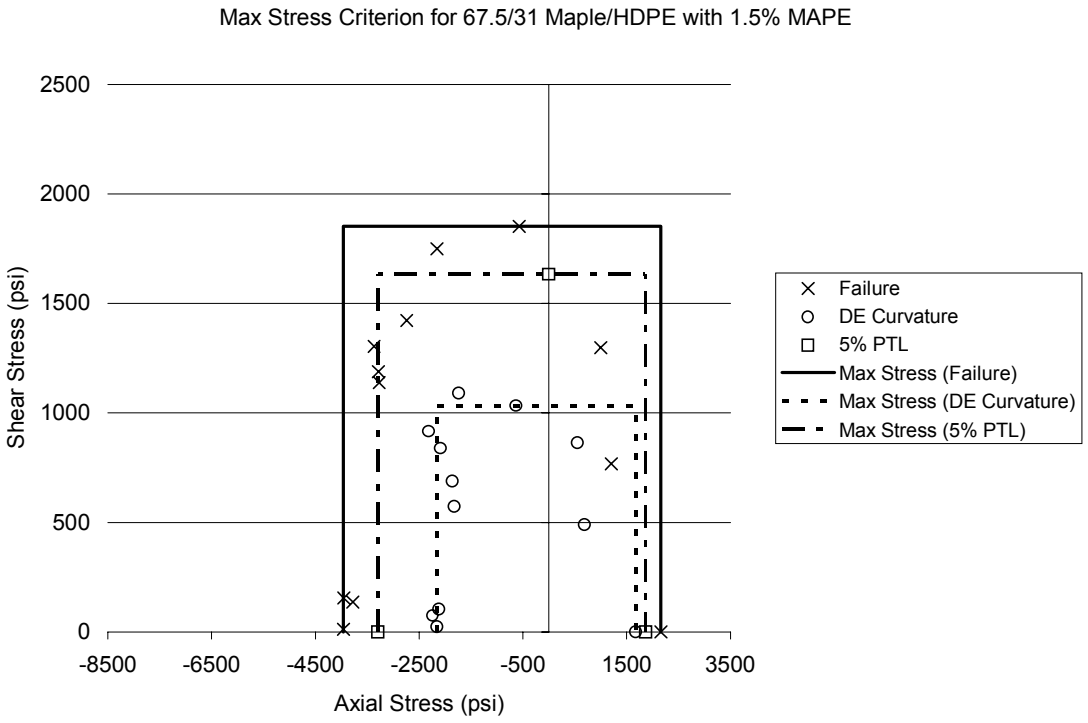

Figure 29: Max Stress Criterion for HDPE w/ MAPE

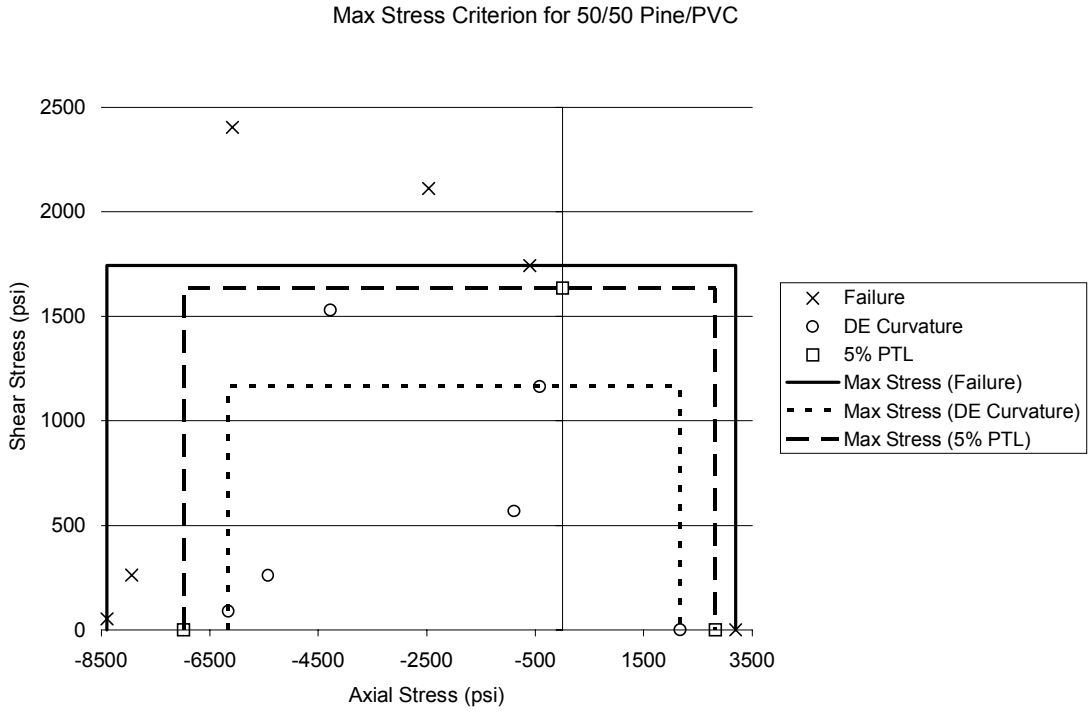

Figure 30: Max Stress Criterion for PVC

The maximum stress limits used for plotting figures 28, 29, and 30 are summarized in the Table 10.

Table 10: Stress Limits Used to Plot Maximum Stress Criterion

Material	Failure Definition	Tension Stress (psi)	Compression Stress (psi)	Shear Stress (psi)
HDPE	Ultimate Strength	1271	-2435	1097
	Max DE Curvature	936	-1465	659
	5% PTL	1119	-2025	913
HDPE w/ MAPE	Ultimate Strength	2156	-3963	1853
	Max DE Curvature	1675	-2156	1032
	5% PTL	1863	-3296	1633
PVC	Ultimate Strength	3196	-8398	1742
	Max DE Curvature	2170	-6154	1163
	5% PTL	2819	-6984	1636

For the 67.5/32.5 Maple/HDPE cylinders in pure compression, barreling of the cylinders (see Figure 46) produced ultimate compressive failures that were not consistent with previous compression test data collected at Washington State University [13]. Consequently, an ultimate compressive stress of –2435 psi was used for the HDPE material as shown in Table 10.

Due to the invalid results (failure at the grip locations for example) obtained in the pure torsion test, only one cylinder for each of the HDPE with MAPE and PVC formulations could be used to provide the ultimate shear strength. However, the shear strengths for HDPE with MAPE and PVC are in-line with previous results.

The dissipated energy curvature values for tension stress in Table 10 are the average of all the tension test data. The shear stress values were found using the values from biaxial specimens in pure torsion. The compression stress values were found using the average values from biaxial specimens in pure compression.

The 5% PTL values for maximum tensile stress shown in Table 10 were calculated directly from the tension test averages and standard deviation. The 5% PTL stresses in compression and shear were calculated using a conservative COV of 8% established in research by Lockyear [13] and Haiar [9]. The basis for the average ($\overline{X}$) and standard deviation ($\hat{s}$) terms used in Equation 5 to calculate 5% PTL tension, compression and shear stresses are shown in Table 11.

Table 11: Derivation of Terms Used to Calculate 5% PTL Stress

Term from Equation 5	HDPE	HDPE w/ MAPE	PVC
Tension $\overline{X}$	Tension Test Avg	Tension Test Avg	Tension Test Avg
Tension Standard Deviation, $\hat{s}$	Tension Test Standard Deviation	Tension Test Standard Deviation	Tension Test Standard Deviation
Comp. Average, $\overline{X}$	Lockyear's Research (-2435 psi)	Biaxial Specimens in Pure Compression	Biaxial Specimens in Pure Compression
Comp. Standard Deviation, $\hat{s}$	Prior Research (8% COV)	Prior Research (8% COV)	Prior Research (8% COV)
Shear Average, $\overline{X}$	Biaxial Specimens in Pure Torsion	Biaxial Specimens in Pure Torsion	Biaxial Specimens in Pure Torsion
Shear Standard Deviation, $\hat{s}$	Prior Research (8% COV)	V-Notch Test Standard Deviation	V-Notch Test Standard Deviation

Maximum Strain Criterion

Without any strain measured in the "2" direction, the maximum strain criterion is reduced to only Equations 9 and 11. Tension test results provided the average tension strain limits ($\varepsilon_1^{(+)}$), while biaxial test data provided the compression and shear strain limits ($\varepsilon_1^{(-)}$ and γ_{MAX}).

Failure envelopes for each wood-plastic formulation are shown in Figure 31, Figure 32, and Figure 33. Each figure shows three failure envelopes representing the ultimate strength, maximum dissipated energy curvature and 5% PTL as failure.

The maximum strain limits used for plotting figures 31, 32, and 33 are summarized in the Table 12.

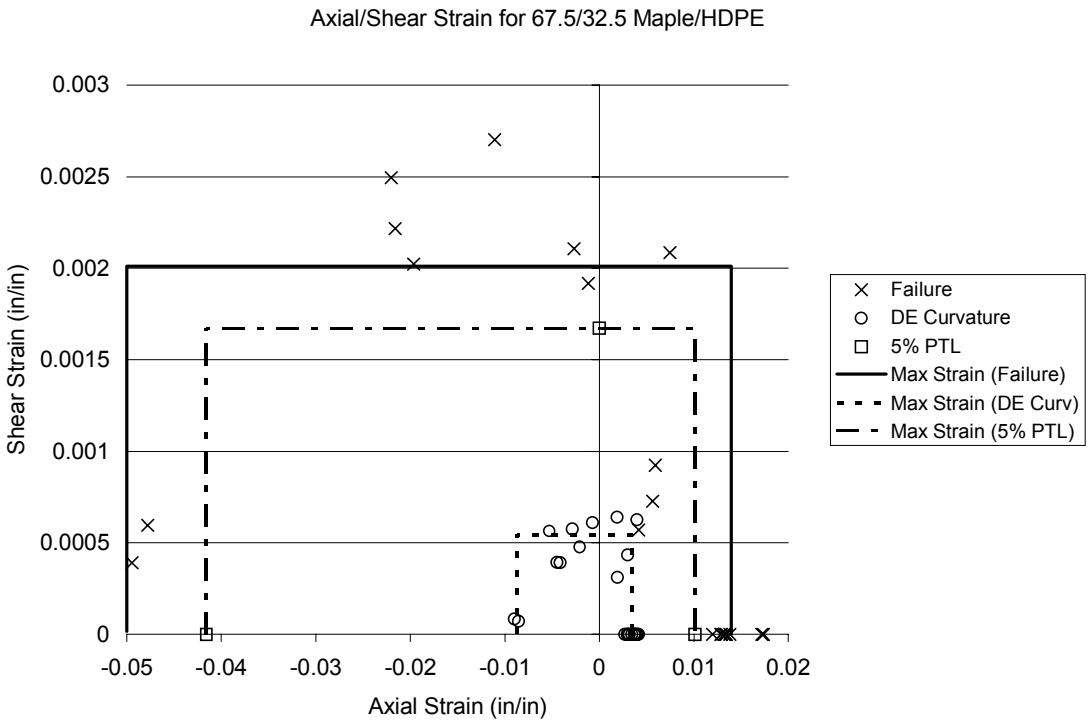

Figure 31: Max Strain Criterion for HDPE

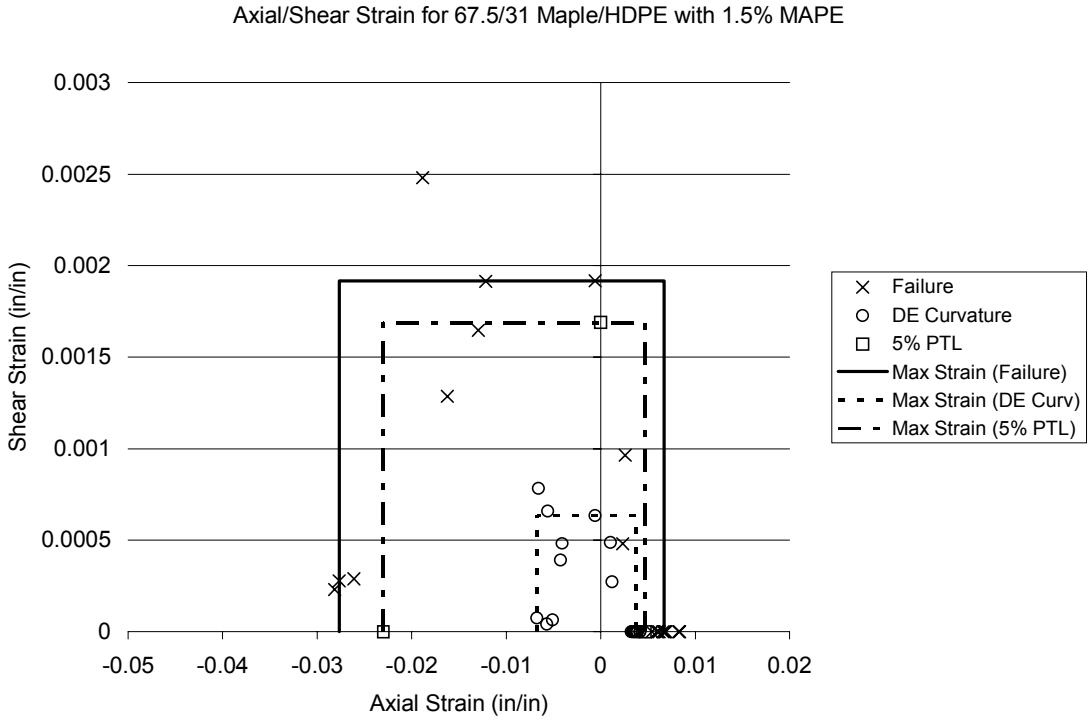

Figure 32: Max Strain Criterion for HDPE w/ MAPE

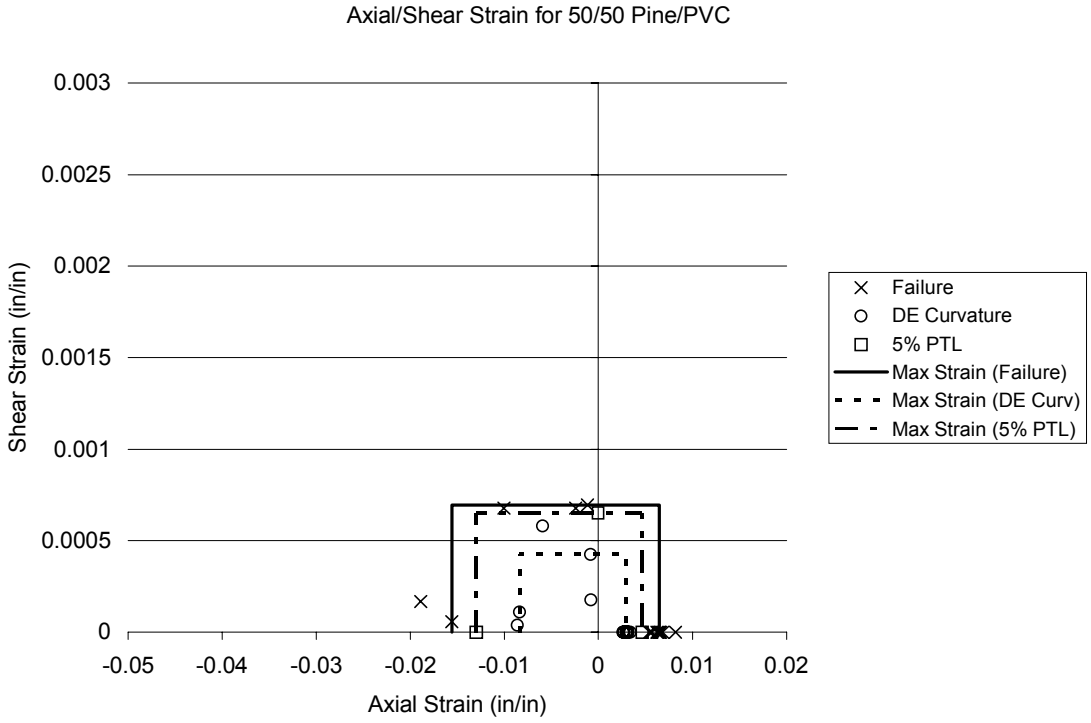

Figure 33: Max Strain Criterion for PVC

Table 12: Strain Limits Used to Plot Maximum Strain Criterion

Material	Failure Definition	Tension Strain (in/in)	Compression Strain (in/in)	Shear Strain (in/in)
HDPE	Ultimate Strength	0.014	-0.050	0.0020
	Max DE Curvature	0.003	-0.009	0.0005
	5% PTL	0.010	0.042	0.0016
HDPE w/ MAPE	Ultimate Strength	0.007	-0.028	0.0019
	Max DE Curvature	0.004	-0.007	0.0006
	5% PTL	0.005	-0.023	0.0017
PVC	Ultimate Strength	0.006	-0.016	0.0007
	Max DE Curvature	0.003	-0.008	0.0004
	5% PTL	0.005	-0.013	0.0006

For the 67.5/32.5 Maple/HDPE cylinders in pure compression, barreling of the cylinders produced ultimate compressive strains that were not consistent with previous compression test data collected at Washington State University [13] (see Figure 46). Consequently, an ultimate compressive strain of -0.05 in/in was used for the HDPE material as shown in Table 12.

Due to the invalid results (failure at the grip locations for example) obtained in the pure torsion test, only one cylinder for each of the HDPE with MAPE and PVC formulations could be used to provide the ultimate shear strain. However, the shear strains for HDPE with MAPE and PVC are in-line with previous results.

The dissipated energy curvature values for tension strain in Table 12 are the average of all the tension test data. The shear strain values were found using the values from biaxial specimens in pure torsion. The compression strain values were found using the average values from biaxial specimens in pure compression.

The 5% PTL values for maximum tensile strain shown in Table 12 were calculated directly from the tension test averages and standard deviation. The 5% PTL compression and shear strains were calculated using a representative COV of 8%

established in research by Lockyear [13] and Haiar [9]. The basis for the average ($\overline{X}$) and standard deviation ($\hat{s}$) terms used in Equation 5 to calculate 5% PTL tension, compression and shear strains are shown in Table 13.

Table 13: Derivation of Terms Used to Calculate 5% PTL Strain

Term from Equation 5	HDPE	HDPE w/ MAPE	PVC
Tension $\overline{X}$	Tension Test Avg	Tension Test Avg	Tension Test Avg
Tension Standard Deviation, $\hat{s}$	Tension Test Standard Deviation	Tension Test Standard Deviation	Tension Test Standard Deviation
Comp. Average, $\overline{X}$	Lockyear's Research (-0.05 in/in)	Biaxial Specimens in Pure Compression	Biaxial Specimens in Pure Compression
Comp. Standard Deviation, $\hat{s}$	Prior Research (8% COV)	Prior Research (8% COV)	Prior Research (8% COV)
Shear Average, $\overline{X}$	Biaxial Specimens in Pure Torsion	Biaxial Specimens in Pure Torsion	Biaxial Specimens in Pure Torsion
Shear Standard Deviation, $\hat{s}$	Prior Research (8% COV)	V-Notch Test Standard Deviation	V-Notch Test Standard Deviation

Maximum Shear Stress Criterion

The yield strengths used to define the maximum shear stress limits (used for plotting figures 34, 35, and 36) are summarized in the Table 15. For reference, the ultimate strength values can be seen in Table 16.

Table 14: Yield Stress Limits Used to Plot Maximum Shear Stress Criterion

Material	Failure Definition	Yield Stress (psi)
HDPE	Ultimate Strength	1290
	Max DE Curvature	859
	5% PTL	957
HDPE w/ MAPE	Ultimate Strength	2009
	Max DE Curvature	1254
	5% PTL	1810
PVC	Ultimate Strength	3254
	Max DE Curvature	2067
	5% PTL	592

The ultimate strengths and maximum DE curvature stresses in Table 14 are the average maximum shear stresses for all combined compression and torsion specimens. The 5% PTL stresses were calculated using the average strength and COV of the compression/torsion test data directly.

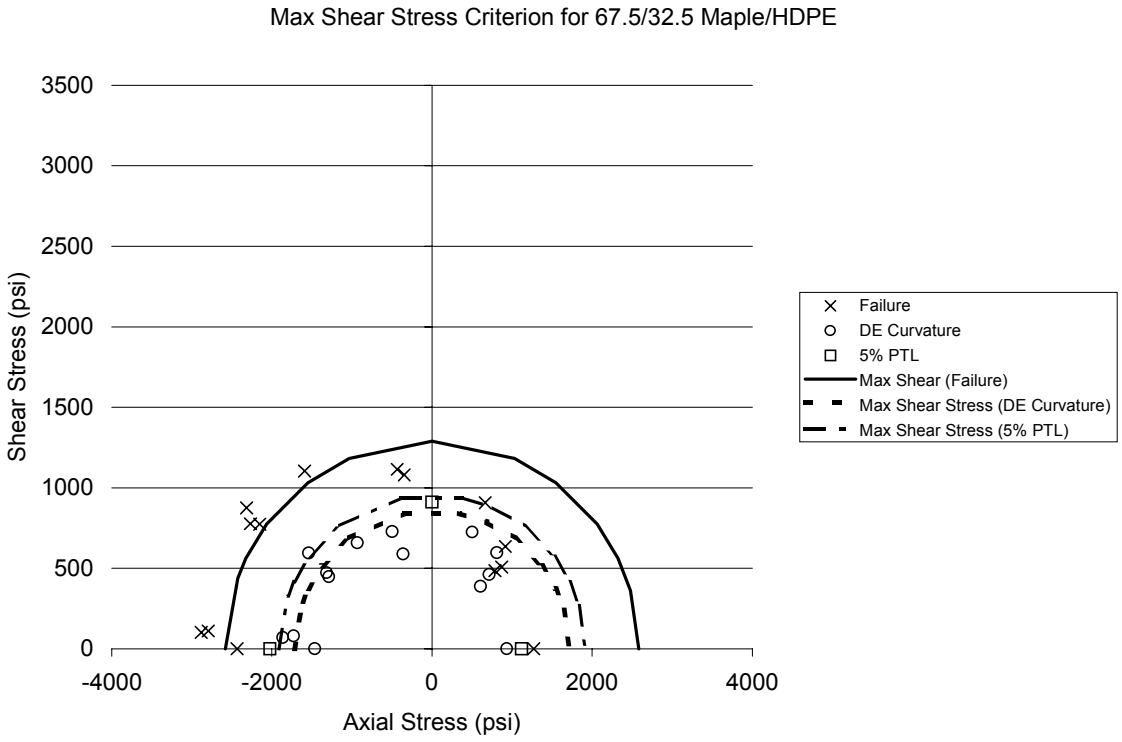

Figure 34: Max Shear Stress Criterion for HDPE

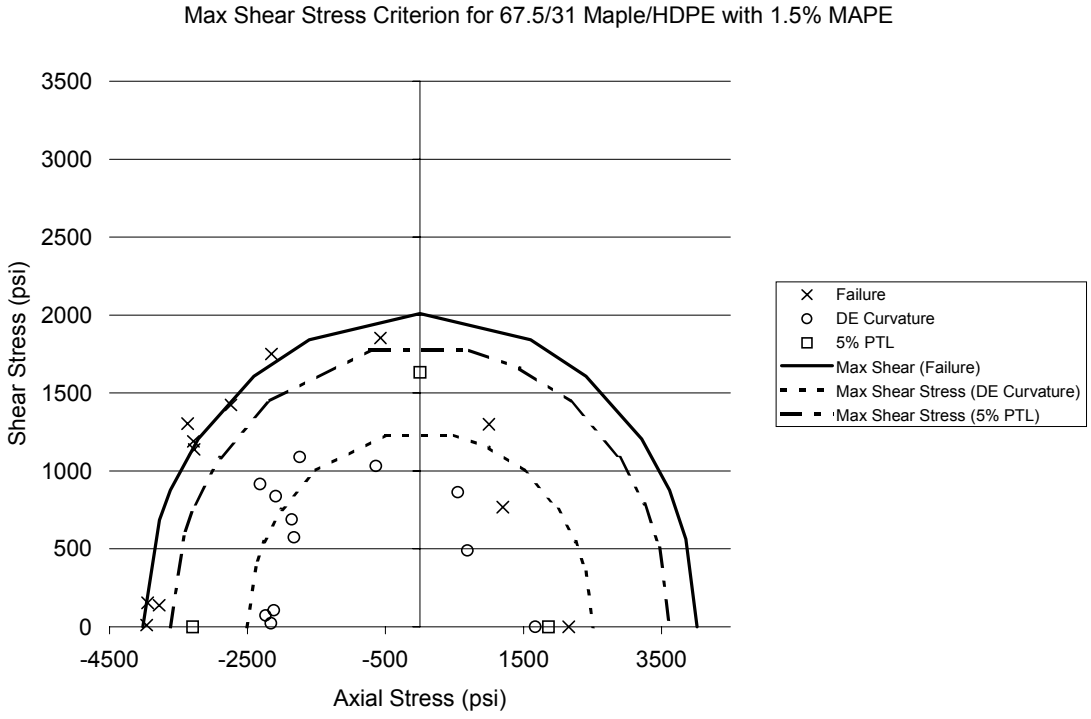

Figure 35: Max Shear Stress Criterion for HDPE w/ MAPE

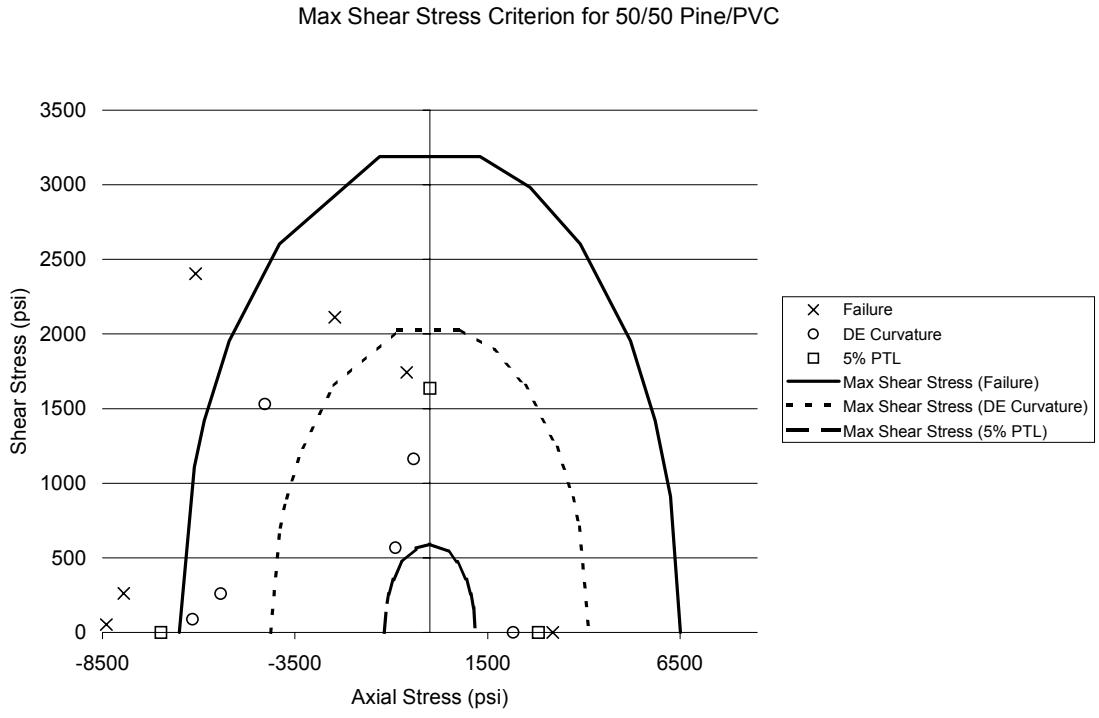

Figure 36: Max Shear Stress Criterion for PVC

Tsai-Wu Criterion

Without any measured stress in the "2" material direction, the plane-stress Tsai-Wu failure criterion reduces to Equation 41.

$$F_1\sigma_1 + F_{11}\sigma_1^2 + F_{66}\tau_{12}^2 = 1 \qquad \text{[Equation 41]}$$

Figures 37, 38 and 39 show the Tsai-Wu criterion for each wood-plastic formulation. Each figure has three Tsai-Wu failure envelopes based on three definitions of failure, 1) ultimate strength, 2) maximum dissipated energy curvature, and 3) the 5% parametric tolerance limit. The figures also show the stresses at failure from the tension and biaxial test specimens.

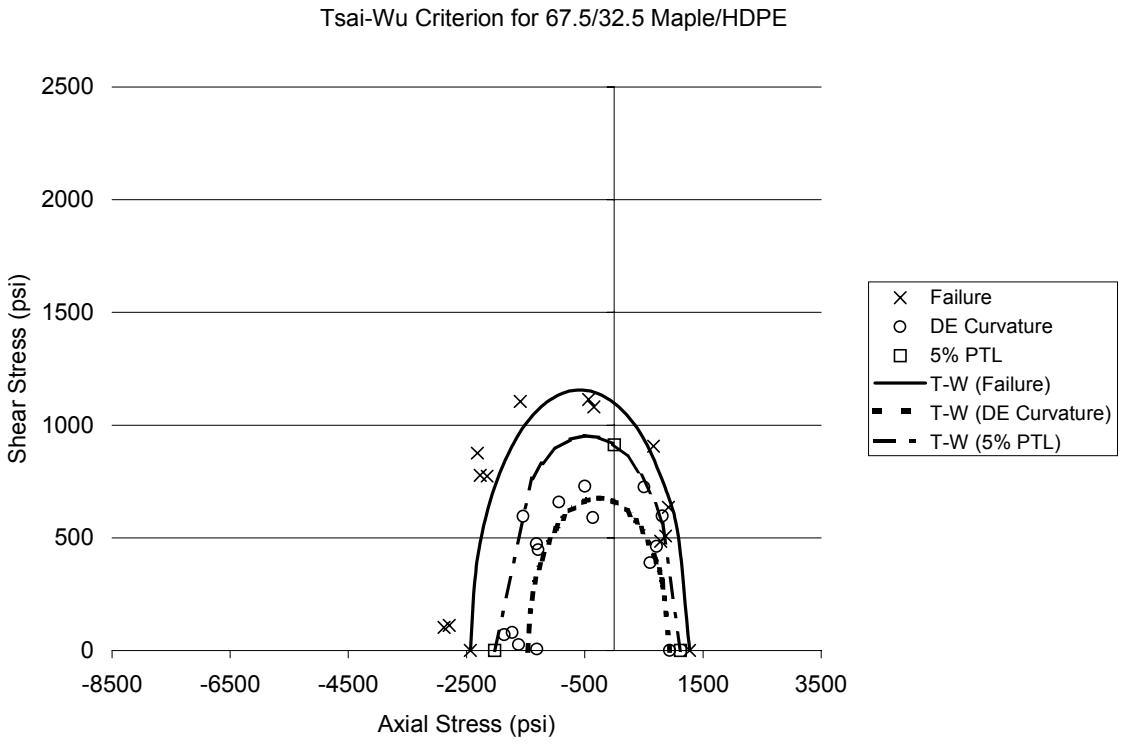

Figure 37: Tsai-Wu criterion for HDPE

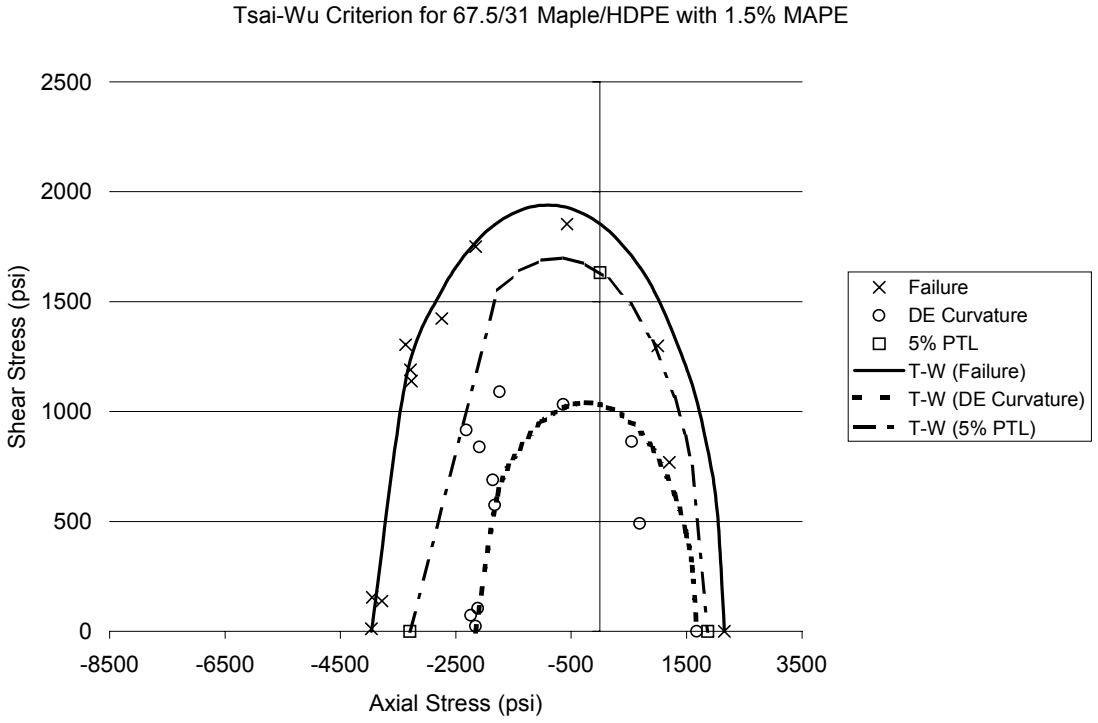

Figure 38: Tsai-Wu criterion for HDPE w/ MAPE

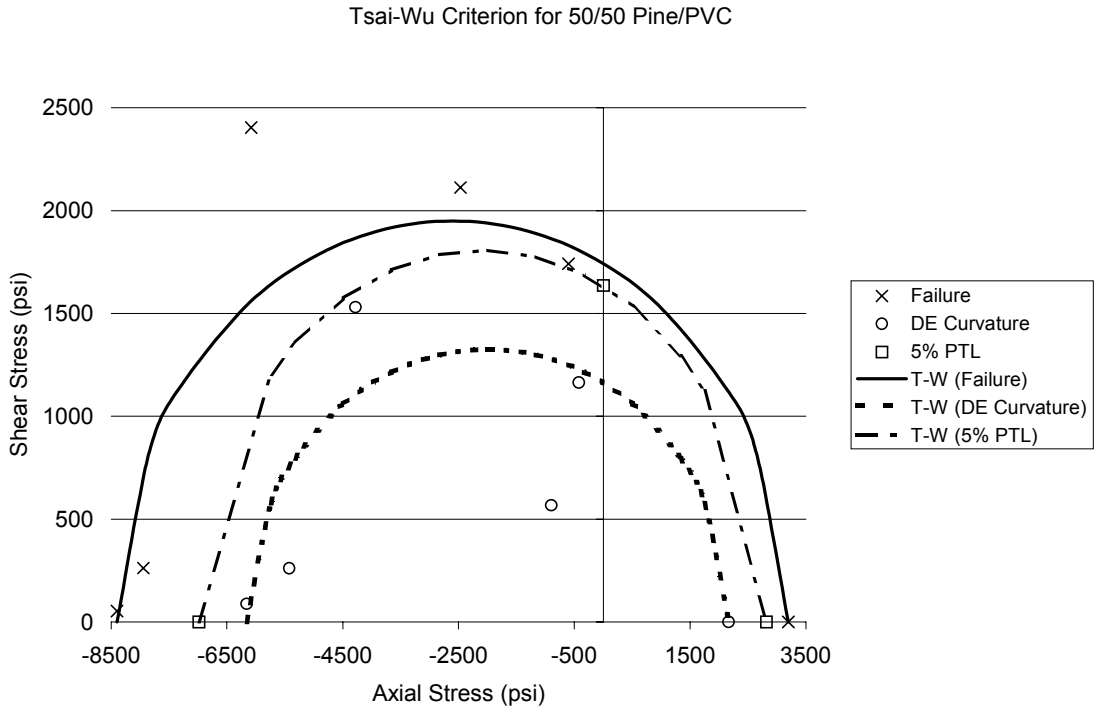

Figure 39: Tsai-Wu criterion for PVC

The values shown in Table 15 were used to develop constants in the Tsai-Wu failure criterion using Equations 20, 21 and 22.

Table 15: Stresses Used to Calculate Tsai-Wu Constants

Material	Failure Definition	Tension Stress (psi)	Compression Stress (psi)	Shear Stress (psi)
HDPE	Ultimate Strength	1271	-2435*	1097
	Max DE Curvature	936	-1465	659
	5% PTL	1119	-2171	913
HDPE w/ MAPE	Ultimate Strength	2156	-3963	1853
	Max DE Curvature	1676	-2156	1032
	5% PTL	1863	-3296	1633
PVC	Ultimate Strength	3196	-8398	1742
	Max DE Curvature	2170	-6154	1163
	5% PTL	2819	-6894	1636

* HDPE Compression stress at failure based on research by Lockyear [13].

Similar to the maximum strain criterion, the tension stress values in Table 15 were calculated directly from tension test results. The compression and shear stresses (ultimate and maximum DE curvature) were derived from biaxial test data. The 5% PTL strengths were calculated using average ($\overline{X}$) and standard deviation ($\hat{s}$) terms explained in Table 13.

Yeh-Stratton Criterion

Without any measured stress in the "2" material direction, the Yeh-Stratton failure criterion reduces to two governing equations.

$$A_1\sigma_1 + C_{12}\tau_{12}^2 = 1 \qquad \text{[Equation 42]}$$

$$A'_1\sigma_1 + C_{12}\tau_{12}^2 = 1 \qquad \text{[Equation 43]}$$

Plots of the Yeh-Stratton criterion for the HDPE, HDPE with MAPE and PVC materials are shown in Figure 40, Figure 41, and Figure 42 respectively. Each figure shows three failure envelopes based on 1) the ultimate strength, 2) the maximum dissipated energy curvature, and 3) the 5% parametric tolerance limit along with the failure test data. The stresses used to formulate the Y-S constants (A_1, A'_1, and C_{12}) were the same stresses used in creation of the Tsai-Wu failure envelopes and are shown in Table 15.

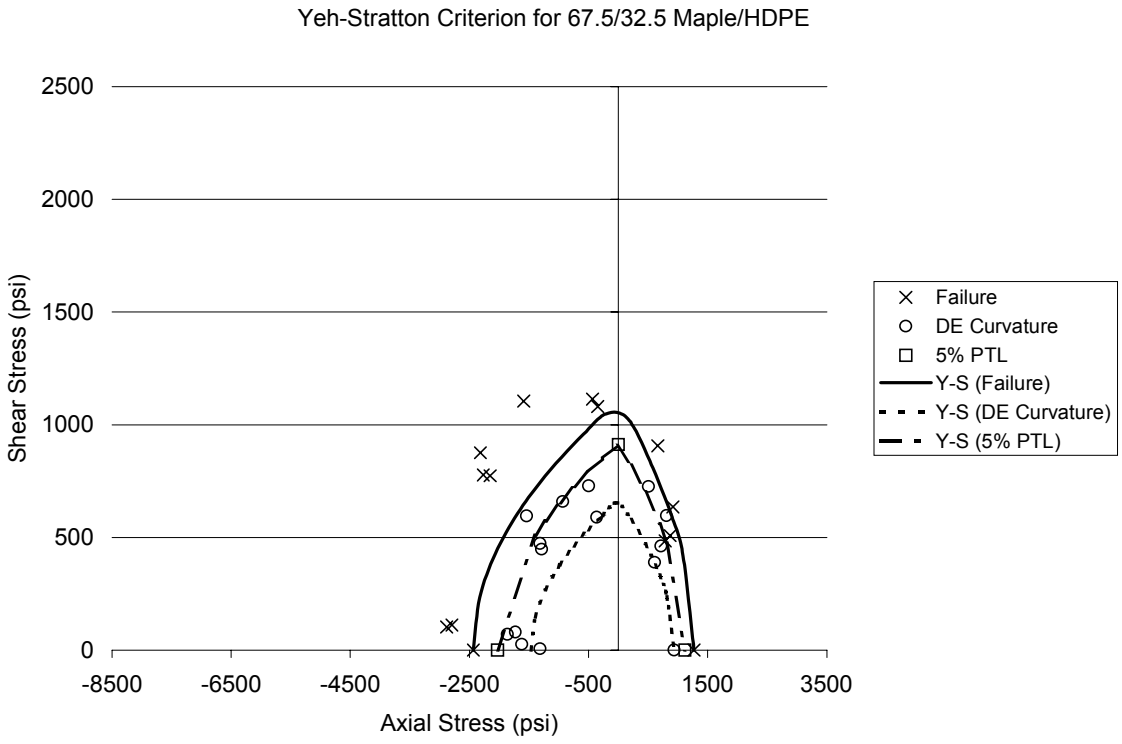

Figure 40: Yeh-Stratton Criterion for HDPE

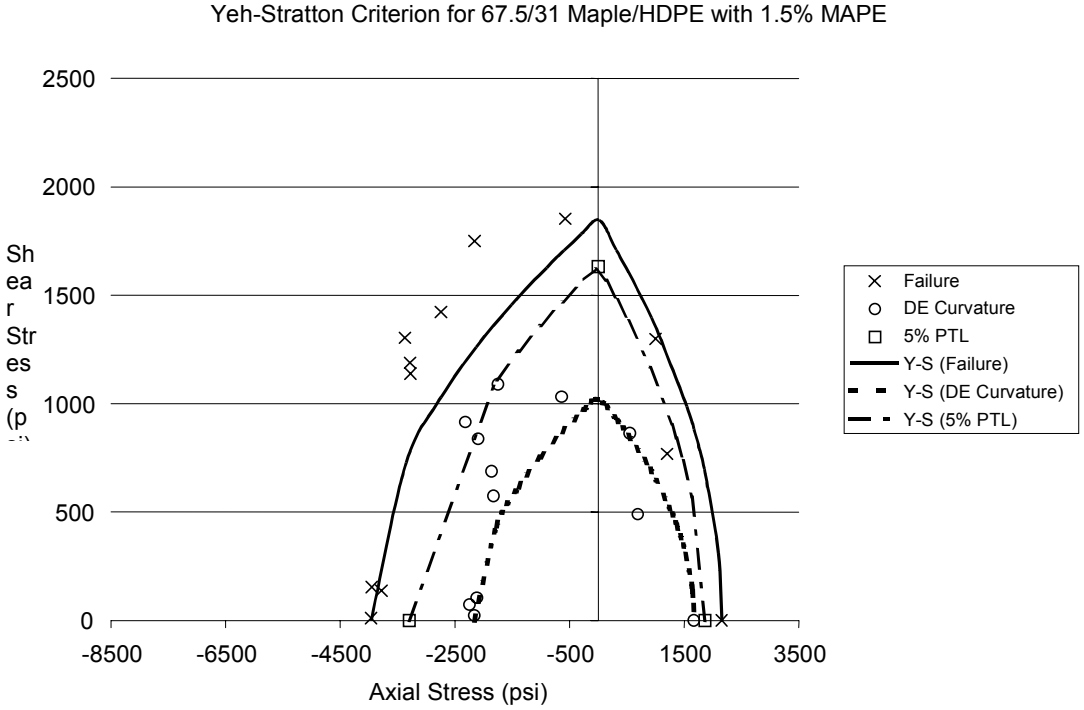

Figure 41: Yeh-Stratton Criterion for HDPE w/ MAPE

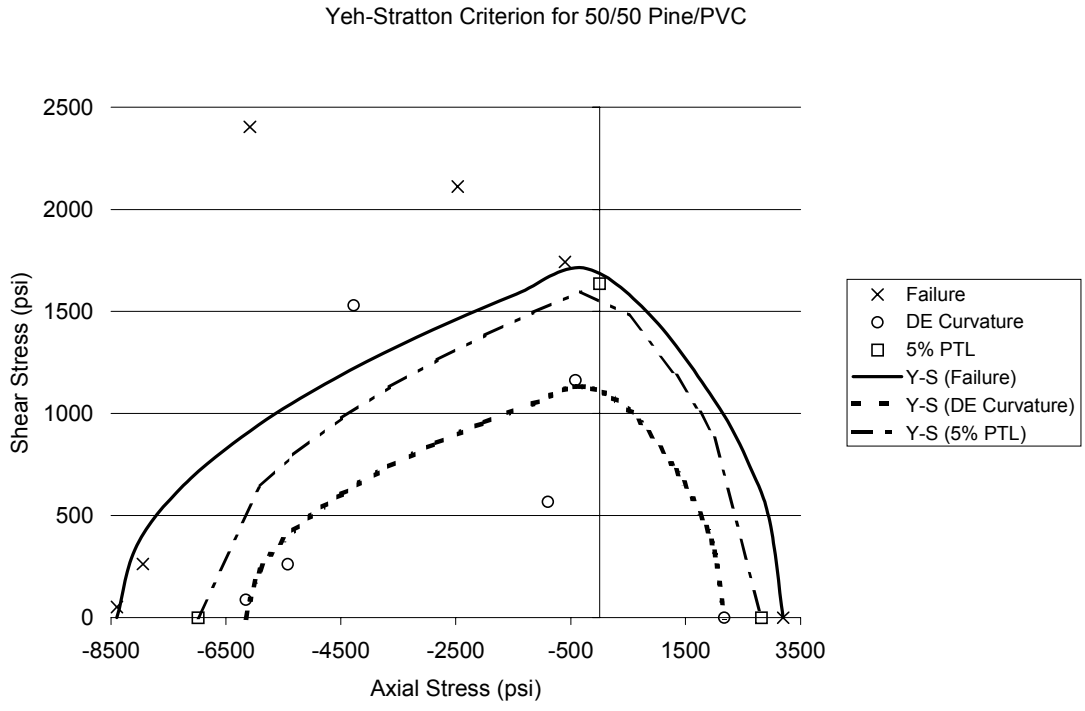

Figure 42: Yeh-Stratton Criterion for PVC

CHAPTER FIVE: DISCUSSION

Test Discussion

Tension Test Discussion

A comparison of the ultimate strengths in Table 7 was done for each material. The PVC formulation had the highest average ultimate tensile stress. The HDPE with MAPE formulation had the second highest average ultimate stress and the HDPE had the lowest average ultimate stress. The HDPE with MAPE was expected to have a higher ultimate strength than HDPE because the MAPE additive is a coupling agent used to increase the bond at the interface of the wood fibers and the polyethylene. If the wood-to-plastic bond were better, a higher strength would be expected.

The 5% PTL stresses and strains are greater than the maximum curvature stresses and strains for all three wood-plastic formulations. While the 5% PTL provides statistical confidence that the material will not fail, it does not give any indication at what rate the material is reaching failure, or how much damage has accumulated in the material up to that load. Consequently, designing a wood-plastic member for the 5% PTL tensile strength could mean that if the member reaches the 5% PTL load, it could be very close to accumulating all of the damage the member can withstand. Note the location of the 5% PTL strength in Figure 43.

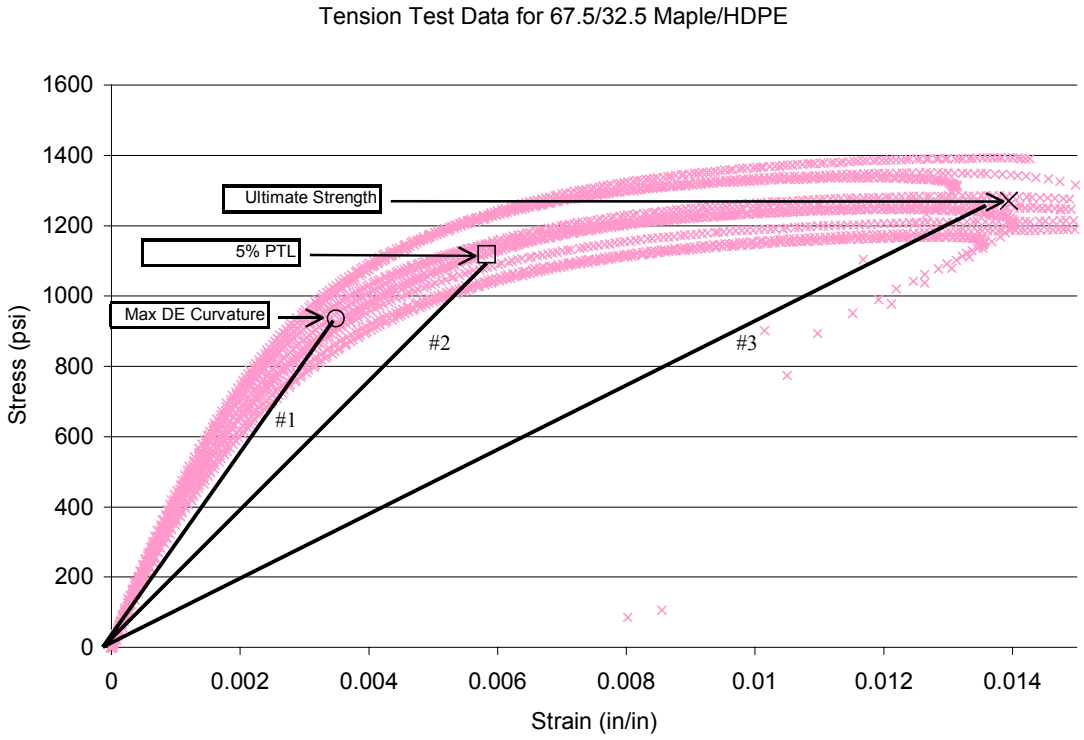

Figure 43: Comparison of 5% PTL and Max DE Curvature Tension Test Results

In Figure 43, line #1 connects the maximum dissipated energy curvature strength to the point of zero stress and lines #2 and #3 connect the 5% PTL and ultimate strengths to the point of zero stress. Because the main mode of damage accumulation in WPC is micro cracking, the slope of line #1 represents the secant stiffness of the test coupon after the maximum DE curvature strength has been reached. Line #1 follows the test data and the change in initial stiffness is kept to a minimum. Compared to line #1, line #2 (whose slope represents the secant stiffness after the 5% PTL strength has been reached) represents a significant decrease in stiffness. It appears that the maximum DE curvature stress also represents a change in material behavior. Designers use the yield strength as the limiting design strength for metals because the yield point indicates a distinct change

in the behavior of the metal. It appears that the maximum curvature strength indicates a similar change in behavior for wood-plastic composites.

The method of using every fifth data point to find maximum curvature in the dissipated energy function was used in order to capture the trend of the raw test data. It may not have been the most efficient way to provide a smooth dissipated energy function. Another approach to calculating the dissipated energy density during a tension test would be to first create a stress function (stress as a function of strain) for each tension specimen. The stress function could be a "best-fit" polynomial or trigonometric function that could be easily used in Equation 3 to provide a best-fit dissipated energy function completely based on strain. Then by taking the second derivative of this best fit dissipated energy function, a maximum curvature could be found.

V-Notch Test Discussion

Haiar [9] performed 5-point shear tests on open-box WPC beams. The average ultimate stress from his thesis was 1133 psi for HDPE and 2931 psi for PVC. The COV for failure stresses for the HDPE and PVC used in his research were 1% and 9% respectively. The average ultimate shear stress from the V-notch tests on HDPE with MAPE was 2138 psi and PVC was 3525 psi. The HDPE with MAPE and PVC ultimate stresses had COV's of 6% and 5% respectively. The ultimate shear stresses in the V-notch tests for PVC are higher than those found by Haiar.

Lockyear noted 45-degree failures in his wood-plastic composite specimens subjected to pure torsion. The same type of 45-degree failures were seen in this research

in all of the v-notch specimens (see Figure 44). Some failure criteria (like Tsai-Wu and Yeh-Stratton) define their terms using the strength at which a failure occurs under a pure shear loading. However, the failures observed in these v-notch tests are not shear failures.

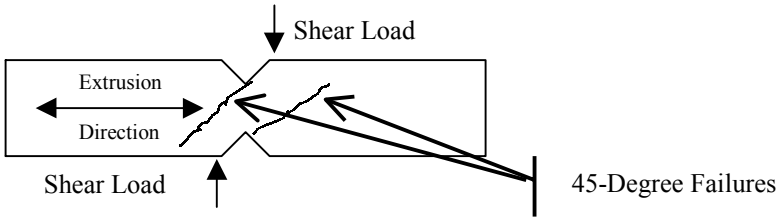

Figure 44: Typical V-notch Specimen Failures

It is hypothesized that dissipated energy density functions derived from shear stress-strain plots should be able to predict the total dissipated energy in the v-notch specimens. Application of strain gages to future v-notch test specimens would provide the shear stress-strain plots. The shear stress-strain plots could be used to calculate a shear dissipated energy density function for calculation of total shear energy dissipated. Although the toe compensation procedure used in this research was derived following ASTM D638, the shear stress-strain data would help to prove the validity of using the toe compensation procedure to calculate total dissipated energy in the v-notch test specimens.

Biaxial Test Discussion

The outside diameter (OD) tolerance used (±0.050 inches) to prepare biaxial test specimens proved to be a problem during these tests. The outside diameter of the test cylinders should have been closer to 1.75±0.01 inches. Test specimens that were 1.78

inches OD were too large to fit into the hydraulic grips. Three specimens with the larger diameter (1.78 inches) were crushed by the hydraulic grips before the any test loads were applied. Figure 45 shows one of the PVC specimens, with the larger outside diameter, in which failure occurred while gripping the specimen. Test specimens that were 1.73 inches OD were too small for the hydraulic grips to hold. The lower limit on outside diameter was not accounted for during specimen preparation and two specimens were too small to be tested.

Figure 45: Failure of a PVC Biaxial Test Specimen Due to Grip Pressure

Examination of specimens after testing showed several specimens in which failures propagated from the grip locations. The reason that failures propagated from the grip locations may be due to tiny cracks that formed when gripping pressure alone was applied. These small cracks appear to have acted as stress risers. Biaxial test data from these grip-failure specimens was removed from research.

Compression loading of the HDPE produced failures in which the cylinder "barreled" outward. Figure 46 shows an HDPE cylinder (top) and a MAPE cylinder (bottom) in pure compression. The barreling occurred under the tip of the biaxial extensometer and caused the compression strain measurements to be artificially small. The ultimate compression strains measured in the HDPE cylinders was less than 80% of the ultimate compression strains noted in previous compression tests performed on HDPE box-shaped members (see Lockyear [13]).

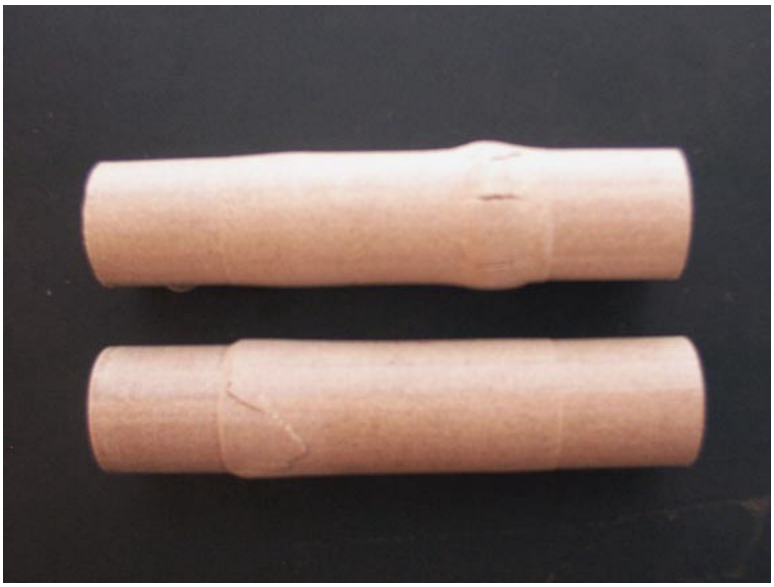

Figure 46: HDPE (top) and HDPE w/ MAPE (bottom) Biaxial Specimen Compression Failures

Lockyear [13] performed static torsion tests on HDPE with 8% talc and PVC wood-plastic composites as part of his research. Figure 47 shows some of Lockyear's torsion test specimens in which failure occurred at 45-degree angles to the loading. Using Mohr's circle for stress transformation, it can be shown that a 45-degree failure under pure shear loading is an indication that the specimen failed in tension rather than

shear. Results of the current research show the same 45-degree failures in the PVC specimens subjected to pure torsion (middle specimen in Figure 48).

Figure 47: Torsion Test Failures of HDPE Specimens (from Lockyear)

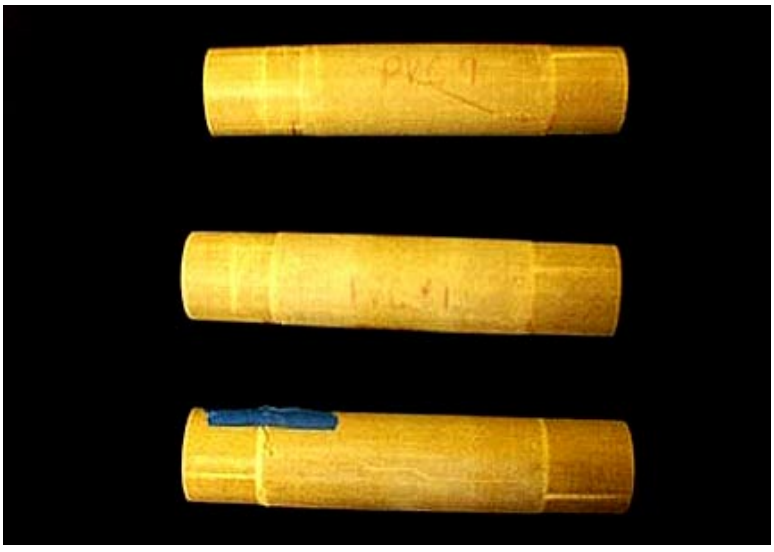

Figure 48: Combined Compression and Shear Failures in PVC Biaxial Test Specimens

Using Mohr's circle transformation, a combined compression and shear loading was expected to shift the angle of failure from 45-degrees to something smaller (with respect to the axis of the cylinder). Figure 48 shows two compression/torsion specimens (top and bottom) and a pure torsion specimen (middle). Note that the angle of the failure plane is smaller in the top and bottom specimens.

A shift in the failure plane was expected to occur in specimens subjected to combined tension and shear. The angle was expected to get larger with respect to the axis of the cylinder. HDPE and HDPE with MAPE specimens (that did not fail in the grips) did have a failure plane at approximately 60° to the axis. The failure angle of the tension/torsion PVC specimens was not recorded because all the specimens failed in the grip locations.

The 45-degree angle of failure under pure torsion loading was not seen in any of the HDPE or HDPE with MAPE specimens. Longitudinal splitting perpendicular to the extrusion direction was the failure mode observed in all of the pure torsion and combined compression and torsion HDPE and HDPE w/ MAPE specimens. Two combined compression and torsion specimens are shown in Figure 49. The specimen on top is HDPE and the bottom specimen is HDPE with MAPE.

Figure 49: Longitudinal Splitting Along the Strand Line of Combined Compression and Torsion HDPE (top) and HDPE w/ MAPE (bottom) Specimens

The longitudinal splits shown in combined compression and torsion specimens seemed to indicate a shear failure. Using Equations 44 and 45, the maximum shear stress and the maximum shear angle were calculated respectively.

$$\tau_1, \tau_2 = \pm \frac{1}{2} \sqrt{(\sigma_x - \sigma_y)^2 + (2\tau_{xy})^2} \qquad \text{[Equation 44]}$$

$$\theta_{\tau 1, \tau 2} = \tfrac{1}{2} \arctan\left(\frac{\sigma_x - \sigma_y}{-2\tau_{xy}}\right) \qquad \text{[Equation 45]}$$

A summary of the maximum shear stresses and angles for each cylinder that failed by longitudinal splitting is shown in Table 16. Again, the MAPE additive increased the ultimate stress of the HDPE wood-plastic formulation. Notice that the coefficient of variation in the maximum shear stresses at failure occurred is similar to results from other testing [9, 13]. Since the PVC specimens had no indication of any

longitudinal splitting failures, they are included in Table 16 in order to provide data for calculation of the yield stress used in the max shear stress criterion.

Table 16: Maximum Shear Stresses at Failure of HDPE and HDPE w/ MAPE Biaxial Test Specimens

Material	Specimen	Maximum Shear Angle (degrees)	Maximum Shear Stress (psi)
HDPE	675-1	5.53	1134.8
	675-2	4.55	1094.6
	675-9	27.14	1325.1
	675-12	27.79	1374.5
	675-13	26.45	1452.0
	675-16	17.87	1361.0
	AVERAGE		1290.3
	COV (%)		11.1%
HDPE w/ MAPE	M2	4.39	1874.8
	M9	27.58	1993.1
	M10	27.04	2027.3
	M11	21.96	1975.2
	M12	26.13	2129.2
	M15	15.81	2054.2
	AVERAGE		2009.0
	COV (%)		4.2%
PVC*	PVC1	4.89	1768.1
	PVC4	44.64	4199.2
	PVC5	43.11	3981.0
	PVC7	25.84	3876.2
	PVC9	15.14	2446.1
	AVERAGE		3254.1
	COV (%)		33.2%

*PVC specimens did not exhibit shear failures. Data is shown for calculation of max shear yield stress.

Longitudinal splitting is of particular interest when one considers how the wood-plastic composites are formed. When the wood-plastic composites are extruded, they go through a stranding die. The stranding die forms the molten plastic and wood into strands, which are then shaped into a specific cross-section while cooling. The longitudinal splits are in the location where the strands bond together to form the final

cross-sectional shape. The shear stresses that are shown in Table 16 are indicative of the strength of the bond lines.

The HDPE and HDPE w/ MAPE materials were expected to fail at 45-degrees to the axis of the cylinder, but this did not happen in this research. One possible reason for this is an unexpected axial compressive load applied during gripping of the specimens. The grips are similar to the self-tightening grips used in tension tests (see ASTM D638). Hydraulic pressure brings a ring down around the grips forcing them inward around the specimen and applying compressive loads to the specimens. Because the load gauge and extensometer were set to zero after closing the first grip, any load due to closing the second hydraulic grip was measured. Compressive pre-load due to gripping alone sometimes exceeded 500 lbs, depending on the outside diameter of the specimens. The addition of axial compressive loads kept the tensile stresses in the 45-degree plane below the maximum shear strength.

The longitudinal shear failures observed in the HDPE and HDPE with MAPE specimens were not noted in any previous research. The longitudinal splitting stresses shown in Table 16 indicate that the maximum shear stress at failure is independent of the amount of compression stress applied. Since there is little or no interaction between normal and shear stresses in HDPE and HDPE with MAPE, a maximum shear stress failure criterion was investigated (see page 57). The maximum shear stress failure criterion was found to predict the observed failures under combined compression and torsion, but not under combined tension and torsion.

The biaxial test methods used in this research involved hours of specimen preparation time and much frustration. While the biaxial tests resulted in new

information about modes of shear failure, the amount of useful test data was small compared to the other useless data received. Inappropriate failure modes and unexpected difficulties in procedure suggest that a better method of biaxial testing should be used in future WPC research. The in-plane loader used by Mast et al [15] to provide test data for creation of dissipated energy functions should provide biaxial data that is more useful.

3-Point Bending Test Discussion

Haiar [9] conducted flat-wise bending tests on HDPE and PVC wood-plastic composite materials with open-box cross-sections. The material formulations were very similar to the HDPE and PVC formulations used in this research. Haiar's research presents coefficients of variation in maximum load of 3% for HDPE and 6% for PVC. The maximum load COV's shown in Table 9 compare well to Haiar's results at 5% for HDPE and 9% for PVC.

The 5% PTL strengths and the maximum dissipated energy curvature strengths are shown Table 9. This Table contains results similar to the tension test results; i.e. the 5% PTL strengths are higher than the maximum curvature strengths. The raw load-displacement data in Appendix D shows the load at maximum dissipated energy curvature resemble a yield load in 3-point bending of metal beams. Bending test results are further discussed in the analytical results section of this paper (page 78).

Analytical Results Discussion

Dissipated Energy Function

Biaxial and tension test results were used to create dissipated energy density functions for HDPE, HDPE with MAPE and PVC wood-plastic composites. The shape of the dissipated energy contour plots show that each combination of normal and shear strain has a different rate of damage accumulation.

The dissipated energy data was examined to see whether there was a simple relationship between the ultimate state of strain and the maximum curvature of the dissipated energy function. Constant and linear relationships were examined, but neither could be statistically determined to represent the relationship of strain vector angle and magnitude of strain at maximum DE curvature. The implication is that the maximum curvature in the dissipated energy function is not related to the combination of normal and shear loading applied to a specimen in a constant or linear way.

The shape of the dissipated energy contour maps shows that each of the three wood-plastic formulations do not dissipate very much energy before they fail under shear loads. The 45-degree failure modes observed in the torsion tests may show why this happened. Under torsion loading, damage was not only accumulating in shear, but also in off-axis tension, producing the 45-degree failures previously noted.

Future research into dissipated energy functions could investigate an automated methodology to calculate dissipated energy. Dissipated energy calculations can be programmed into a finite element code for uniaxial tension, compression and shear based on the hyperbolic tangent model presented by Murphy [18]. A comparison between the

current test results and the uniaxial dissipated energy functions in combined tension and shear, or compression and shear could provide more information about the behavior of wood-plastic composites under combined loading.

Dissipated Energy during 3-Point Bending Tests

Table 17 shows the values used to create Figure 25, Figure 26, and Figure 27. The table shows the dissipated energy of the 3-point bending specimens that correspond to the six displacements chosen in the methodology section of this paper.

Notice in Table 17 that the percent difference between dissipated energy predictions and test data at small displacements (i.e. ε_t curvature) is higher than the percent difference at other displacements. Although the percent difference is high, the absolute magnitude of the difference is not significantly higher than the other displacements.

Table 17: Predicted vs. Actual Dissipated Energy of WPC Coupons in 3-Point Bending

Material	Comments	Disp. (in)	Predicted DE (in-lbs)	Test DE (in-lbs)	% Diff
HDPE	no load	0	0	0	0.0%
	ε_t curvature	0.0415	0.0037	0.0015	59.0%
	Max ε_t	0.0797	0.0450	0.0476	5.9%
	Bending DE Curvature	0.0852	0.0586	0.0665	13.6%
	5% PTL Bending	0.1246	0.2323	0.2162	6.9%
	Ultimate Strength	0.1875	0.5897	0.6245	5.9%
MAPE	no load	0	0	0	0.0%
	ε_t curvature	0.0441	0.0074	0.0059	20.0%
	Max ε_t	0.0668	0.0264	0.0260	1.5%
	Bending DE Curvature	0.1023	0.1336	0.1183	11.5%
	5% PTL Bending	0.1075	0.1641	0.1413	13.9%
	Ultimate Strength	0.1409	0.4142	0.3814	7.9%
PVC	no load	0	0	0	0.0%
	ε_t curvature	0.0471	0.0050	0.0061	22.1%
	Max ε_t	0.0675	0.0206	0.0207	0.6%
	Bending DE Curvature	0.0805	0.0670	0.0699	4.4%
	5% PTL Bending	0.0844	0.0837	0.0965	15.4%
	Ultimate Strength	0.1253	0.3331	0.3589	7.8%

It can reasonably be assumed from Table 17, that dissipated energy can be predicted for a beam coupon in 3-point bending. Haiar also used moment-curvature relations to predict the displacement of HDPE and PVC beams in 3-point bending. He observed that displacements of full-size, rectangular, three-box cross-section beams were predictable up to failure using tension and compression stress-strain relationships. Lockyear [13] was also able to predict load-displacement behavior of wood-plastic beams in bending. Because Haiar and Lockyear could both predict load-displacement behavior

of WPC beams, it is logical that the strain states within the beams must be predictable, and dissipated energy for full size WPC beams in bending should be predictable.

In order to predict the total energy dissipated in the 3-point bending coupons, some assumptions were made. Previous research at Washington State University [13] used the hyperbolic tangent function to approximate the stress-strain relationship in WPC. Using this function implies that the material will have a constant stress after the ultimate strength has been reached. Figure 50 shows an example of a tension test stress-strain curve in which a line was added to indicate constant stress-strain relationship after maximum stress is reached. If this assumption were used to create the dissipated energy functions for tension, the material would continue to dissipate energy after the maximum tension strain (see Figure 51). For this research, the uniaxial tension and compression stresses were held constant after the ultimate strength was reached, and the rate of energy dissipation was assumed to be zero (see Figure 51).

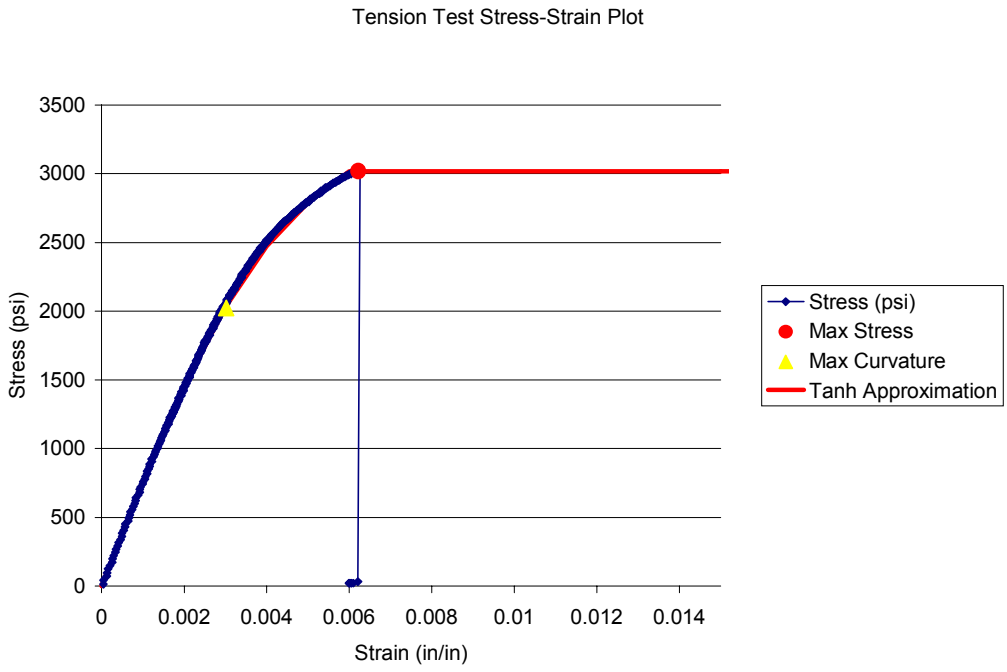

Figure 50: PVC stress-strain plot using a hyperbolic tangent approximation of stress-strain relationship to hold the stress constant after max stress is reached.

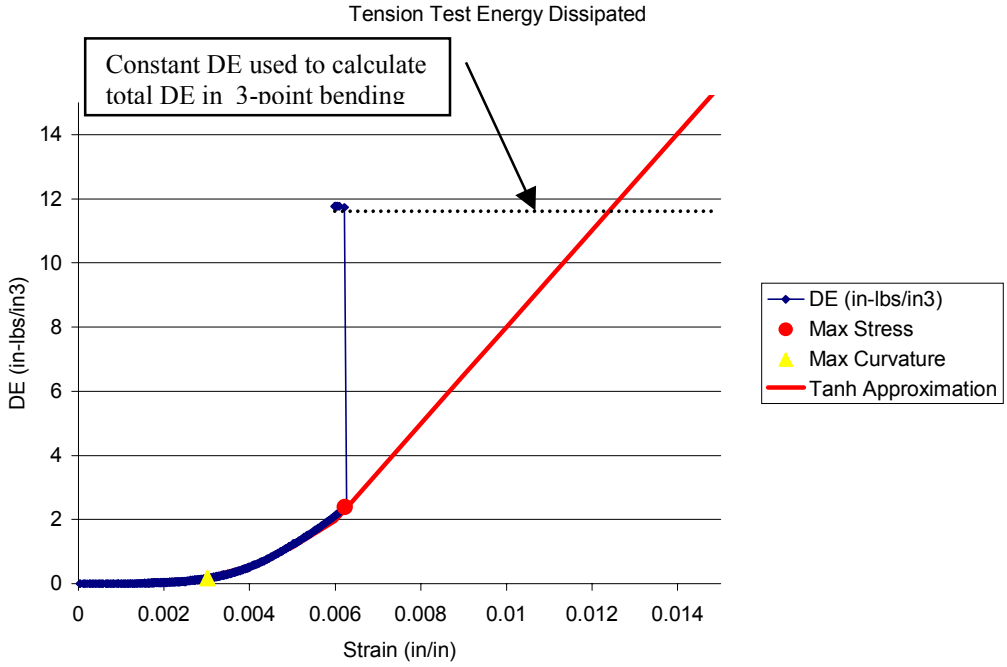

Figure 51: PVC dissipated energy plot using a hyperbolic tangent approximation of stress-strain relationship to hold the stress constant after max stress is reached.

The application of dissipated energy in a 3-point bending test has interesting results when one considers a beam design problem. Using the maximum tension strain as a design limit for wood-plastic composite beams in bending provides a design limit in which the total dissipated energy in the beam is kept just below the maximum curvature. In other words, the rate of damage accumulation in a wood-plastic beam is low when the maximum tension strain is reached.

Tension and compression dissipated energy density functions were used to predict dissipated energy in 3-point bending tests. Haiar used a similar concept when he programmed moment-curvature equations into a finite element code to predict displacements of beams from tension and compression stress-strain relationships. Programming uniaxial dissipated energy density functions into a finite element code would easily allow designers to analyze the energy dissipated by complex beam shapes or complex beam loads.

An investigation to see whether the total dissipated energy could be predicted in assemblies of wood-plastic members could also be accomplished in future research. If this is possible, damage to a WPC structure can be assessed in terms of damage to the members that make up the structure. Designers could use dissipated energy to optimize structural designs based on damage accumulation.

Comparison with Failure Theories

To compare failure criteria with test results, the average difference between each failure criteria and the biaxial test results was calculated. The ultimate strength from

each tension and biaxial specimen was compared to the value predicted each failure criteria. The difference between the predicted value and the tested value was calculated as a percentage of the predicted values.

Maximum Stress Criterion

The failure modes observed in biaxial tests on HDPE and HDPE with MAPE materials suggest that a maximum stress criterion would predict ultimate strength under tension, compression and biaxial compression torsion loading. However, under combined tension and torsion loading, the HDPE and MAPE formulations are not limited by the strength in a principal material direction. The limiting strength under this combined loading is in an off-axis direction (as shown by the 45-degree failure surface). Table 18 shows the difference between the maximum stress failure criterion and the biaxial test results. The differences have been divided into combined compression/torsion and tension/torsion quadrants of stress space for the HDPE, HDPE with MAPE and PVC wood-plastic formulations.

Table 18: Difference Between Max Stress Criterion Failure Criterion and Biaxial Test Results

Material	Average Difference (%) Under Compression and Torsion	Average Difference (%) Under Tension and Torsion
HDPE	**9.8**	**29.7**
HDPE w/ MAPE	**12.5**	**37.8**
PVC*	**19.6**	**N/A**

* All combined tension and torsion PVC specimens failed in the test grips.

Designers can use the maximum stress criterion to define failure under uniaxial loading, but not under any biaxial loading. This criterion does a better job predicting

failure under biaxial compression/torsion loading than it does predicting failure under biaxial tension/torsion loading, but the criterion lacks accuracy in either of these two quadrants of stress space.

Maximum Strain Criterion

The maximum strain criterion works well to predict ultimate strain under uniaxial loading because the criterion was defined using uniaxial test data. However, the maximum strain criterion did not work well to predict ultimate strain of ductile WPC under biaxial shear loads. Gibson [8] noted the same results when he compared the maximum strain criterion with brittle and ductile fiber-reinforced composites. Table 19 shows the average difference between the maximum strain criterion and the biaxial test results for all combinations of shear and normal loading in HDPE, HDPE with MAPE and PVC wood-plastic formulations.

Table 19: Average Difference Between Max Strain Criterion Failure Criterion and Biaxial Test Results

Material	Average Difference (%)
HDPE	**33.3**
HDPE w/ MAPE	**28.5**
PVC	**9.6**

In addition to the ultimate strength failure envelope, two other failure envelopes for the maximum strain criterion (based on max dissipated energy curvature and 5% PTL) were drawn for each wood-plastic composite formulation. When compared to the ultimate strength failure envelope, the failure envelope based on maximum dissipated energy curvature is more conservative in pure compression than it is in pure torsion and

more conservative in pure torsion than it is in pure tension. Since the rate of energy dissipation is a measure of material stability, looking at when the material becomes unstable in tension and compression tests could help to explain the increasing conservatism displayed in the maximum dissipated energy failure envelope. Tension instability in WPC specimens occurs just before tension failure is observed and compression instability in WPC specimens occurs long before ultimate compression strength is observed.

Designers using the maximum strain criterion to define failure need to be aware that the criterion accurately predicts failure under uniaxial loading, but not under biaxial shear and normal loads. The percent error is larger for WPC that are more ductile. In addition, using the maximum curvature in the DE function as a design limit may have economic consequences when compression and shear loads are critical.

Maximum Shear Stress Criterion

The longitudinal splitting observed in biaxial tests on HDPE and HDPE with MAPE materials suggest that a maximum shear stress criterion would predict ultimate strength under tension, compression and biaxial compression torsion loading. However, under combined tension and torsion loading, the HDPE and MAPE formulations are not limited by the shear strength in a principal material direction. The limiting strength is in an off-axis direction (as shown by the 45-degree failure surface). Table 20 shows the difference between the maximum shear stress criterion and the biaxial test results. The differences have been divided into compression/torsion and

tension/torsion quadrants of stress space for HDPE, HDPE with MAPE and PVC wood-plastic formulations.

Table 20: Difference Between Max Shear Stress Criterion Failure Criterion and Biaxial Test Results

Material	Average Difference (%) Under Compression and Torsion	Average Difference (%) Under Tension and Torsion
HDPE	**6.7**	**29.7**
HDPE w/ MAPE	**2.3**	**31.6**
PVC*	**21.4**	**N/A**

* All combined tension and torsion PVC specimens failed in the test grips.

Designers can use the maximum shear stress criterion to define failure under combined compression and torsion loading in HDPE and HDPE with MAPE wood-plastic composites. The criterion does not work to predict failure in the PVC formulation. This was expected because all of the PVC compression/torsion specimens exhibited off-axis failures. The failure surfaces depended on the combination axial and torsion stresses applied.

Tsai-Wu Criterion

By looking at Figures 37, 38, and 39, it appears that the criterion was more accurate for the HDPE formulations (with and without MAPE) than the PVC formulation. An investigation of the linear shear stress term (F_{16}) was done to see if adding shear terms to the Tsai-Wu criterion would help improve the accuracy of failure prediction. The ability of the Tsai-Wu criterion to predict failure in HDPE, HDPE with MAPE, and PVC wood-plastic composites was measured using the average difference between the Tsai-Wu criterion and the biaxial test results.

While it is agreed that the sign of the shear stress should not affect predictions of failure, the interaction term (F_{16}) in the Tsai-Wu criterion could be used in absolute value form. The plane stress Tsai-Wu criterion was rewritten to include the interaction term as Equation 46.

$$F_1\sigma_1 + F_2\sigma_2 + F_{11}\sigma_1^2 + F_{22}\sigma_2^2 + F_{66}\tau_{12}^2 + F_{12}\sigma_1\sigma_2 + F_{16}\sigma_1|\tau_{12}| + F_{26}\sigma_2|\tau_{12}| = 1$$

[Equation 46]

All of the "F" constants can be found using the same methods described in chapter two. Only the linear shear stress (F_{16} and F_{26}) terms still need to be defined. These two terms can be defined using the same methodology used to define the other F terms. Under only a combined axial and shear load, many terms in the plane stress Tsai-Wu criterion drop out. Equation 46 can then be rearranged to give F_{16} as shown in Equation 47.

$$F_{16} = \frac{1}{\sigma_1\tau_{12}}(1 - F_1\sigma_1 - F_{11}\sigma_1^2 - F_{66}\tau_{12}^2) \qquad \text{[Equation 47]}$$

Equation 47 requires known combinations of axial and shear (σ_1 and τ_{12}) failure stresses in order to determine F_{16}. Using Wu's suggestion that the F_{12} term be calculated for each quadrant of stress-strain space, the F_{16} term was calculated for both tension and compression axial loads. The average values of all the F_{16} constants in tension and compression are shown in Table 21.

Table 21: Linear Shear Stress Interaction Constants in Tsai-Wu Criterion

Material	F_{16} (psi^{-2}) tension	F_{16} (psi^{-2}) compression
HDPE	1.57E-07	2.39E-07
HDPE w/ MAPE	1.44E-07	-2.47E-08
PVC*	5.84E-09	5.84E-09

*Since all of the PVC combined tension and shear specimens failed upon gripping, the compression F_{16} was also used as the tension F_{16} for purposes of plotting failure envelopes.

Figure 52, Figure 53, and Figure 54 show the Tsai-Wu criterion (with and without the F_{16} interaction term) superimposed on the test data for the three material formulations. For reference, the stresses at maximum curvature in the DE function have also been included.

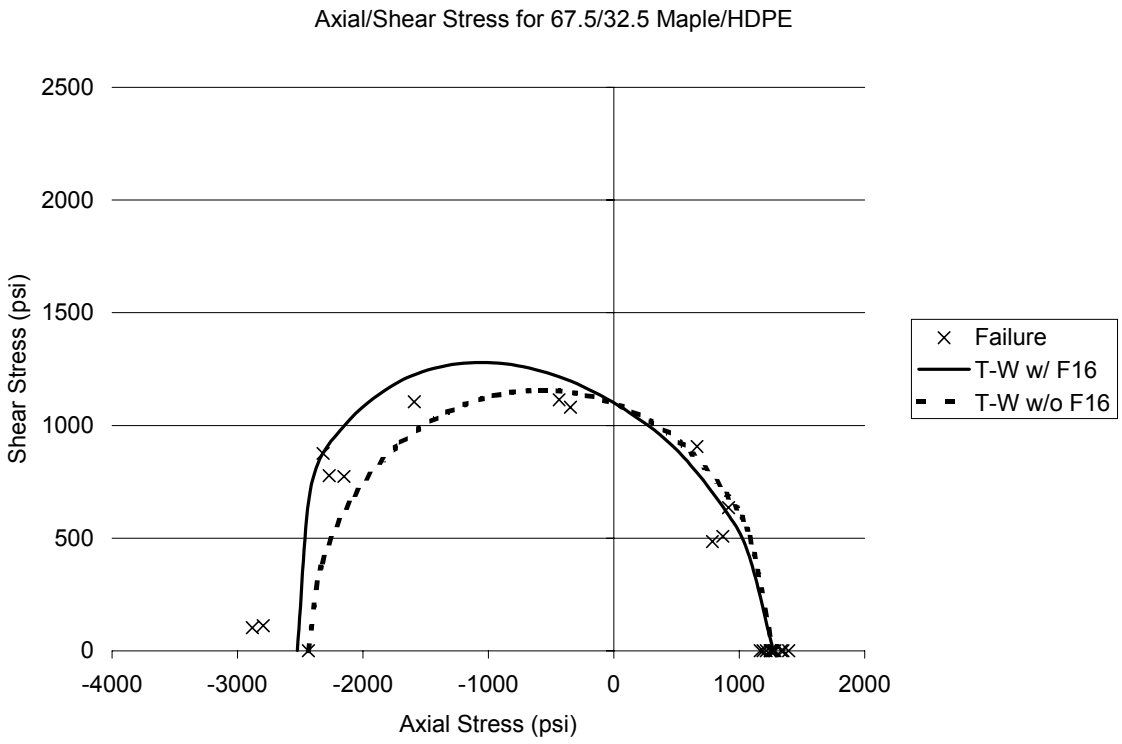

Figure 52: Tsai-Wu Criterion w/ and w/o Shear Stress Interaction Constants (HDPE)

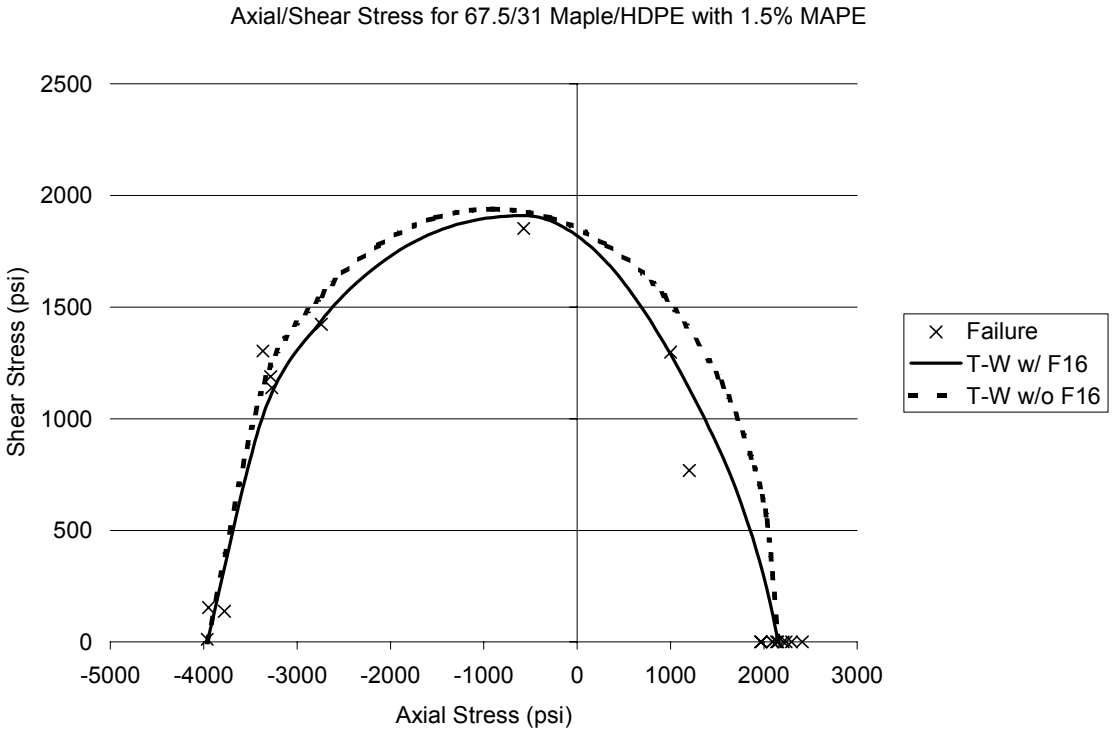

Figure 53: Tsai-Wu Criterion w/ and w/o Shear Stress Interaction Constants (HDPE w/ MAPE)

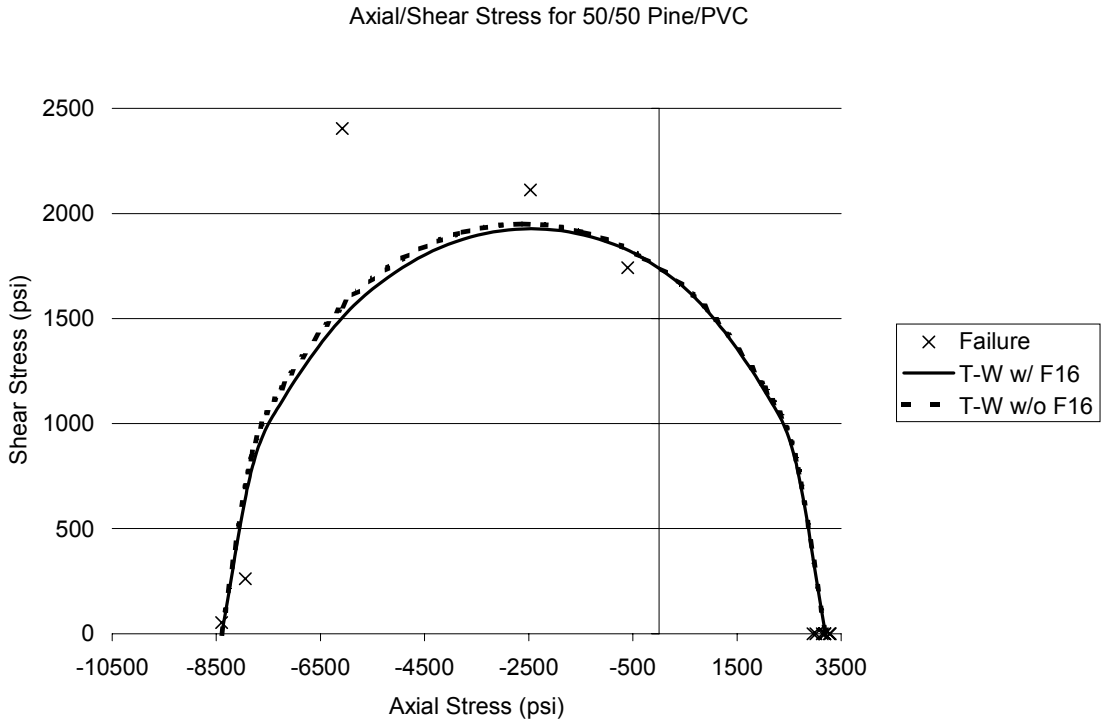

Figure 54: Tsai-Wu Criterion w/ and w/o Shear Stress Interaction Constants (PVC)

The average difference between the biaxial test results (for all combinations of normal and shear loading tested) and the Tsai-Wu criterion, with and without the F_{16} term, is shown in Table 22 below.

Table 22: Average Difference between Tsai-Wu Criterion and Biaxial Test Results with and without Shear Stress Interaction Terms

Material	Average Difference w/o F_{16} (%)	Average difference w/ F_{16} (%)
HDPE	**12.1**	**10.0**
HDPE w/ MAPE	**9.3**	**10.0**
PVC	**14.9**	**16.0**

The addition of the shear interaction term does not reduce the difference between the failure criterion and the biaxial test results. This supports the biaxial test results, which showed that the interaction between normal and shear stresses is based on the maximum shear stress. If a failure criterion is trying to accurately predict failure of WPC under compression and shear, it must account for the maximum shear stress.

Structural designers who want to use the Tsai-Wu criterion to determine failure in wood-plastic composites under combined normal and shear loading should understand that the criterion works better for ductile WPC. The criterion is less accurate for brittle WPC, and adding terms to account for interaction of normal and shear stresses has almost no effect on the accuracy of combined normal/shear failure predictions.

Yeh-Stratton Criterion

Figures 40, 41 and 42 plotted the Yeh-Stratton criterion against biaxial and tension test data. It appears that the criterion is not accurately predicting failure in these three wood-plastic composites. The criterion under-predicted the strength of all three wood-plastic composites under combined compression and shear.

Although the criterion (as presented by Yeh and Lee [24]) does not include interaction terms between axial and shear stresses, a $D_{1,12}$ term was created in this thesis and investigated to determine if the Yeh-Stratton criterion could better predict ultimate stresses and match biaxial test results. Equations 48 and 49, show the limiting plane stress Yeh-Stratton criterion with the $D_{1,12}$ interaction term included for tension and compression respectively.

$$A_1\sigma_1 + C_{12}\tau_{12}^2 + D_{1,12}\sigma_1|\tau_{12}| = 1 \qquad \text{[Equation 48]}$$

$$A'_1\sigma_1 + C_{12}\tau_{12}^2 + D'_{1,12}\sigma_1|\tau_{12}| = 1 \qquad \text{[Equation 49]}$$

The value of $D_{1,12}$ was determined by rearranging Equations 48 and 49. Tension and compression interaction terms are shown in Equations 51 and 50 respectively.

$$D_{1,12} = \frac{1}{\sigma_1|\tau_{12}|}(1 - A_1\sigma_1 - C_{12}\tau_{12}^2) \qquad \text{[Equation 50]}$$

$$D'_{1,12} = \frac{1}{\sigma_1|\tau_{12}|}(1 - A'_1\sigma_1 - C_{12}\tau_{12}^2) \qquad \text{[Equation 51]}$$

Axial and shear stress values obtained from biaxial test data were used to calculate the interaction terms in Equations 50 and 51. A value of the interaction constant was calculated for each biaxial test, but the average values of the shear interaction term (for each material) are shown in Table 23.

Table 23: Yeh-Stratton Interaction Constants

Material	$D_{1,12}$ (psi^{-2})	$D'_{1,12}$ (psi^{-2})
HDPE	7.04E-8	3.79E-7
HDPE w/ MAPE	1.64E-7	4.95E-8
PVC*	6.26E-8	6.26E-8

*Since all of the PVC combined tension and shear specimens failed upon gripping, the compression $D'_{1,12}$ was also used as the tension $D_{1,12}$ for purposes of plotting failure envelopes.

In Figure 55, Figure 56 and Figure 57, the Yeh-Stratton criterion is plotted with and without the linear shear stress interaction term, $D_{1.12}$. The values used to plot the "Y-S w/ D112" lines are given in Table 23.

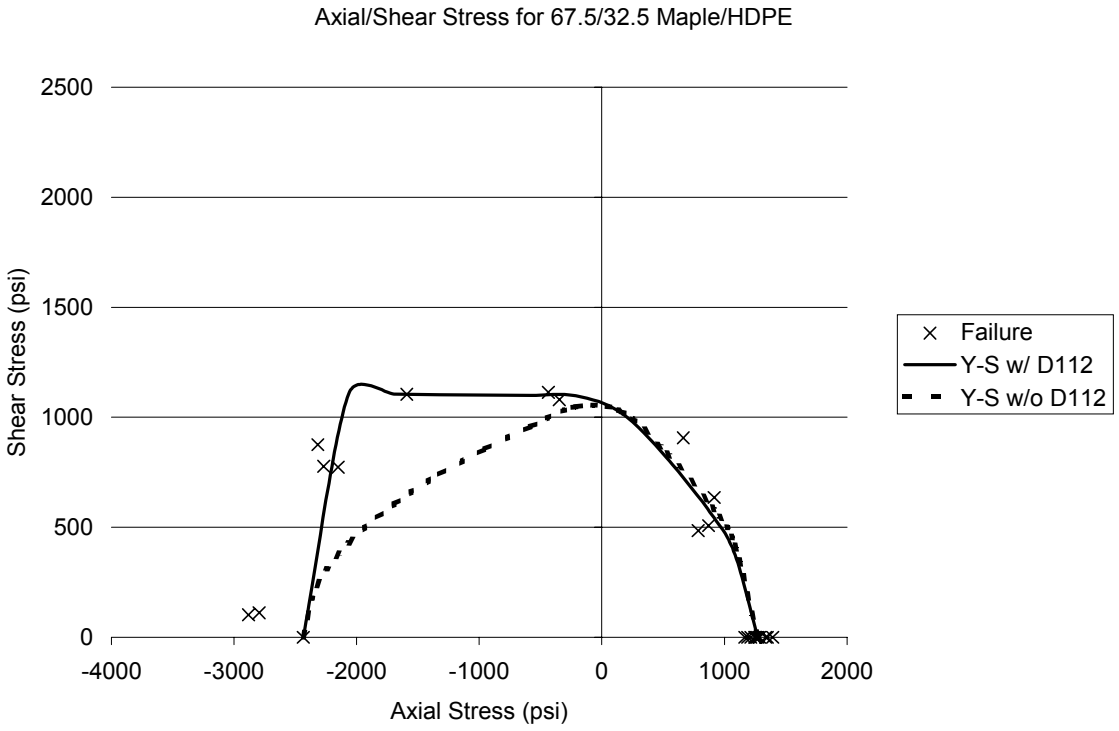

Figure 55: Yeh-Stratton Criterion w/ and w/o Shear Stress Interaction Constants (HDPE)

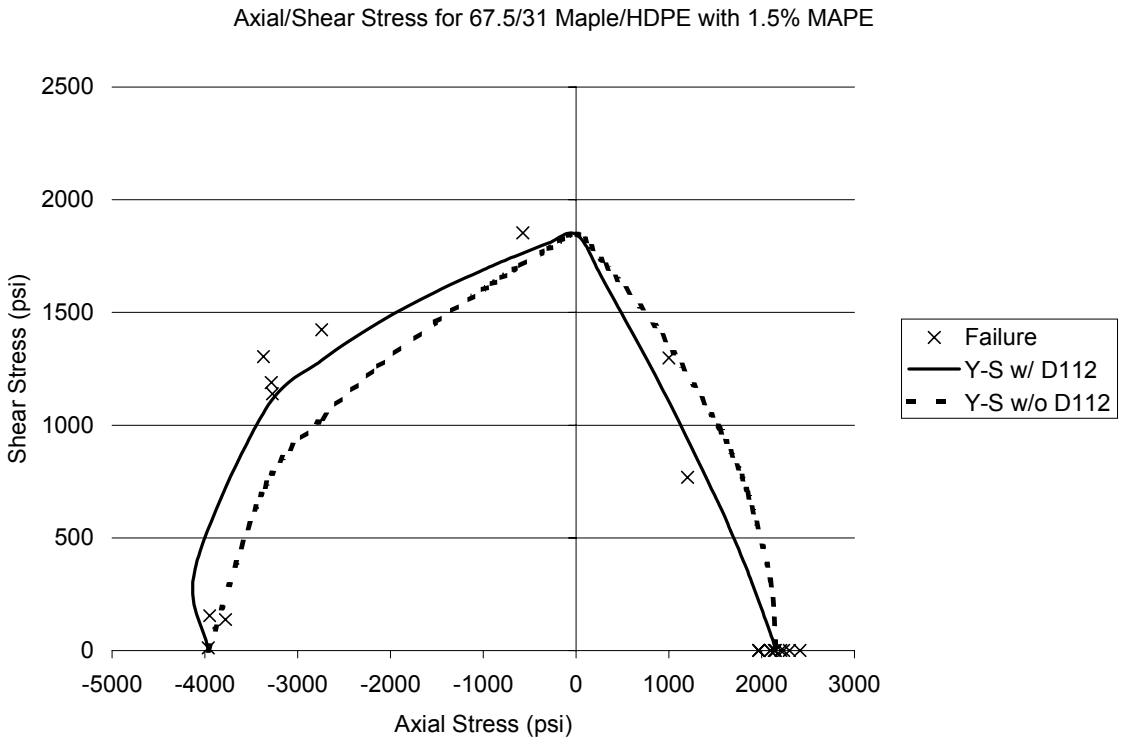

Figure 56: Yeh-Stratton Criterion w/ and w/o Shear Stress Interaction Constants (HDPE w/ MAPE)

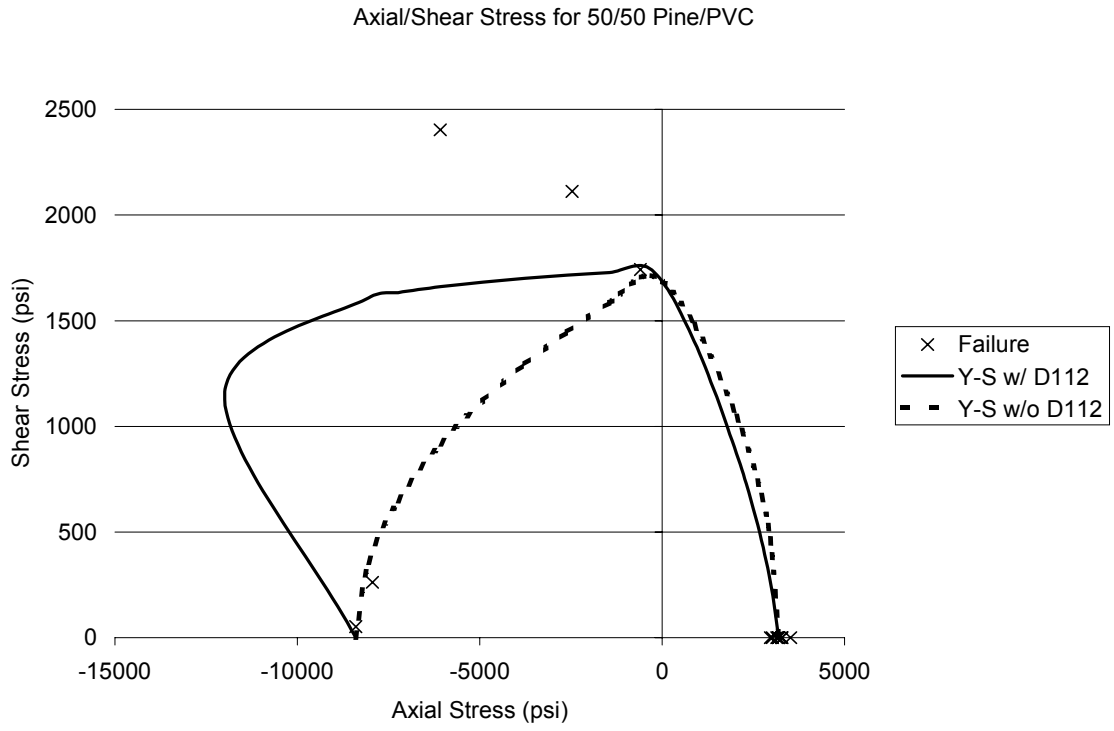

Figure 57: Yeh-Stratton Criterion w/ and w/o Shear Stress Interaction Constants (PVC)

The average difference between the biaxial test results (for all combinations of normal and shear stress tested) and the Yeh-Stratton criterion with and without the proposed $D_{1,12}$ terms is shown in Table 24.

Table 24: Average Difference between Yeh-Stratton Criterion and Biaxial Test Results with and without Shear Stress Interaction Constants

Material	Average Difference w/o $D_{1,12}$ (%)	Average difference w/ $D_{1,12}$ (%)
HDPE	**36.5**	**15.8**
HDPE w/ MAPE	**15.8**	**7.8**
PVC	**39.0**	**22.9**

With the $D_{1,12}$ terms, the resulting average difference is approximately the same as the Tsai-Wu criterion (see Table 22). Still, the Yeh-Stratton equation cannot represent compression/shear failures using a quadratic equation with linear terms included.

In their conclusion, Yeh and Lee state that the Yeh-Stratton criterion is "among the most accurate and reliable." The conclusion does not seem to hold for these wood-plastic composites under combined normal and shear loading. The criterion as presented by Yeh and Lee assumes that the axial/shear stress interaction can be described with a single quadratic shear stress term. If the criterion is modified to include both linear and quadratic shear stress terms, the Yeh-Stratton criterion starts to represent the biaxial test data, but still lacks accuracy. Rather than adding more terms, a failure criterion needs to account for the failure modes observed in biaxial tests, i.e. longitudinal splitting of HDPE and HDPE with MAPE specimens, and the off-axis tension failures of the PVC specimens.

CHAPTER SIX: SUMMARY AND CONCLUSION

Summary

Wood-plastic composites with high wood-fiber content can be characterized by dissipated energy. This thesis used tension and biaxial test data to create dissipated energy density functions for three different wood-plastic composite formulations: HDPE, HDPE with MAPE, and PVC. The procedure used to calculate dissipated energy was similar to the procedure used by researchers at the Naval Research Laboratory [15, 16, and 17]. The dissipated energy density functions were presented as contour maps allowing a user to quickly assess the rates of damage accumulation under combined shear and normal loads.

The total energy dissipated by a wood-plastic coupon under 3-point bending was calculated for each wood-plastic formulation. The total energy dissipated was predictable using tension and compression dissipated energy density functions and beam theory. If the dissipated energy calculations were programmed into a structural analysis program, there is an opportunity for future researchers to analyze WPC beams and assemblies not only in terms of internal stresses, but also in terms of accumulated damage.

One of the problems facing designers who would like to use wood-plastic composites is the lack of a distinct change in material behavior that indicates failure is eminent. This thesis defines allowable design strengths based on curvature in the dissipated energy functions. The maximum curvature in the dissipated energy function indicates a change in material stability, just as the yield point indicates a change in the

stability of metals. The maximum dissipated energy curvature strength would provide designers with an allowable stress to use in current design methodologies.

Testing conducted in this research provided an opportunity to examine how wood-plastic composites behave under biaxial loading. The results of the biaxial testing showed that true shear failures could be induced in HDPE and HDPE with MAPE formulations by applying a combination of compression and shear loads to biaxial test cylinders. The shear failures were contrary to previous torsion test results that had shown off-axis tension failures.

Conclusion

The first objective of this thesis was to characterize three formulations of wood-plastic composites using dissipated energy.

- The PVC formulation generally dissipated energy at a faster rate than the HDPE and HDPE with MAPE formulations.
- All three wood-plastic formulations accumulate damage under shear loading more quickly than under tension or compression loading.
- There is no simple relationship between the applied combination of normal/shear stresses and the maximum curvature in the dissipated energy function, a fact that is reflected in the shape of the dissipated energy contour plots.
- Uniaxial tension and compression dissipated energy density functions can be used with beam theory to predict the total energy dissipated by a beam in flexure.

The second objective of this thesis was to compare the strength based on curvature in the dissipated energy functions to the 5% PTL and the ultimate strengths.

- Strengths corresponding to the maximum curvature in the dissipated energy function represent a strength at which WPC materials undergo a change in behavior.
- All 5% PTL strengths were higher than strengths based on curvature in the dissipated energy functions. Maximum curvature tension stresses were 63%-79% of ultimate while 5% PTL tension stresses were 81%-84% of ultimate.
- The maximum curvature strength is more conservative in compression than it is in shear, and more conservative in shear than it is in tension.
- Design values based on the 5% parametric tolerance limit provide confidence against failure, but provide no consistent rate of damage accumulation.
- The maximum curvature in the dissipated energy of a beam in 3-point bending occurs after maximum tensile strain in the extreme fiber has been reached.

The last objective was to investigate the ability of three failure theories to predict failure in WPC materials.

- No single failure theory examined in this thesis worked to predict failure for all quadrants of normal/shear space.
- Failure of HDPE and HDPE with MAPE formulations under combined compression and shear stresses is governed by the maximum shear strength.

- Of the failure criteria examined here, the maximum shear stress (Tresca) criterion predicted the observed shear failures in the HDPE and HDPE with MAPE wood-plastic formulations.
- None of the failure criteria examined in this thesis worked to predict failure of the three WPC formulations under combined tension and shear loading. However, the Tsai-Wu criterion had the smallest percent difference in this quadrant of stress space.
- The linear shear stress terms in the Tsai-Wu and Yeh-Stratton criteria are often neglected. Including the linear shear stress terms had no effect in the Tsai-Wu criterion, but did affect the Yeh-Stratton criterion.

More research could be done on wood-plastic composites and dissipated energy including:

- Better biaxial test methods are available and additional test data could verify dissipated energy density functions for combined normal and shear loading, as well as, providing dissipated energy density functions for combined normal stresses.
- Dissipated energy calculations could be programmed into a finite-element code to calculate dissipated energy in an assembly of wood-plastic composite members.
- This thesis performed a preliminary investigation of using existing failure criteria to predict failure in wood-plastic composites. To determine which failure criterion can accurately predict failure of WPC, many more test specimens will have to be tested. New tests should include combined normal loading.

REFERENCES

1. Abu-Farsakh, G. A., K. S. Numayr and Kh. A. Hamad. (1997). "A Micro-mechanical Model for Predicting the Compressive Strength of Fibrous Composite Materials." *Composites Science and Technology*, 57, 1415-1422.

2. Biegler, M. W. and M. M. Mehrabadi. (1995). "An Energy-Based Constitutive Model for Anisotropic Solids Subject to Damage." *Mechanics of Materials*, 19, 151-164.

3. Brandt, Christopher. Masters Thesis (2001). *Load-Duration Behavior of Extruded Wood-Plastic Composites*. Washington State University.

4. Brünig, Michael. (2001). "A Framework for Large Strain Elastic-plastic Damage Mechanics Based on Metric Transformations." *International Journal of Engineering Science*, 39, 1033-1056.

5. Brostow, Witold and Roger Corneliussen (Ed.). (1986). *Failure of Plastics*. New York: Hanser Publishers.

6. Christensen, R. M. (1997). "Stress Based Yield/Failure Criteria for Fiber Composites." *International Journal of Solids and Structures*, 34, 529-543.

7. Cook, Robert D., Malkus, David S. and Plesha, Michael E. (1989). *Concepts and Applications of Finite Element Analysis Third Ed*. New York: John Wiley and Sons.

8. Gibson, Ronald F., (1994). *Principles of Composite Material Mechanics.* New York: McGraw-Hill, Inc.

9. Haiar, Kevin. Masters Thesis (2000). *Performance and Design of Prototype Wood-Plastic Composite Sections*. Washington State University.

10. Hashin, Z. (1980). "Failure Criteria for Unidirectional Fiber Composites." *Journal of Applied Mechanics*, 47, 329-334

11. Hermanson, John C., Timothy Adcock and Michael P. Wolcott. (1999). "Section Design of Wood Plastic Composites." *Washington State University*

12. Hyer, Michael W. (1998). *Stress Analysis of Fiber Reinforced Composite Materials*. Boston: WCB/McGraw-Hill.

13. Lockyear, Scott. Masters Thesis (1999). *Mechanical Analysis of Transversely Loaded Wood/Plastic Sections*. Washington State University.

14. Lui, J.Y., (1984) "Evaluation of the Tensor Polynomial Strength Theory for Wood." *Journal of Composite Materials*, 18, 216-226.

15. Mast, P. W. et al. (1995). "Characterization of Strain-Induced Damage in Composites Based on the Dissipated Energy Part I. Basic Scheme and Formulation." *Theoretical and Applied Fracture Mechanics*, 22, 71-96.

16. Mast, P. W. et al. (1995). "Characterization of Strain-Induced Damage in Composites Based on the Dissipated Energy Part II. Composite Specimens and Naval Structures." *Theoretical and Applied Fracture Mechanics*, 22, 97-114.

17. Mast, P. W. et al. (1995). "Characterization of Strain-Induced Damage in Composites Based on the Dissipated Energy Part III. General Material Constitutive Relation." *Theoretical and Applied Fracture Mechanics*, 22, 115-125.

18. Murphy, Joseph F., "Characterization of Nonlinear Materials." *USDA Forest Products Laboratory Technical Note*. Madison, WI.

19. Oguni, K. and Ravichandran, G. (2000). "An Energy-Based Model of Longitudinal Splitting in Unidirectional Fiber-Reinforced Composites." *Journal of Applied Mechanics*, Vol. 67, 437-443

20. Philpot, Timothy, Kenneth Fridley and David Rosowsky. (1994). "Energy-Based Failure Criterion for Wood." *Journal of Materials in Civil Engineering*, 6, 578-594

21. Powell, Peter C. (1983). *Engineering with Polymers*. New York: Chapman and Hall.

22. Rangaraj, Sudarshan V. Masters Thesis (1999). *Durability Assessment and Modeling of Wood-Thermoplastic Composites*. Washington State University.

23. Ugural, A. C. and S. K. Fenster. (1995). *Advanced Strength and Applied Elasticity.* New Jersey: Prentice Hall PTR.

24. Yeh, Hsien-Yang and Robert Chun-Yen Lee. (1995). "Simple Analysis of the Yeh-Stratton Failure Criterion on Composite Materials." *Engineering Fracture Mechanics*, 51, 37-49

APPENDIX A: TENSION TEST RESULTS

Included in this appendix is a summary of the tension tests performed in this research. Stress-Strain plots are shown for all three material formulations. Plots of dissipated energy density vs. strain are also shown.

The plots labeled HDPE show test data from the 67.5/32.5 Maple/HDPE formulation. Plots labeled HDPE w/ MAPE show test data from the 67.5/31 Maple/HDPE with 1.5% MAPE formulation. Plots labeled PVC show test data from the 50/50 Pine/PVC formulation.

Noted in all the plots are the average value for maximum stress (denoted with X), the average value of maximum curvature in the dissipated energy function (denoted with 0) and the value of the 5% parametric tolerance limit stress (denoted by □).

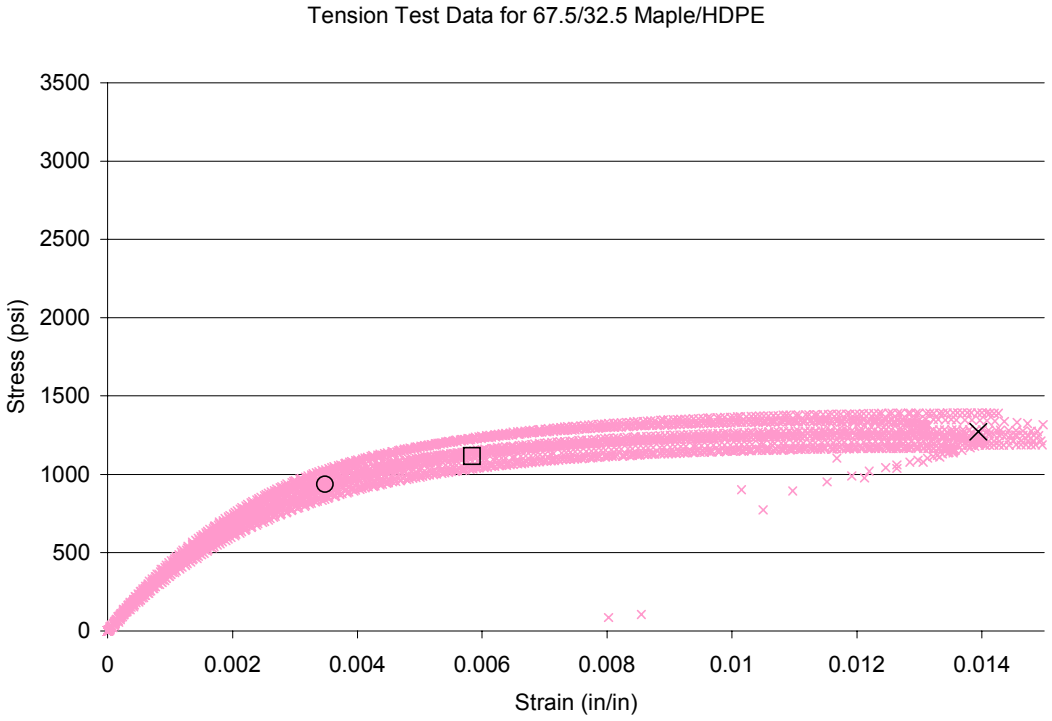
Tension Test Data for 67.5/32.5 Maple/HDPE
Stress (psi)
3500
3000
2500
2000
1500
1000
500
0
0
0.002
0.004
0.006
0.008
0.01
0.012
0.014
Strain (in/in)

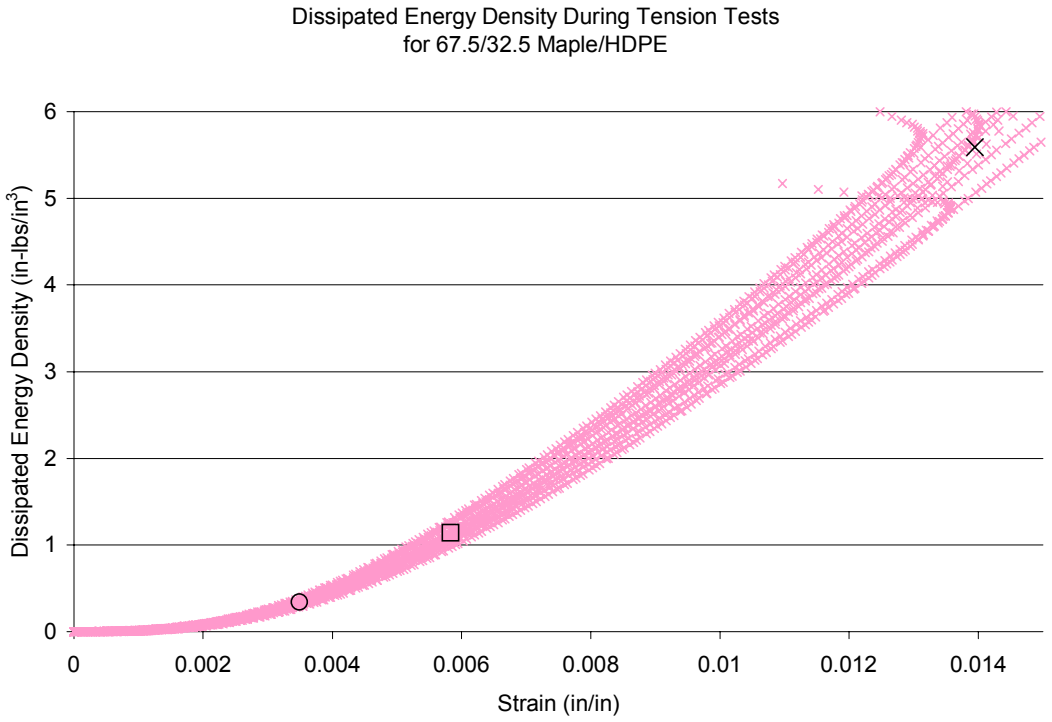
Dissipated Energy Density During Tension Tests
for 67.5/32.5 Maple/HDPE
Dissipated Energy Density (in-lbs/in3)
6
5
4
3
2
1
0
0
0.002
0.004
0.006
0.008
0.01
0.012
0.014
Strain (in/in)

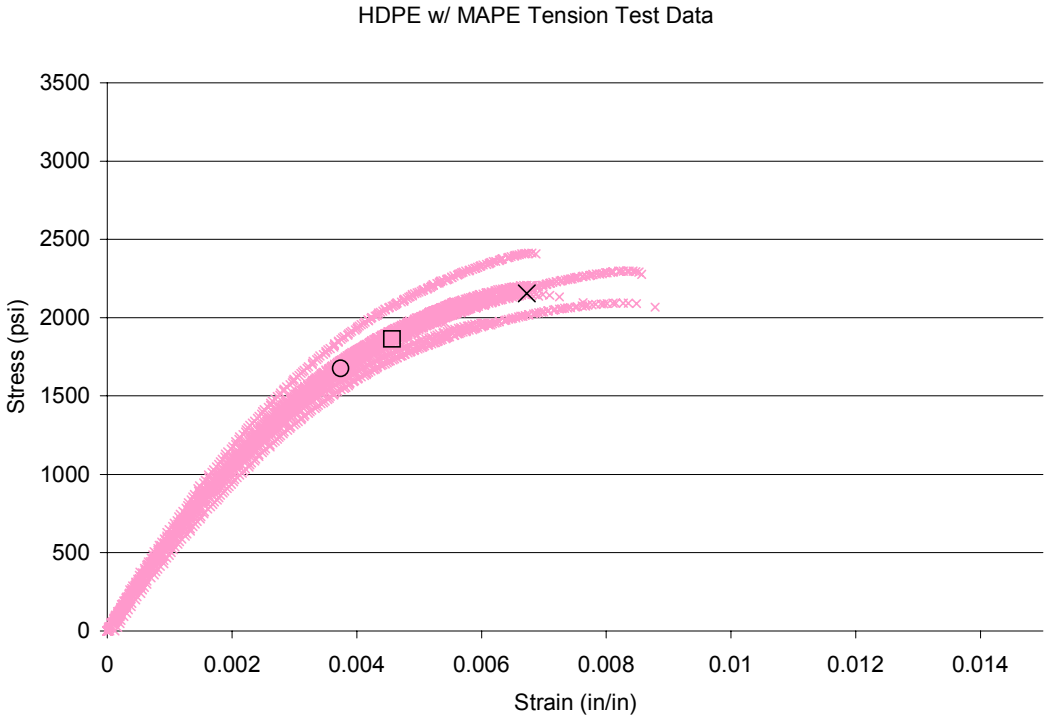
HDPE w/ MAPE Tension Test Data
Stress (psi)
3500
3000
2500
2000
1500
1000
500
0
0
0.002
0.004
0.006
0.008
0.01
0.012
0.014
Strain (in/in)

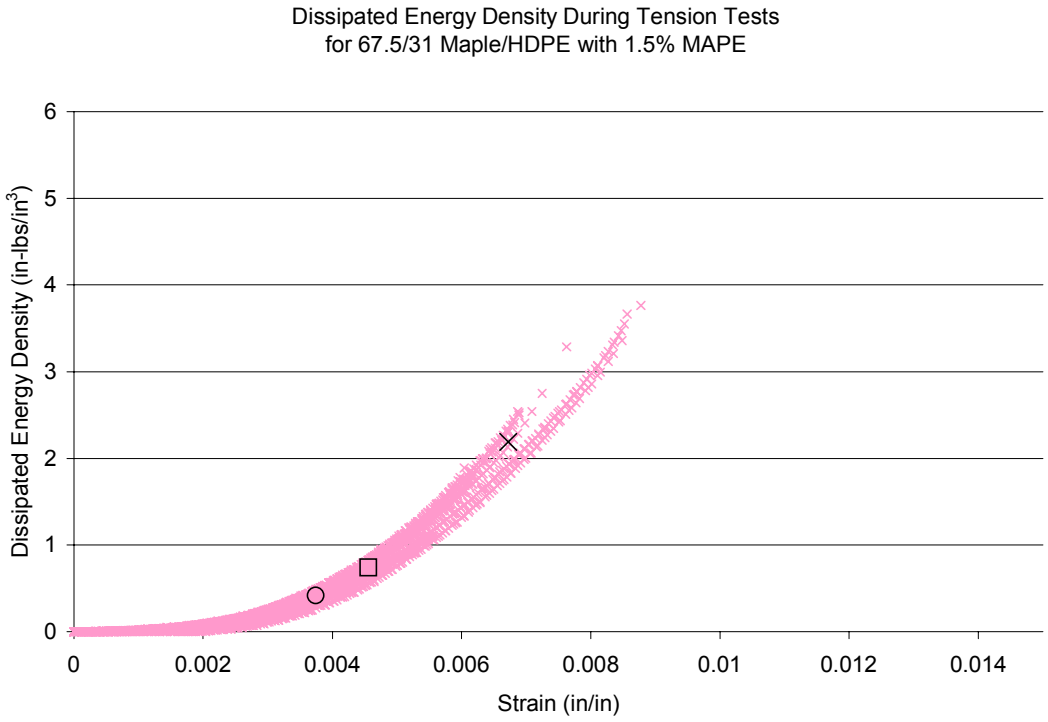
Dissipated Energy Density During Tension Tests
for 67.5/31 Maple/HDPE with 1.5% MAPE
Dissipated Energy Density (in-lbs/in3)
6
5
4
3
2
1
0
0
0.002
0.004
0.006
0.008
0.01
0.012
0.014
Strain (in/in)

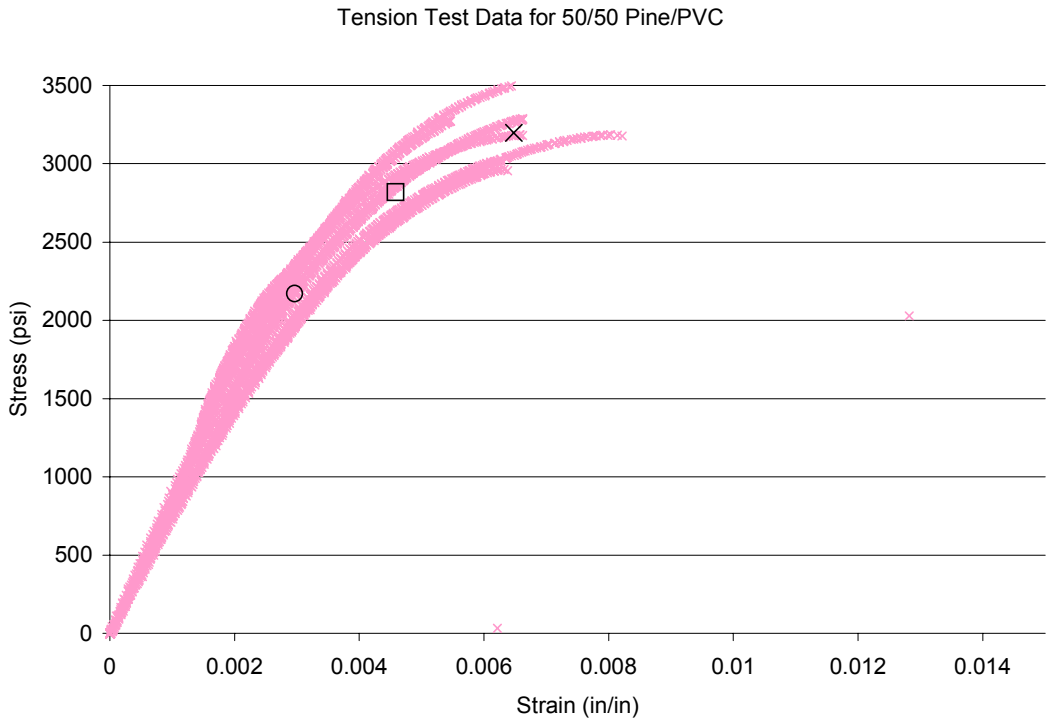
Tension Test Data for 50/50 Pine/PVC
Stress (psi)
3500
3000
2500
2000
1500
1000
500
0
0
0.002
0.004
0.006
0.008
0.01
0.012
0.014
Strain (in/in)

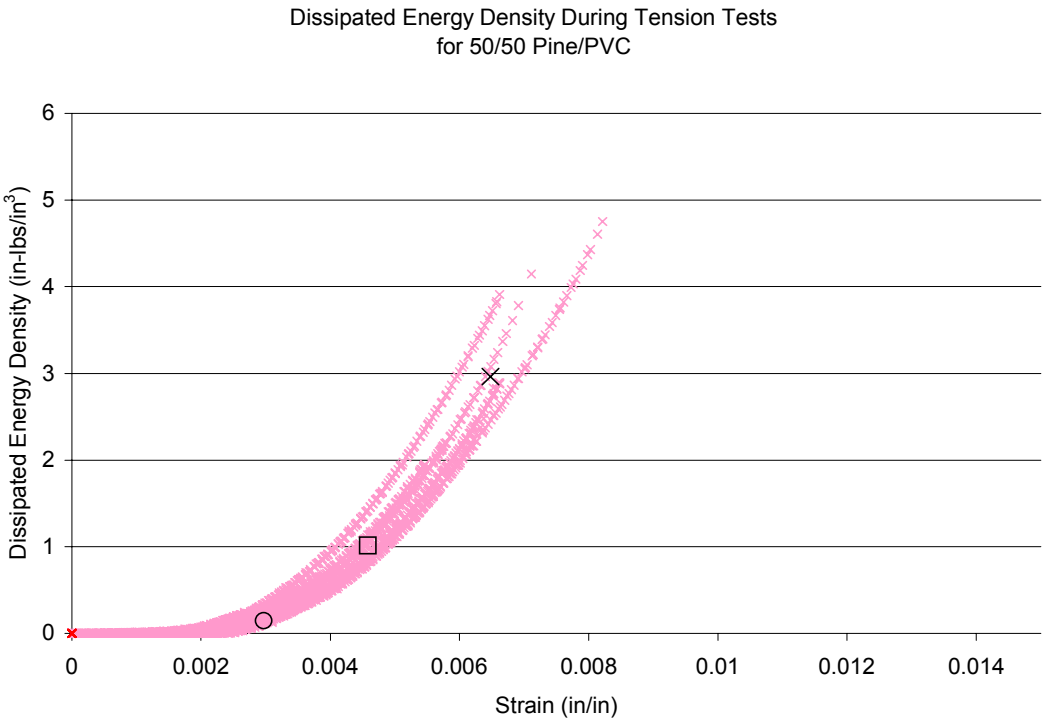
Dissipated Energy Density During Tension Tests
for 50/50 Pine/PVC
Dissipated Energy Density (in-lbs/in3)
6
5
4
3
2
1
0
0
0.002
0.004
0.006
0.008
0.01
0.012
0.014
Strain (in/in)

APPENDIX B: V-NOTCH SHEAR TEST RESULTS

Included in this appendix is a summary of the v-notch shear tests performed in this research. Load-Displacement plots are shown for the HDPE with MAPE and PVC wood-plastic formulations. Plots of dissipated energy density vs. displacement are also shown.

Plots labeled HDPE w/ MAPE show test data from the 67.5/31 Maple/HDPE with 1.5% MAPE formulation. Plots labeled PVC show test data from the 50/50 Pine/PVC formulation.

Noted in all the plots are the average value for maximum stress (denoted with X), the average value of maximum curvature in the dissipated energy function (denoted with 0) and the value of the 5% parametric tolerance limit stress (denoted by □).

V-Notch Shear Test Data for 67.5/31 Maple/HDPE with MAPE

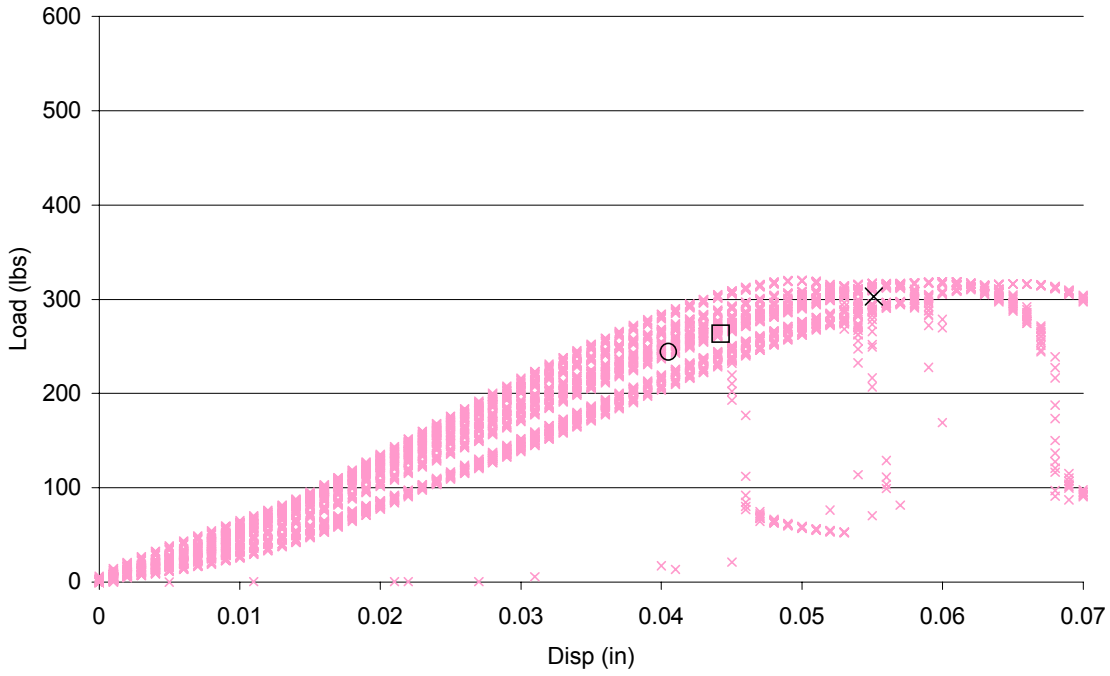

V-Notch Shear Test Data for 67.5/31 Maple/HDPE with 1.5 MAPE

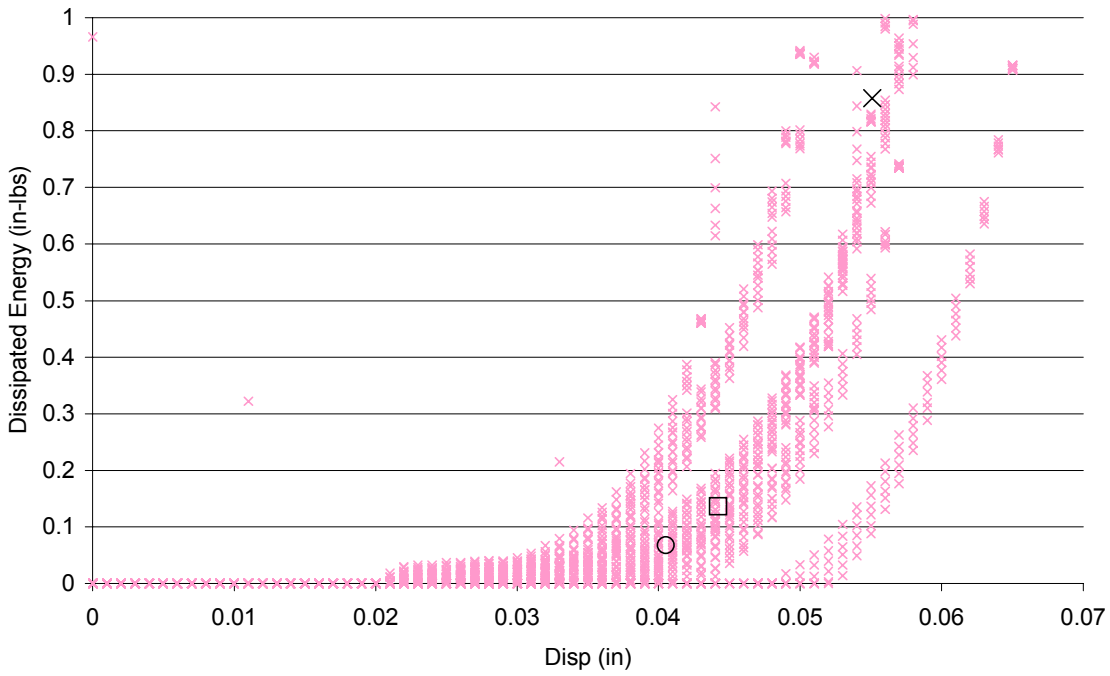

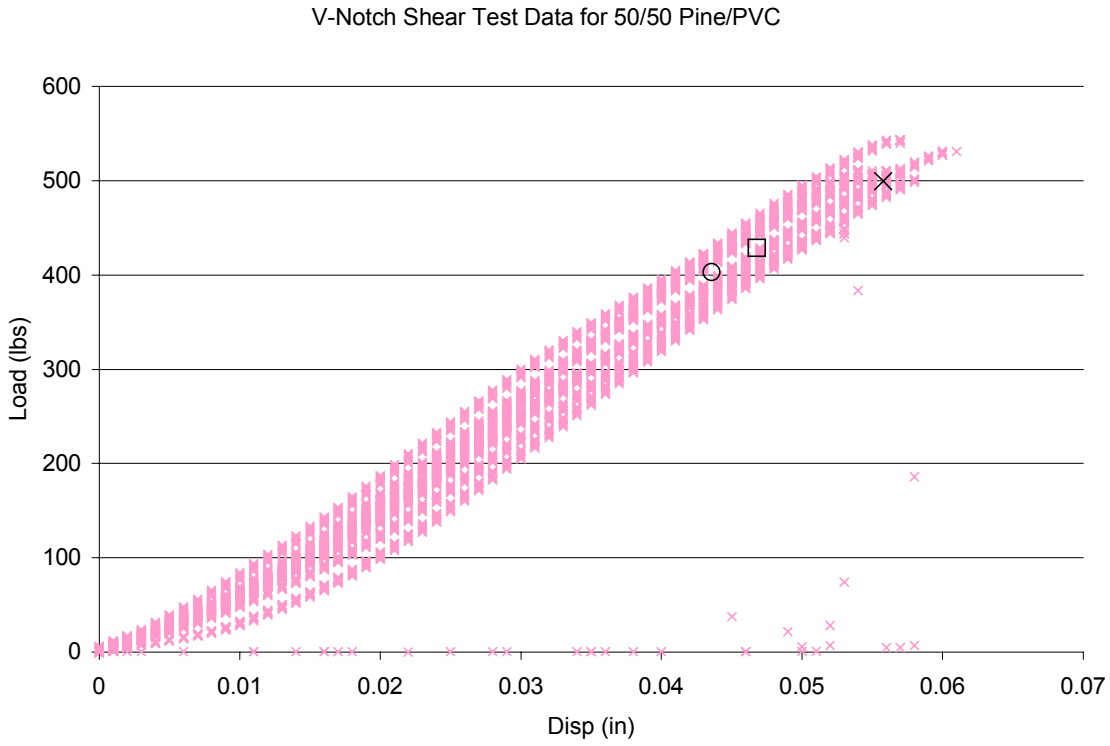
V-Notch Shear Test Data for 50/50 Pine/PVC
Load (lbs)
600
500
400
300
200
100
0
0
0.01
0.02
0.03
0.04
0.05
0.06
0.07
Disp (in)

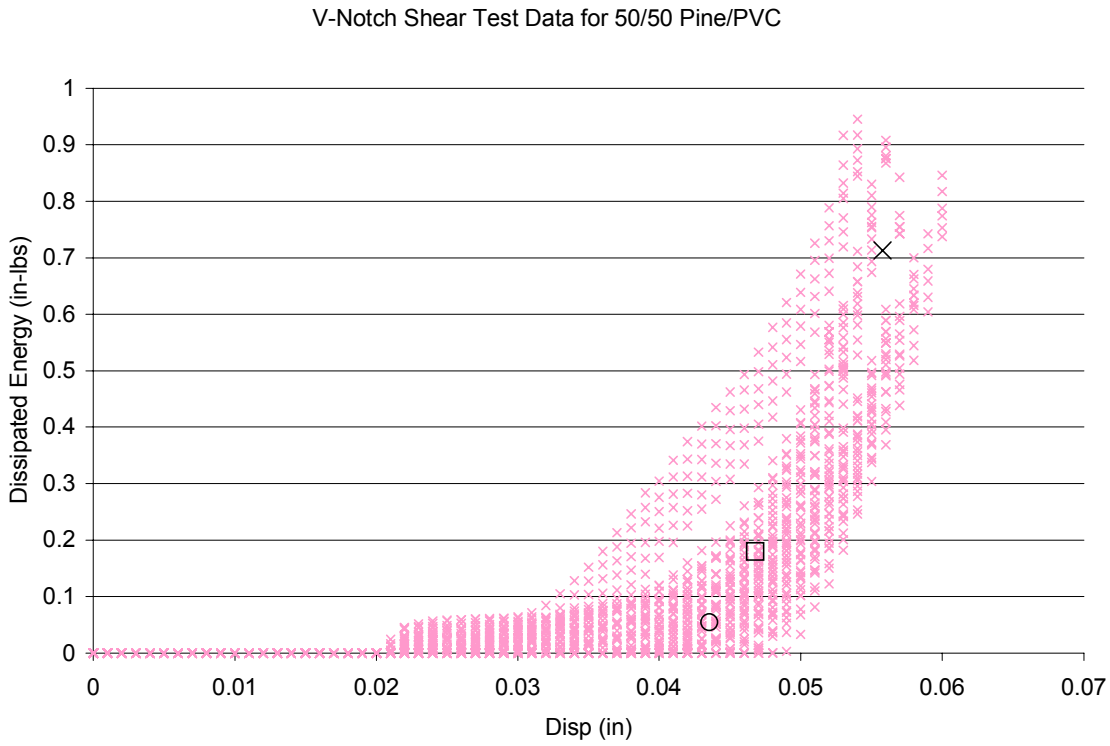
V-Notch Shear Test Data for 50/50 Pine/PVC
Dissipated Energy (in-lbs)
1
0.9
0.8
0.7
0.6
0.5
0.4
0.3
0.2
0.1
0
0
0.01
0.02
0.03
0.04
0.05
0.06
0.07
Disp (in)

APPENDIX C: BIAXIAL TEST RESULTS

The following charts are plots of dissipated energy density vs principal strain for the biaxial tests performed. The plots labeled with the material and the specimen number. A chart of the displacement rates at which each test specimen was loaded is below.

67.5/32.5 Cylinder #	Axial rate (in/min)	Twist rate (rad/min)	Princ Strain (in/in/min)	Princ Strain (in/in/min)	Princ Strain angle (degrees from ε_c or ε_t)
1	0	0.04857	0.0050	-0.0050	90.0
2	0	0.04857	0.0050	-0.0050	90.0
3	-0.0425	0	0.0000	-0.0100	0.0
4	-0.0425	0	0.0000	-0.0100	0.0
5	-0.03518	0.00402	0.0000	-0.0083	-5.7
6	-0.03518	0.00402	0.0000	-0.0083	-5.7
7	0.03518	0.0402	0.0100	-0.0017	45.0
8	0.03518	0.0402	0.0100	-0.0017	45.0
9	-0.03518	0.0402	0.0017	-0.0100	-45.0
12	-0.03518	0.0402	0.0017	-0.0100	-45.0
13	-0.0471	0.065	0.0031	-0.0142	-50.4
14	0.0471	0.065	0.0142	-0.0031	50.4
15	0.02355	0.065	0.0100	-0.0045	67.5
16	-0.02355	0.065	0.0045	-0.0100	-67.5
MAPE					
2	0	0.04857	0.0100	-0.0100	90.0
3	-0.0425	0	0.0000	-0.0100	0.0
5	-0.03518	0.00402	0.0001	-0.0084	-5.7
6	-0.03518	0.00402	0.0001	-0.0084	-5.7
9	-0.03518	0.0402	0.0051	-0.0134	-45.0
10	-0.03518	0.0402	0.0051	-0.0134	-45.0
11	-0.0471	0.065	0.0089	-0.0200	-50.4
12	-0.0471	0.065	0.0089	-0.0200	-50.4
13	0.0471	0.065	0.0200	-0.0089	50.4
14	0.02355	0.065	0.0164	-0.0109	67.5
15	-0.02355	0.065	0.0109	-0.0164	-67.5
PVC					
1	0	0.04857	0.0100	-0.0100	90.0
4	-0.0425	0	0.0000	-0.0100	0.0
5	-0.03518	0.00201	0.0000	-0.0083	-2.9
7	0.04156	0.056	0.0148	-0.0065	49.7
9	-0.02771	0.0765	0.0128	-0.0193	-67.5

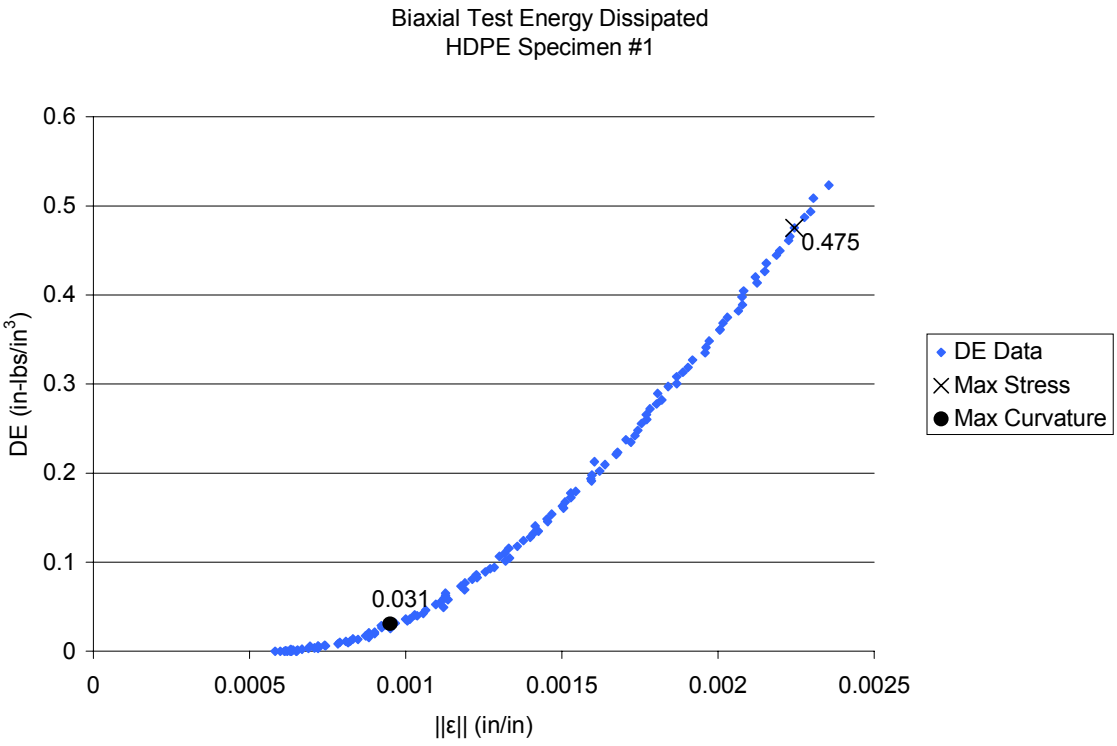
Biaxial Test Energy Dissipated
HDPE Specimen #1
DE (in-lbs/in3)
0.6
0.5
0.4
0.3
0.2
0.1
0
0.475
0.031
0
0.0005
0.001
0.0015
0.002
0.0025
||ε|| (in/in)
DE Data
Max Stress
Max Curvature

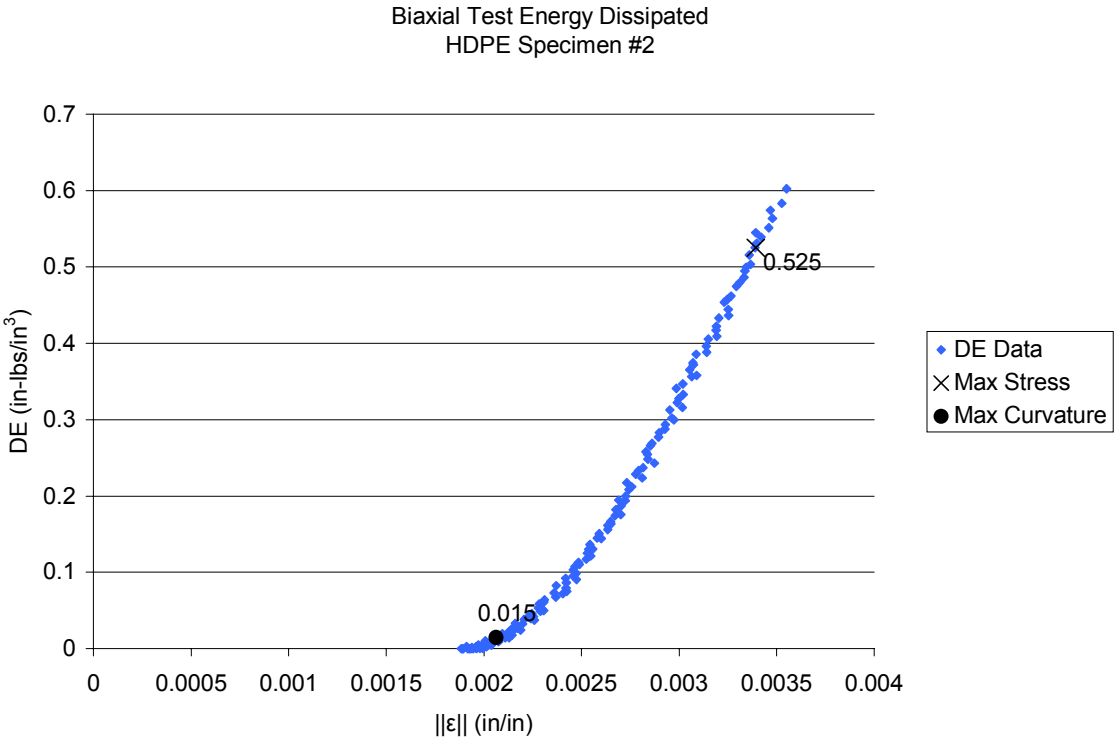
Biaxial Test Energy Dissipated
HDPE Specimen #2
DE (in-lbs/in3)
0.7
0.6
0.5
0.4
0.3
0.2
0.1
0
0.525
0.015
0
0.0005
0.001
0.0015
0.002
0.0025
0.003
0.0035
0.004
||ε|| (in/in)
DE Data
Max Stress
Max Curvature

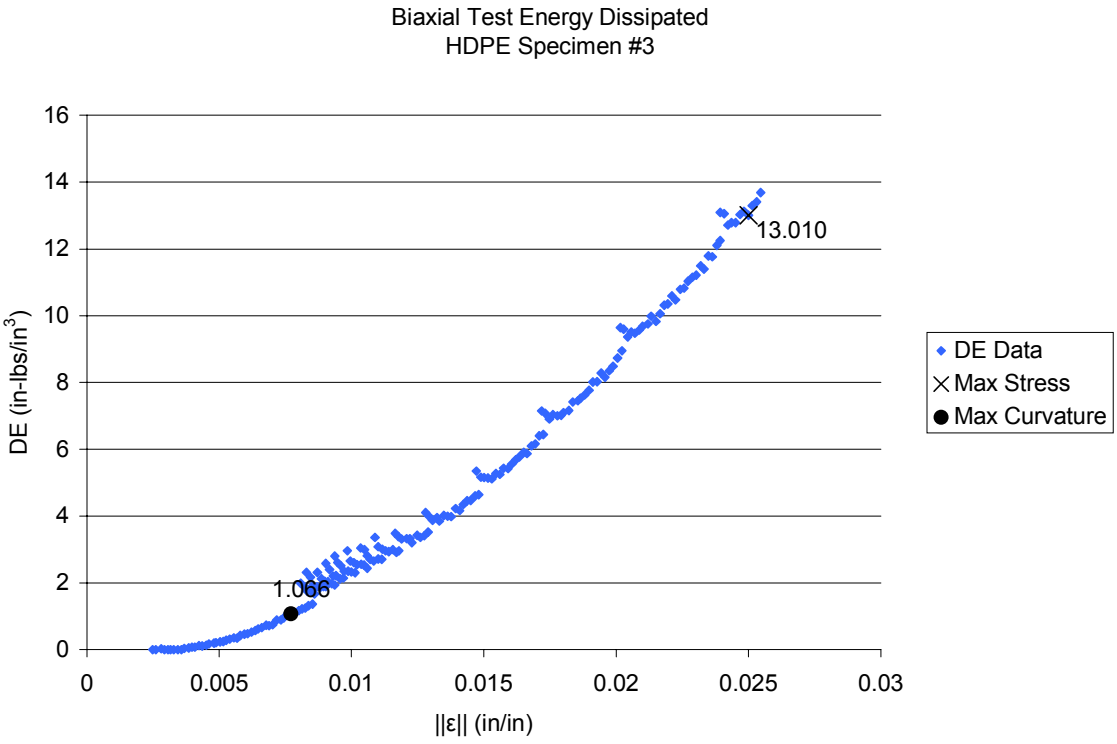
Biaxial Test Energy Dissipated
HDPE Specimen #3
DE (in-lbs/in3)
16
14
12
10
8
6
4
2
0
0
0.005
0.01
0.015
0.02
0.025
0.03
||ε|| (in/in)
13.010
1.066
DE Data
Max Stress
Max Curvature

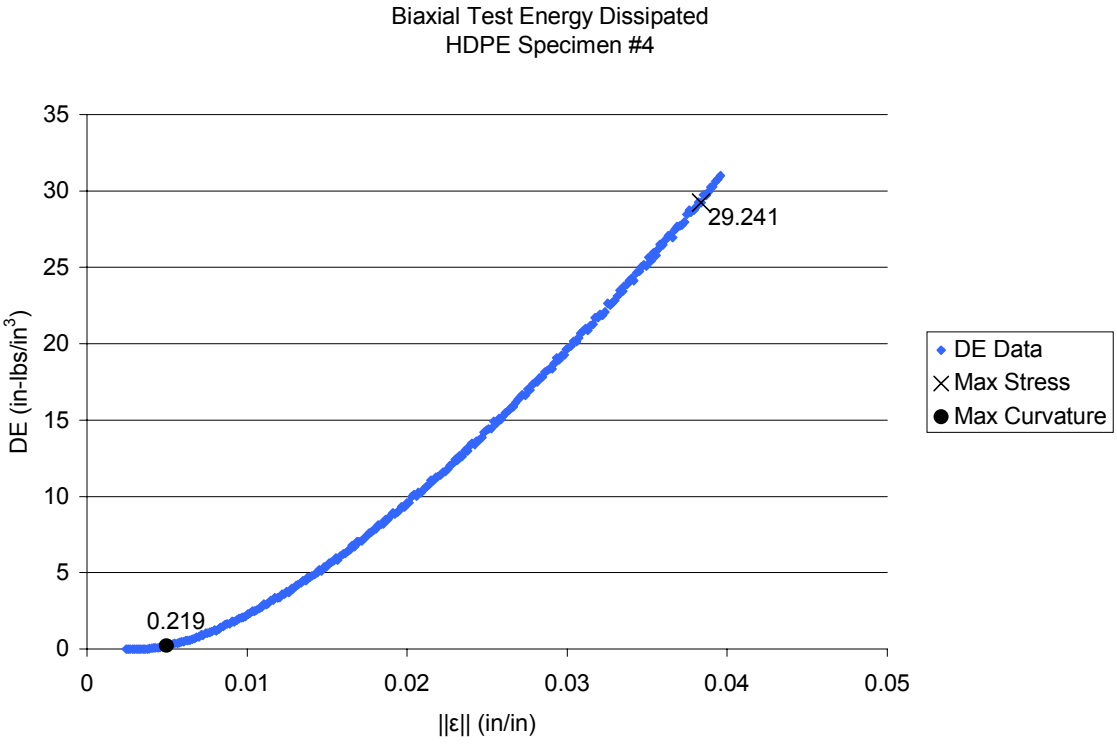
Biaxial Test Energy Dissipated
HDPE Specimen #4
DE (in-lbs/in3)
35
30
25
20
15
10
5
0
0
0.01
0.02
0.03
0.04
0.05
||ε|| (in/in)
29.241
0.219
DE Data
Max Stress
Max Curvature

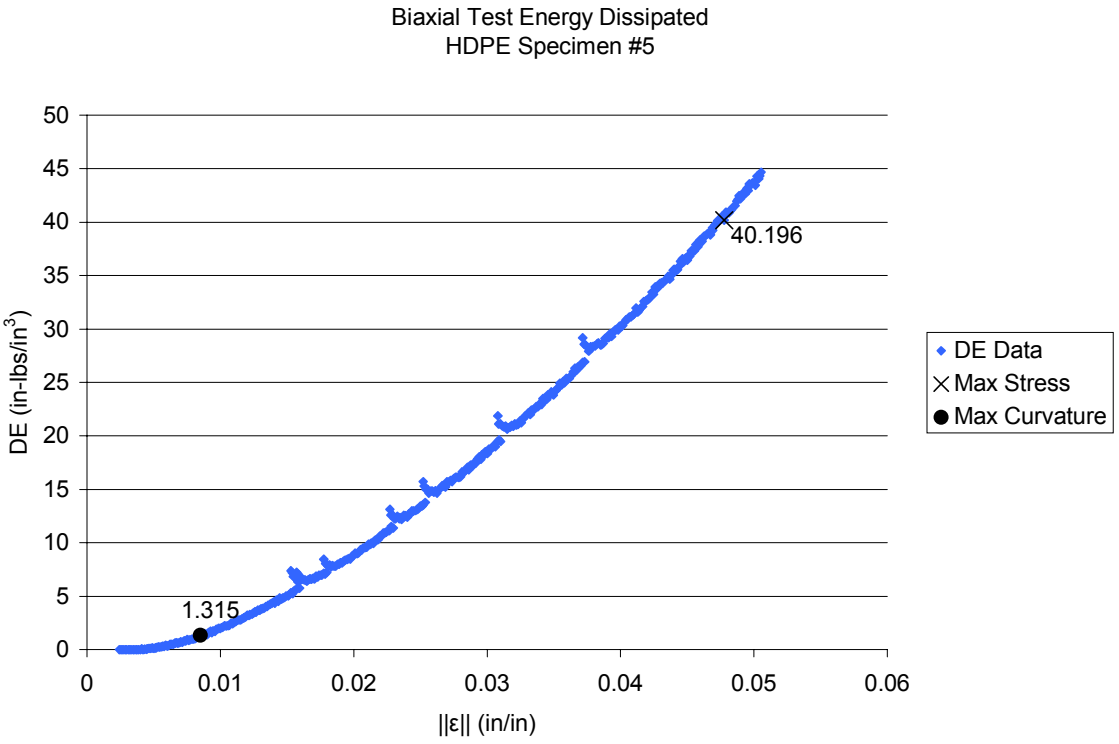
Biaxial Test Energy Dissipated
HDPE Specimen #5
DE (in-lbs/in3)
50
45
40
35
30
25
20
15
10
5
0
40.196
1.315
0
0.01
0.02
0.03
0.04
0.05
0.06
||ε|| (in/in)
DE Data
Max Stress
Max Curvature

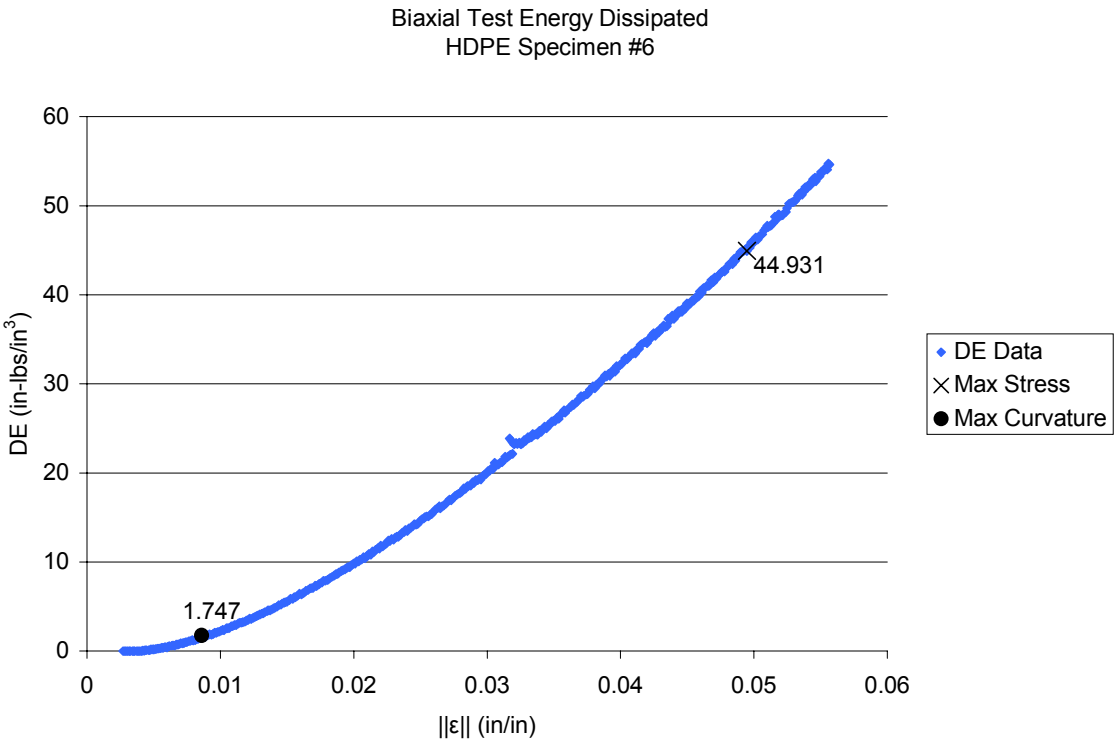
Biaxial Test Energy Dissipated
HDPE Specimen #6
DE (in-lbs/in3)
60
50
40
30
20
10
0
44.931
1.747
0
0.01
0.02
0.03
0.04
0.05
0.06
||ε|| (in/in)
DE Data
Max Stress
Max Curvature

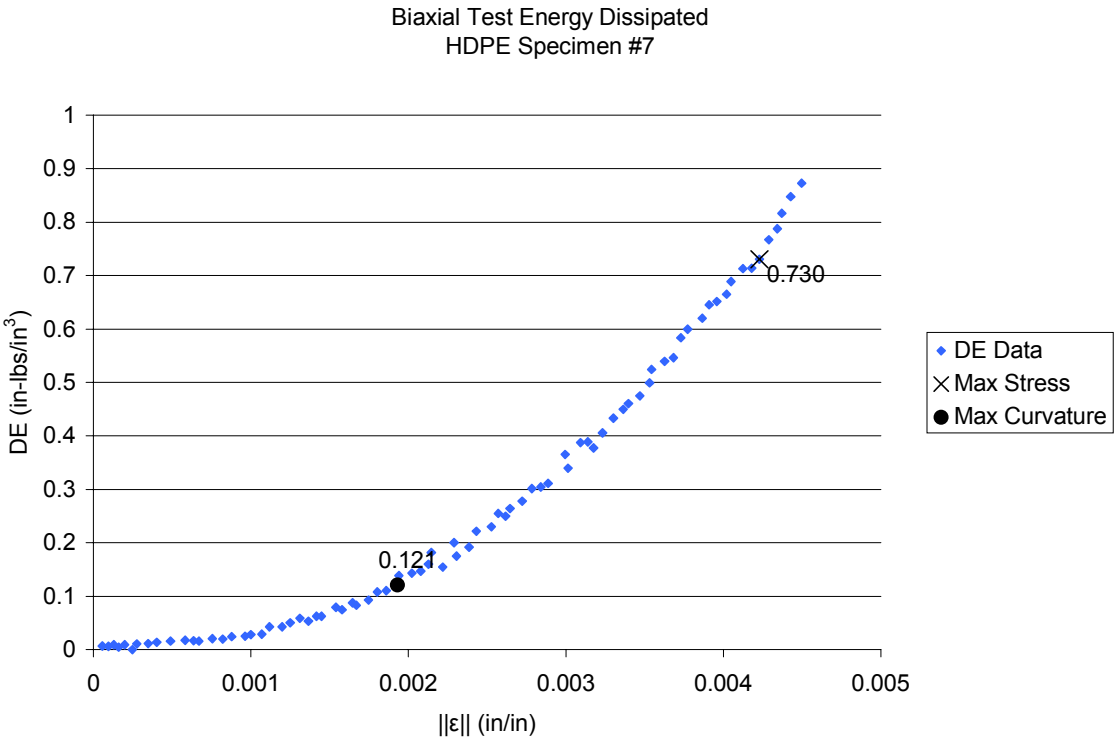
Biaxial Test Energy Dissipated
HDPE Specimen #7
DE (in-lbs/in3)
1
0.9
0.8
0.7
0.6
0.5
0.4
0.3
0.2
0.1
0
0.730
0.121
0
0.001
0.002
0.003
0.004
0.005
||ε|| (in/in)
DE Data
Max Stress
Max Curvature

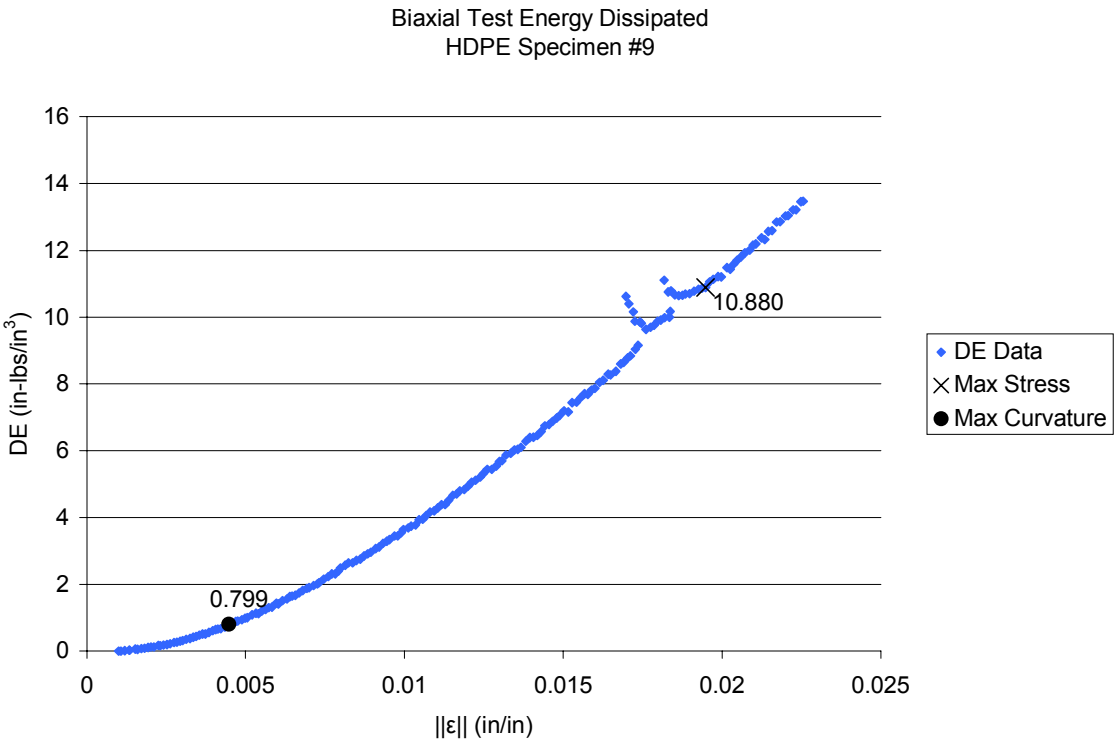
Biaxial Test Energy Dissipated
HDPE Specimen #9
DE (in-lbs/in3)
16
14
12
10
8
6
4
2
0
10.880
0.799
0
0.005
0.01
0.015
0.02
0.025
||ε|| (in/in)
DE Data
Max Stress
Max Curvature

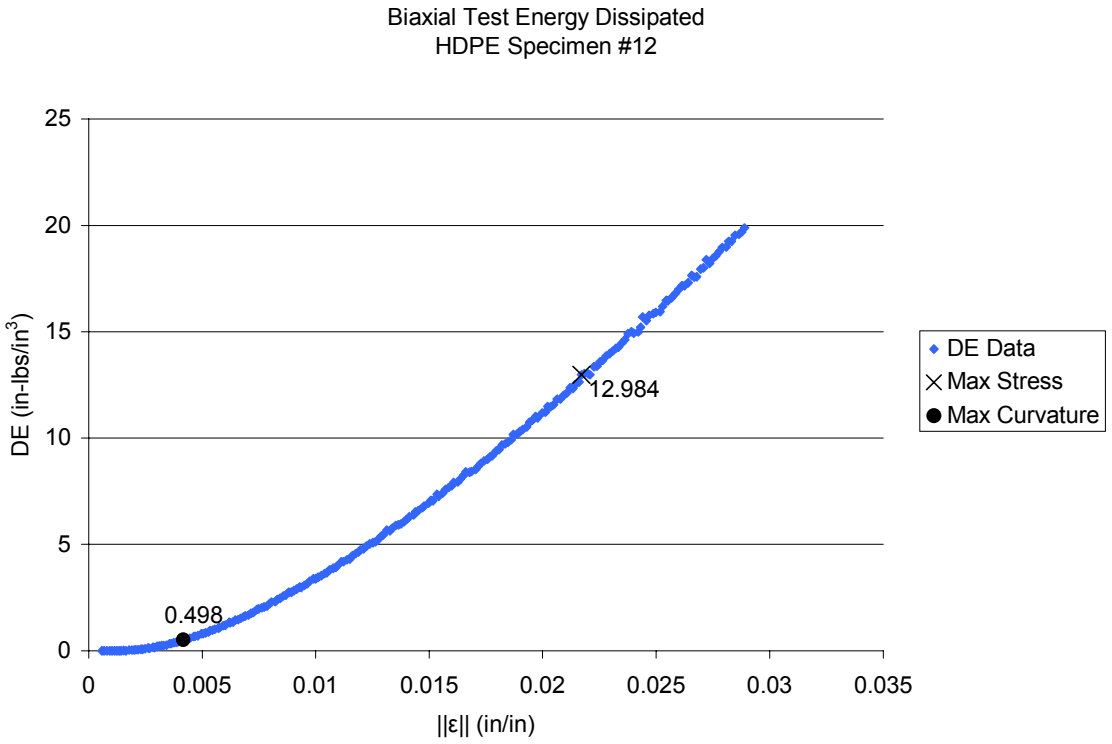
Biaxial Test Energy Dissipated
HDPE Specimen #12
DE (in-lbs/in3)
25
20
15
10
5
0
0
0.005
0.01
0.015
0.02
0.025
0.03
0.035
||ε|| (in/in)
12.984
0.498
DE Data
Max Stress
Max Curvature

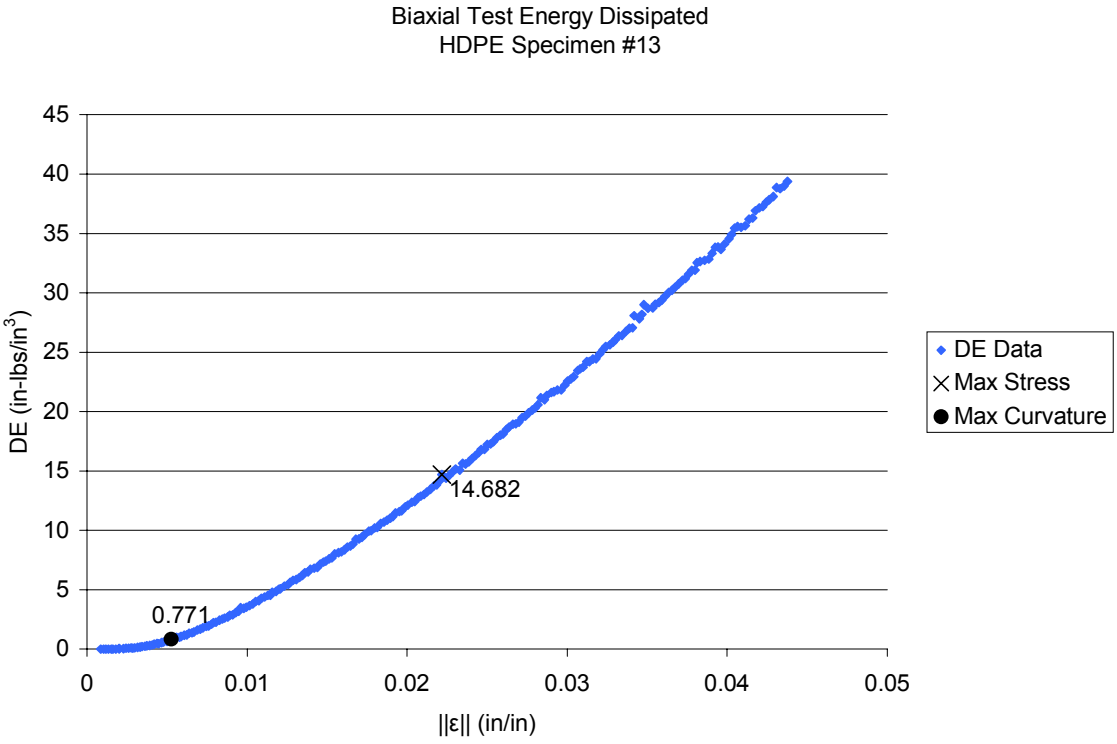
Biaxial Test Energy Dissipated
HDPE Specimen #13
DE (in-lbs/in3)
45
40
35
30
25
20
15
10
5
0
0
0.01
0.02
0.03
0.04
0.05
||ε|| (in/in)
14.682
0.771
DE Data
Max Stress
Max Curvature

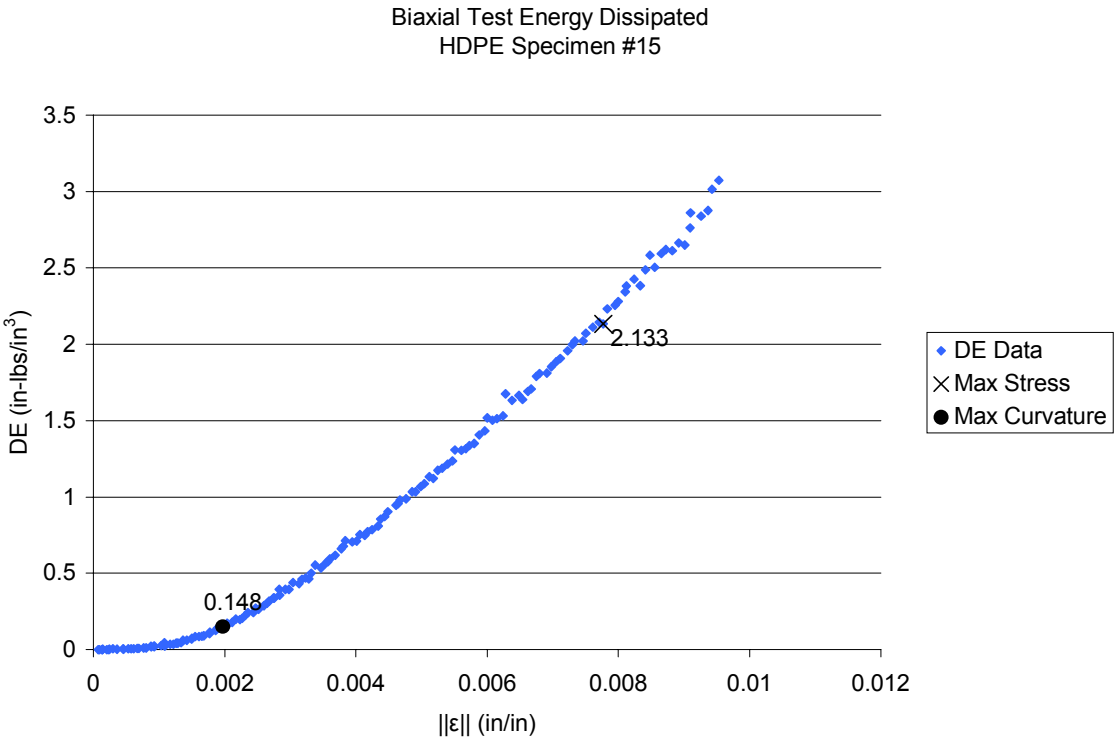
Biaxial Test Energy Dissipated
HDPE Specimen #15
DE (in-lbs/in3)
||ε|| (in/in)
0.148
2.133
DE Data
Max Stress
Max Curvature

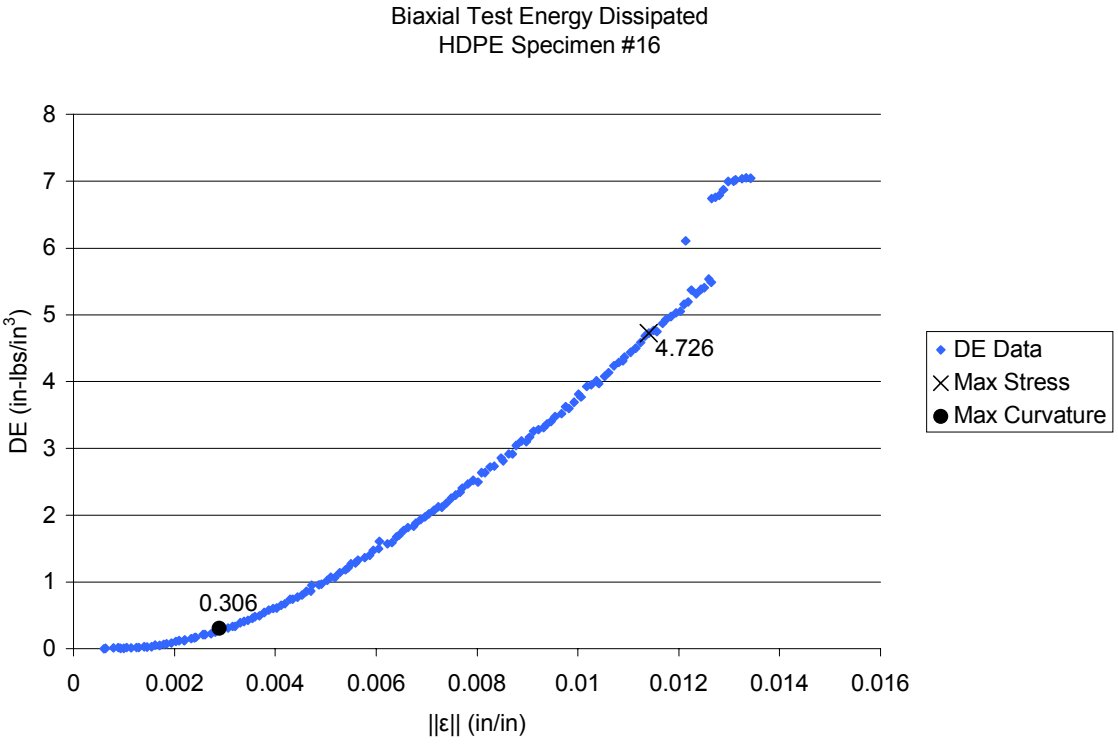
Biaxial Test Energy Dissipated
HDPE Specimen #16
DE (in-lbs/in3)
||ε|| (in/in)
0.306
4.726
DE Data
Max Stress
Max Curvature

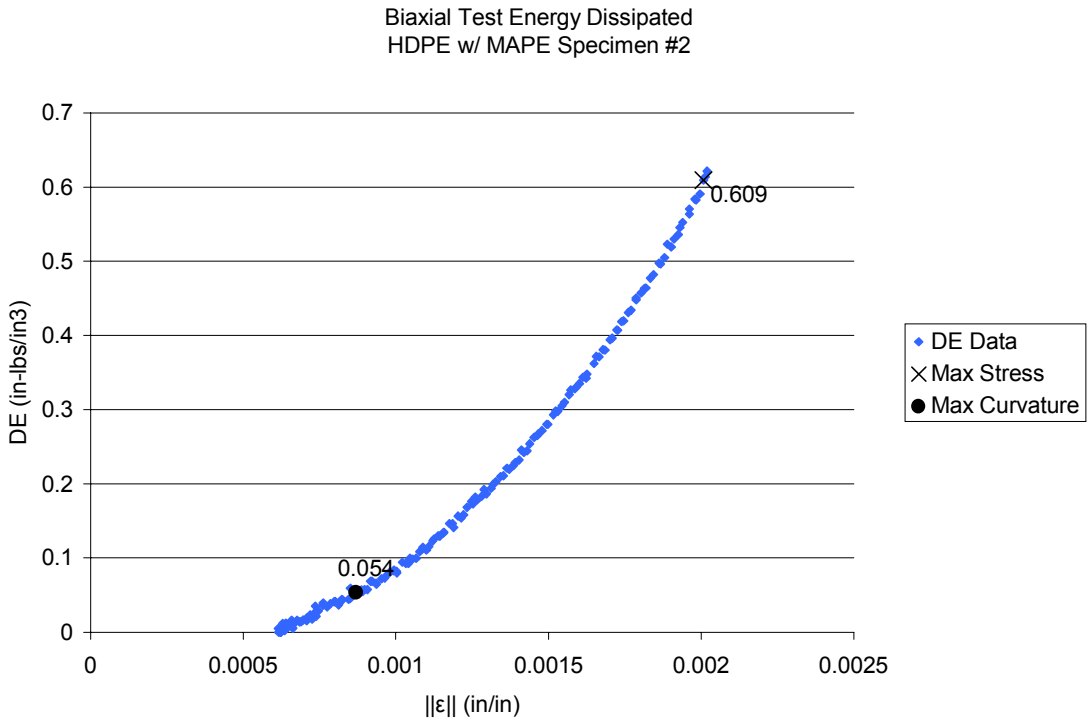
Biaxial Test Energy Dissipated
HDPE w/ MAPE Specimen #2
DE (in-lbs/in3)
0.7
0.6
0.5
0.4
0.3
0.2
0.1
0
0.609
0.054
0
0.0005
0.001
0.0015
0.002
0.0025
||ε|| (in/in)
DE Data
Max Stress
Max Curvature

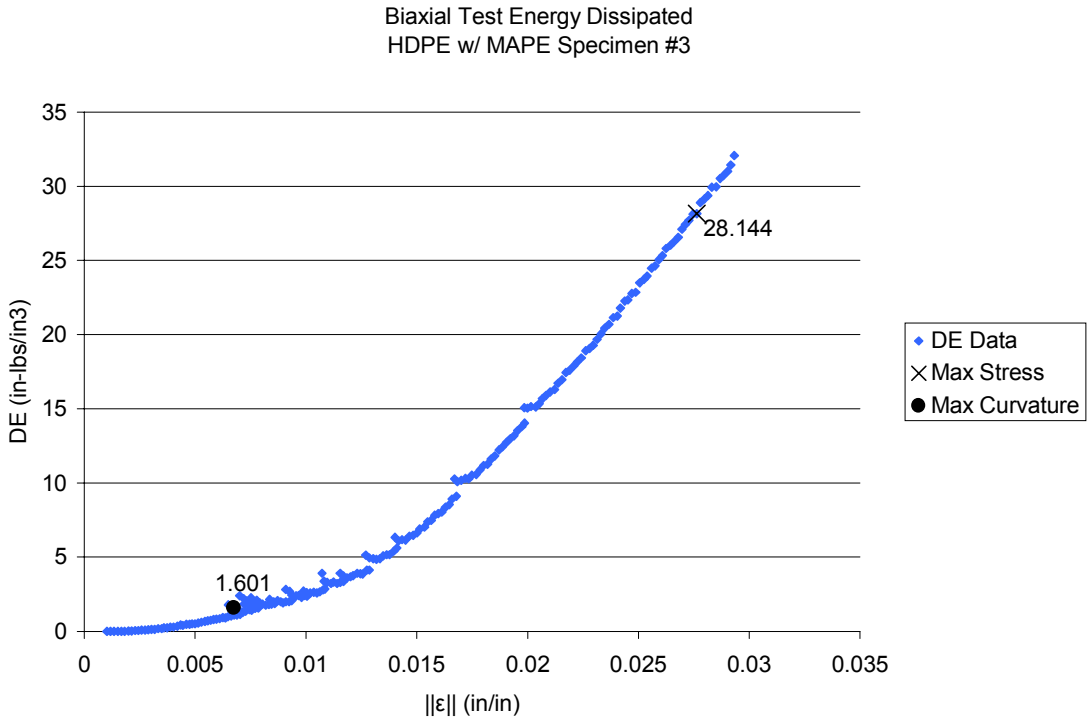
Biaxial Test Energy Dissipated
HDPE w/ MAPE Specimen #3
DE (in-lbs/in3)
35
30
25
20
15
10
5
0
28.144
1.601
0
0.005
0.01
0.015
0.02
0.025
0.03
0.035
||ε|| (in/in)
DE Data
Max Stress
Max Curvature

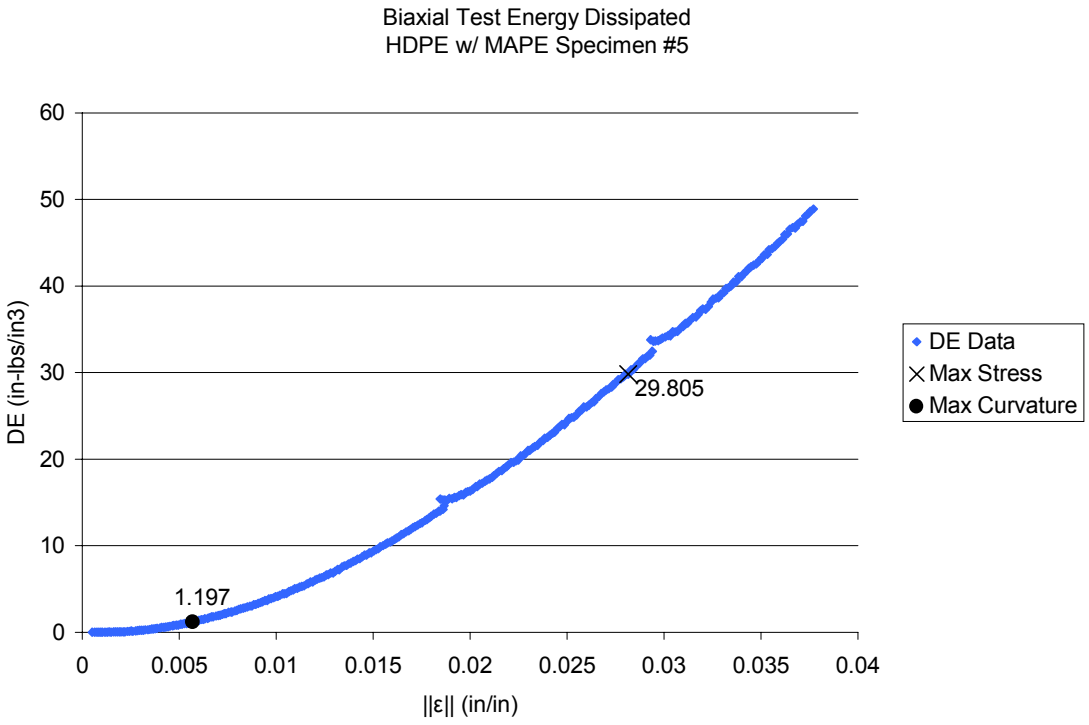
Biaxial Test Energy Dissipated
HDPE w/ MAPE Specimen #5
DE (in-lbs/in3)
60
50
40
30
20
10
0
0
0.005
0.01
0.015
0.02
0.025
0.03
0.035
0.04
||ε|| (in/in)
1.197
29.805
DE Data
Max Stress
Max Curvature

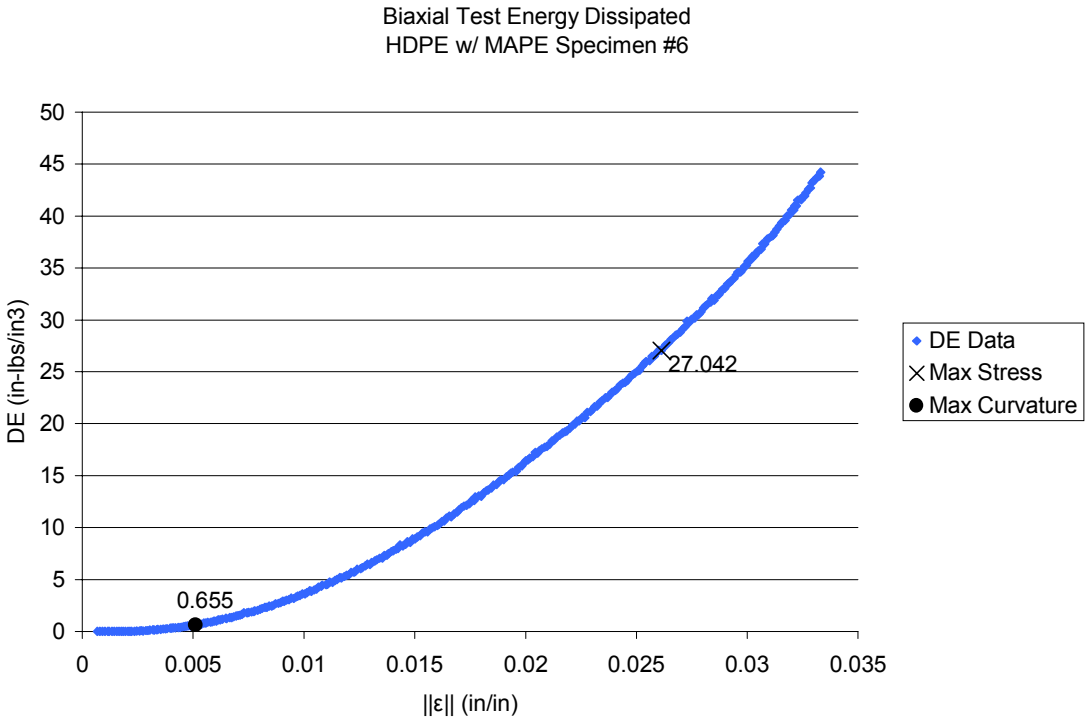
Biaxial Test Energy Dissipated
HDPE w/ MAPE Specimen #6
DE (in-lbs/in3)
50
45
40
35
30
25
20
15
10
5
0
0
0.005
0.01
0.015
0.02
0.025
0.03
0.035
||ε|| (in/in)
0.655
27.042
DE Data
Max Stress
Max Curvature

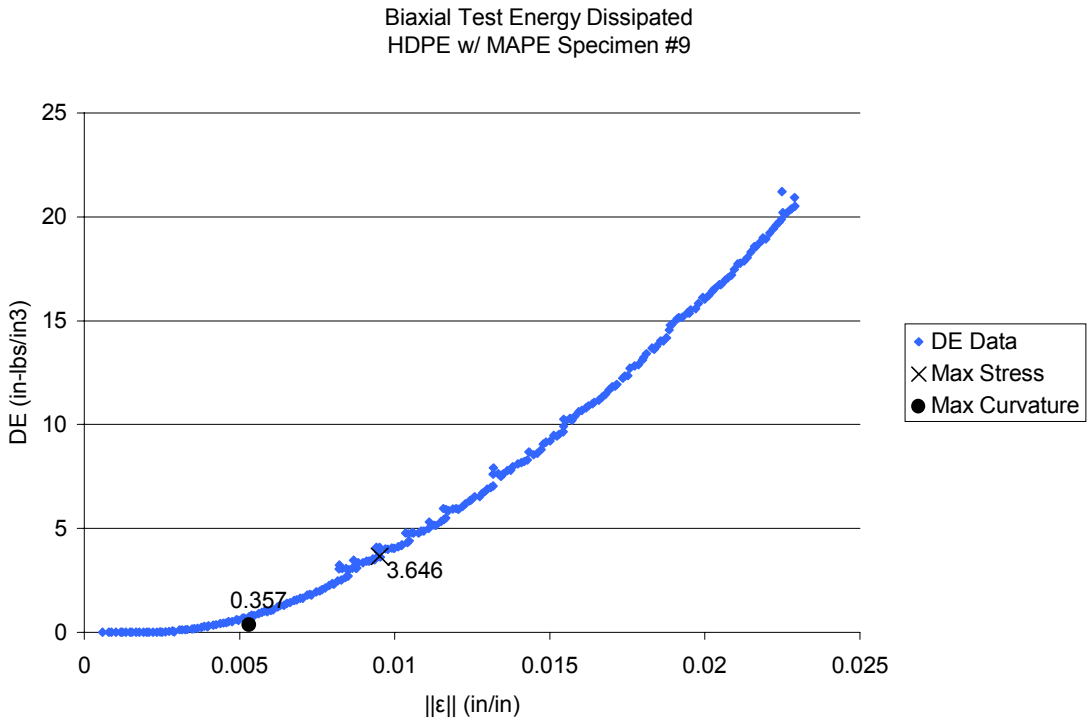
Biaxial Test Energy Dissipated
HDPE w/ MAPE Specimen #9
DE (in-lbs/in3)
25
20
15
10
5
0
0
0.005
0.01
0.015
0.02
0.025
||ε|| (in/in)
0.357
3.646
DE Data
Max Stress
Max Curvature

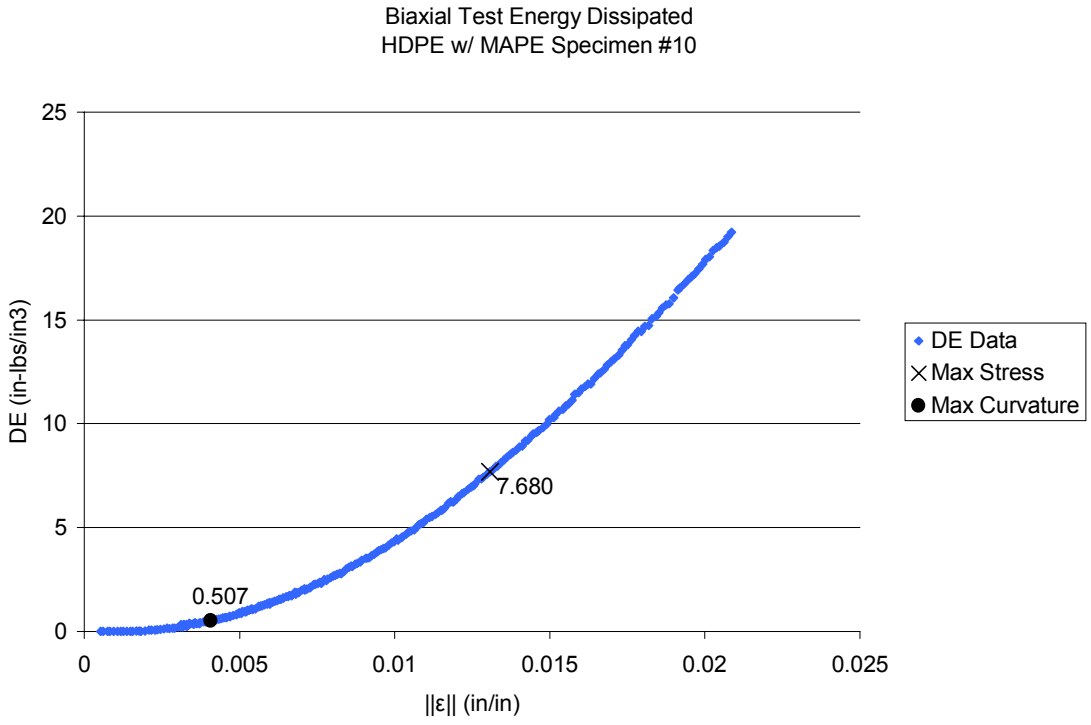
Biaxial Test Energy Dissipated
HDPE w/ MAPE Specimen #10
DE (in-lbs/in3)
25
20
15
10
5
0
0
0.005
0.01
0.015
0.02
0.025
||ε|| (in/in)
0.507
7.680
DE Data
Max Stress
Max Curvature

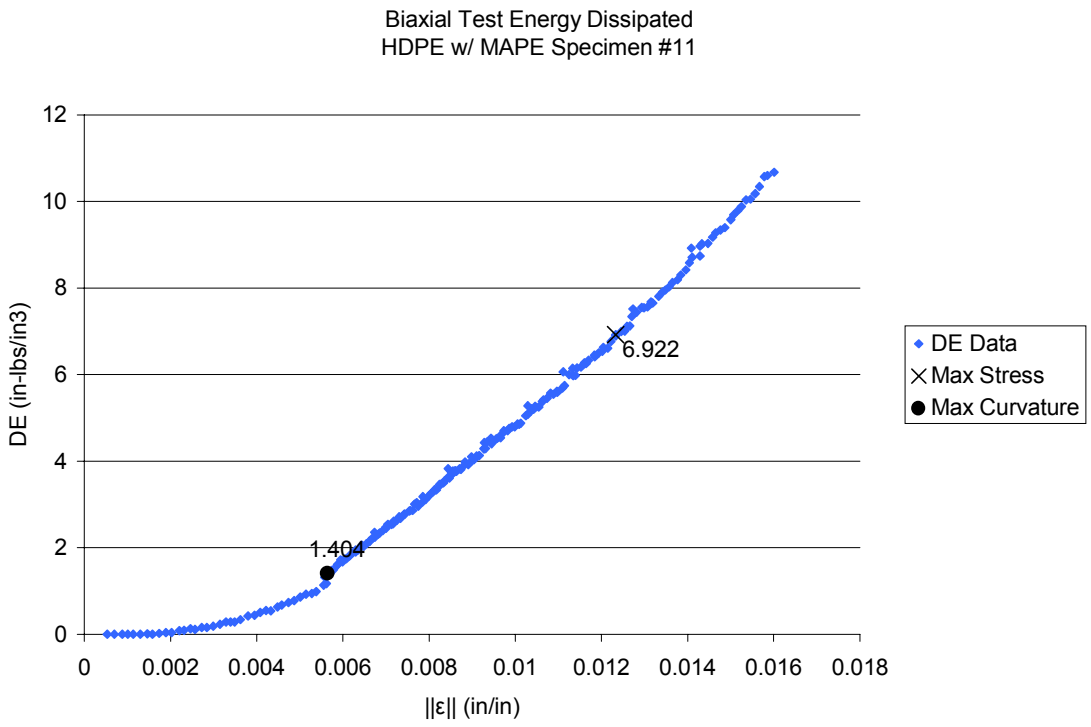
Biaxial Test Energy Dissipated
HDPE w/ MAPE Specimen #11
DE (in-lbs/in3)
12
10
8
6
4
2
0
0
0.002
0.004
0.006
0.008
0.01
0.012
0.014
0.016
0.018
||ε|| (in/in)
6.922
1.404
DE Data
Max Stress
Max Curvature

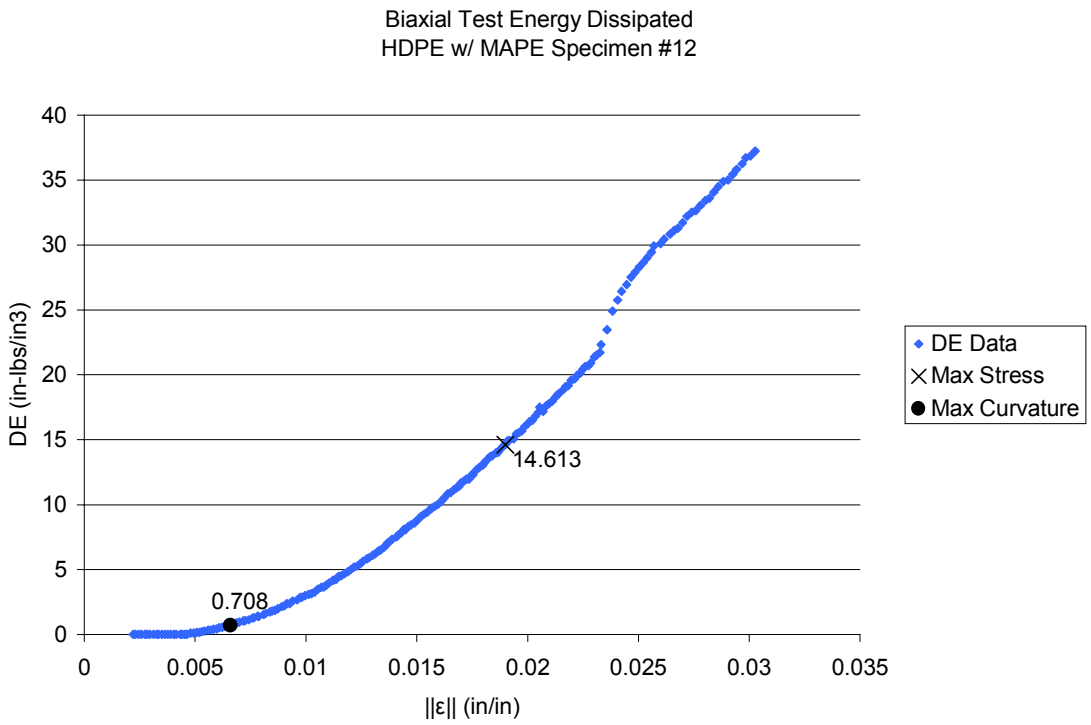
Biaxial Test Energy Dissipated
HDPE w/ MAPE Specimen #12
DE (in-lbs/in3)
40
35
30
25
20
15
10
5
0
0
0.005
0.01
0.015
0.02
0.025
0.03
0.035
||ε|| (in/in)
14.613
0.708
DE Data
Max Stress
Max Curvature

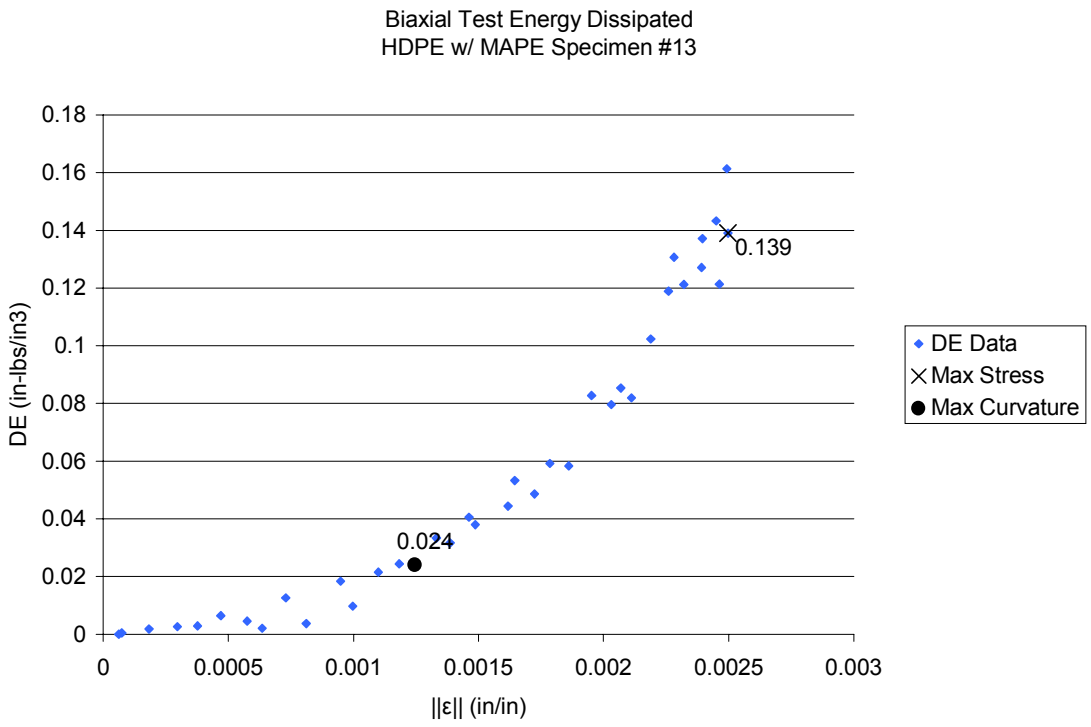
Biaxial Test Energy Dissipated
HDPE w/ MAPE Specimen #13
DE (in-lbs/in3)
0.18
0.16
0.14
0.12
0.1
0.08
0.06
0.04
0.02
0
0.139
0.024
0
0.0005
0.001
0.0015
0.002
0.0025
0.003
||ε|| (in/in)
DE Data
Max Stress
Max Curvature

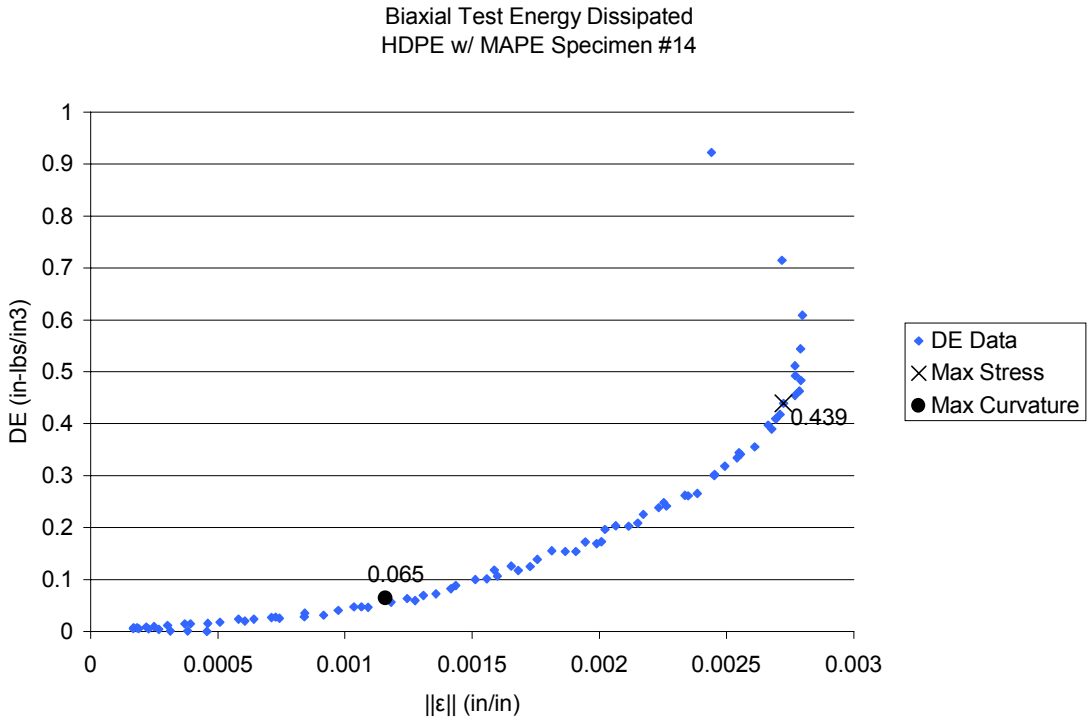
Biaxial Test Energy Dissipated
HDPE w/ MAPE Specimen #14
DE (in-lbs/in3)
1
0.9
0.8
0.7
0.6
0.5
0.4
0.3
0.2
0.1
0
0.439
0.065
0
0.0005
0.001
0.0015
0.002
0.0025
0.003
||ε|| (in/in)
DE Data
Max Stress
Max Curvature

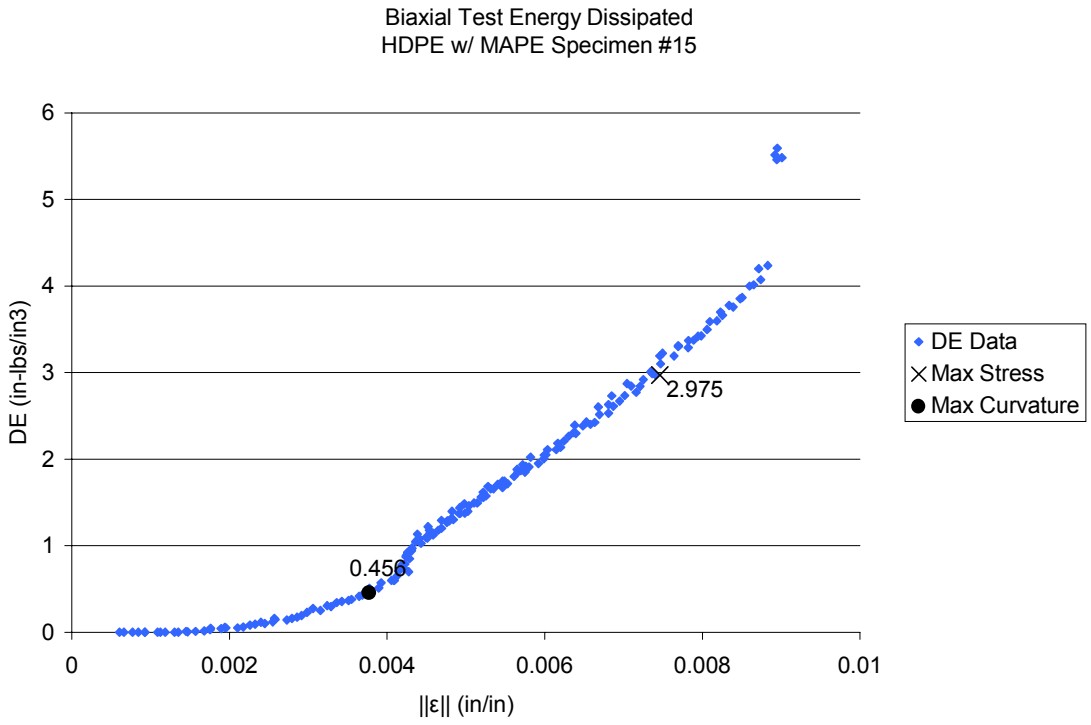
Biaxial Test Energy Dissipated
HDPE w/ MAPE Specimen #15
DE (in-lbs/in3)
||ε|| (in/in)
0
1
2
3
4
5
6
0
0.002
0.004
0.006
0.008
0.01
0.456
2.975
DE Data
Max Stress
Max Curvature

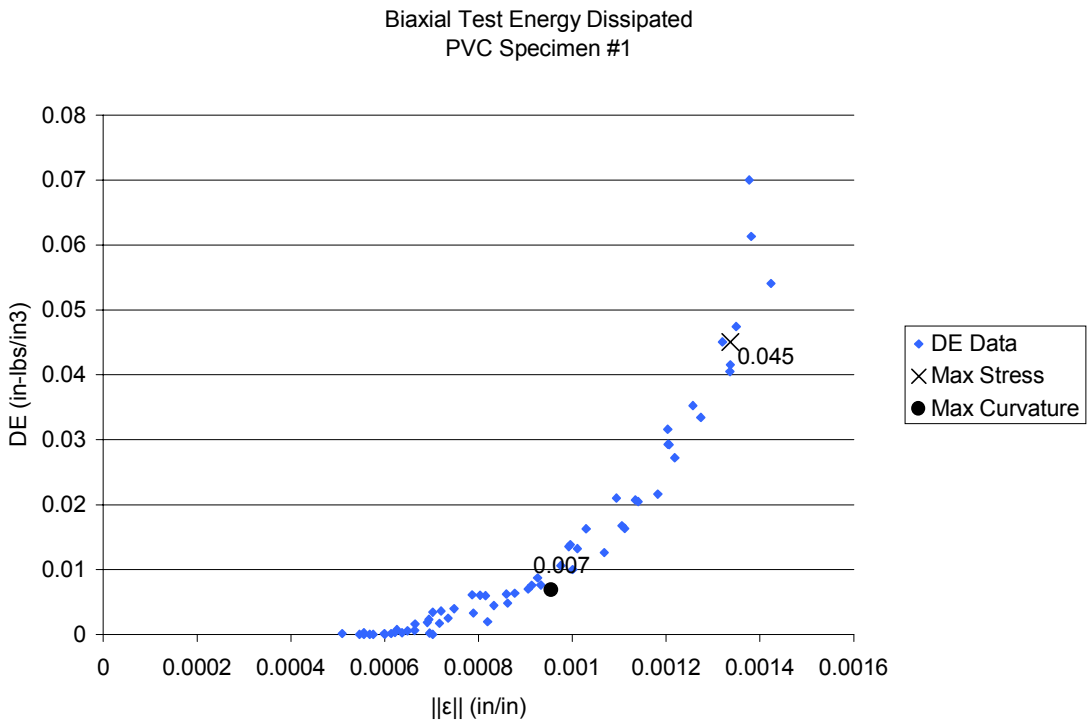
Biaxial Test Energy Dissipated
PVC Specimen #1
DE (in-lbs/in3)
||ε|| (in/in)
0
0.01
0.02
0.03
0.04
0.05
0.06
0.07
0.08
0
0.0002
0.0004
0.0006
0.0008
0.001
0.0012
0.0014
0.0016
0.007
0.045
DE Data
Max Stress
Max Curvature

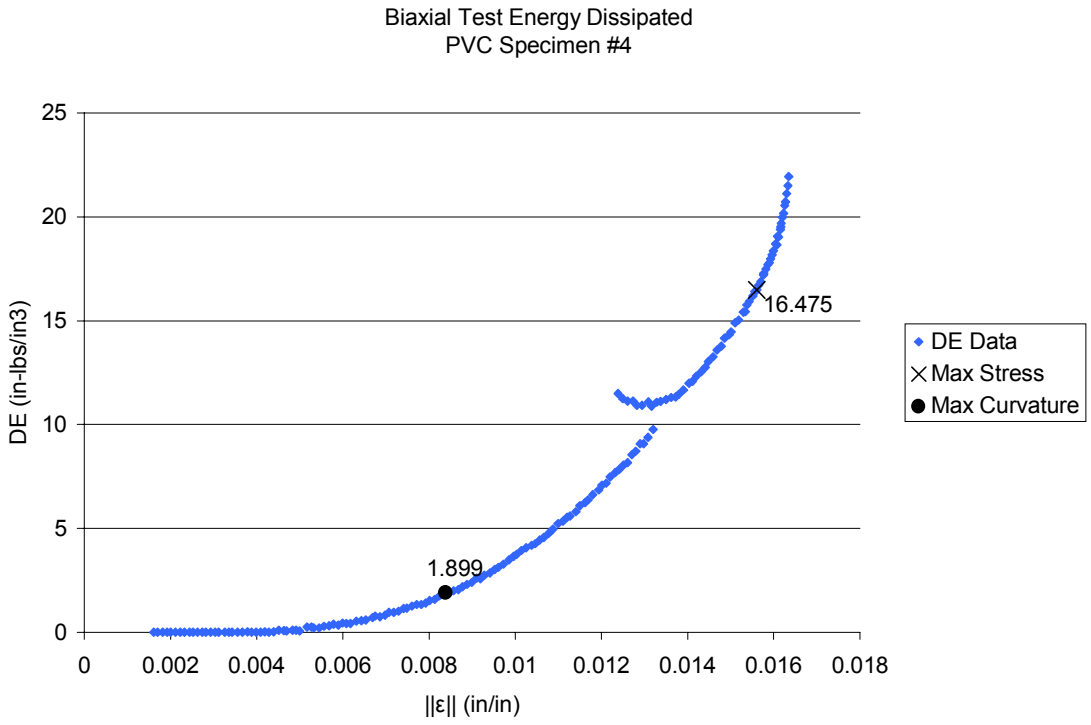
Biaxial Test Energy Dissipated
PVC Specimen #4
DE (in-lbs/in3)
25
20
15
10
5
0
0
0.002
0.004
0.006
0.008
0.01
0.012
0.014
0.016
0.018
||ε|| (in/in)
16.475
1.899
DE Data
Max Stress
Max Curvature

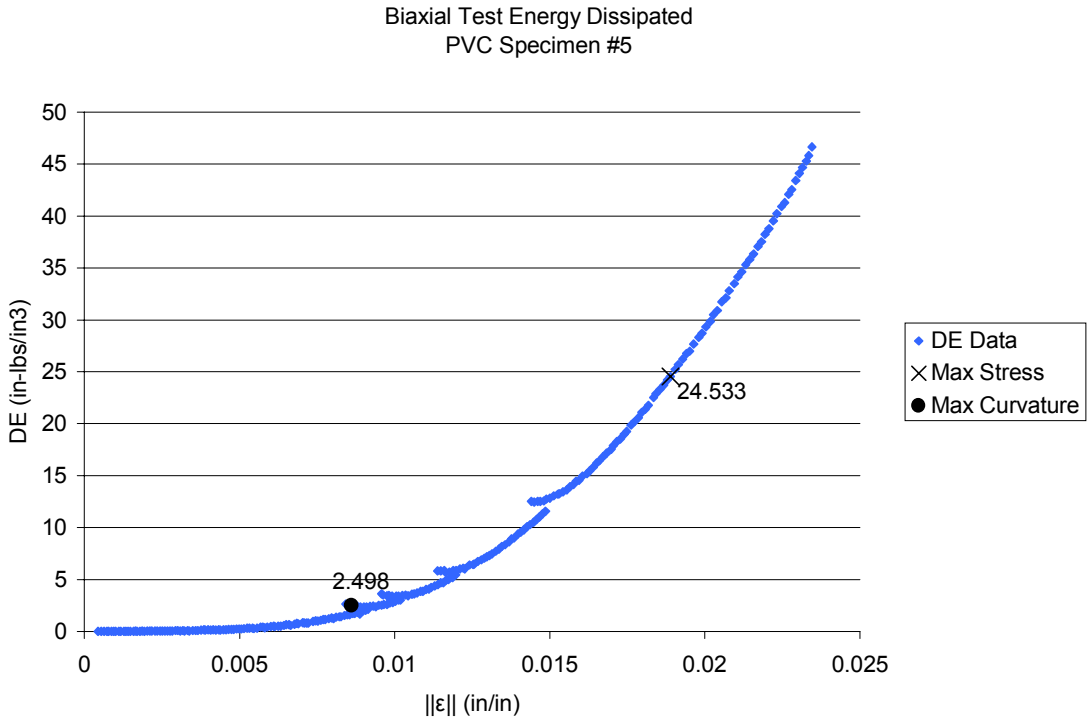
Biaxial Test Energy Dissipated
PVC Specimen #5
DE (in-lbs/in3)
50
45
40
35
30
25
20
15
10
5
0
0
0.005
0.01
0.015
0.02
0.025
||ε|| (in/in)
24.533
2.498
DE Data
Max Stress
Max Curvature

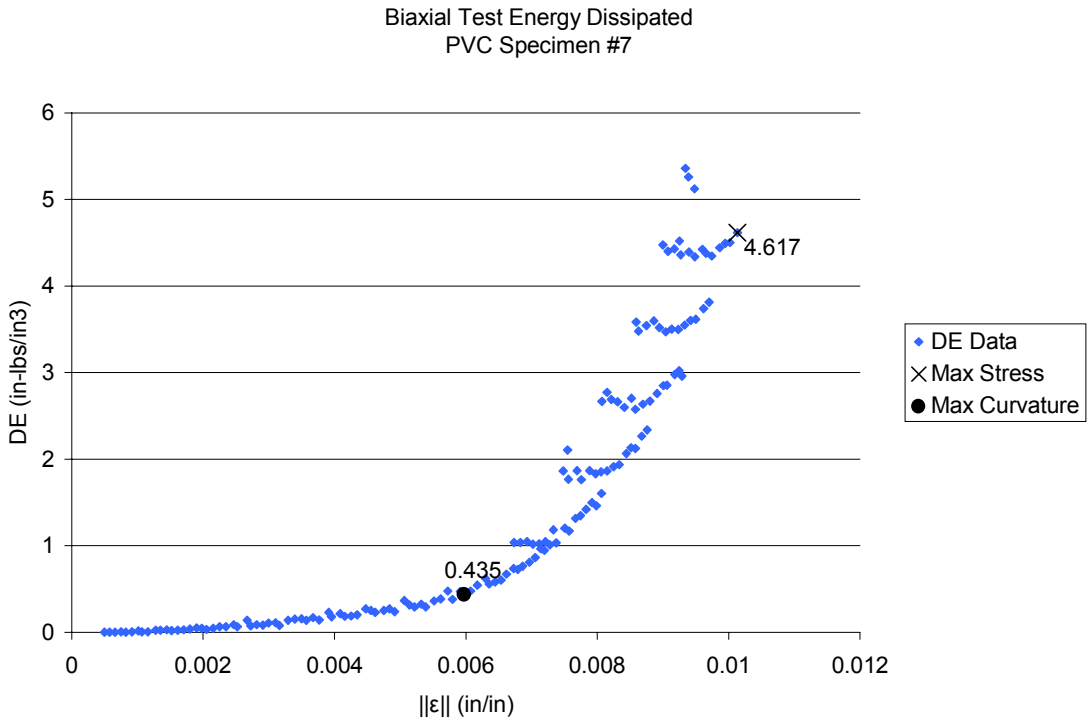
Biaxial Test Energy Dissipated
PVC Specimen #7
DE (in-lbs/in3)
||ε|| (in/in)
4.617
0.435
DE Data
Max Stress
Max Curvature

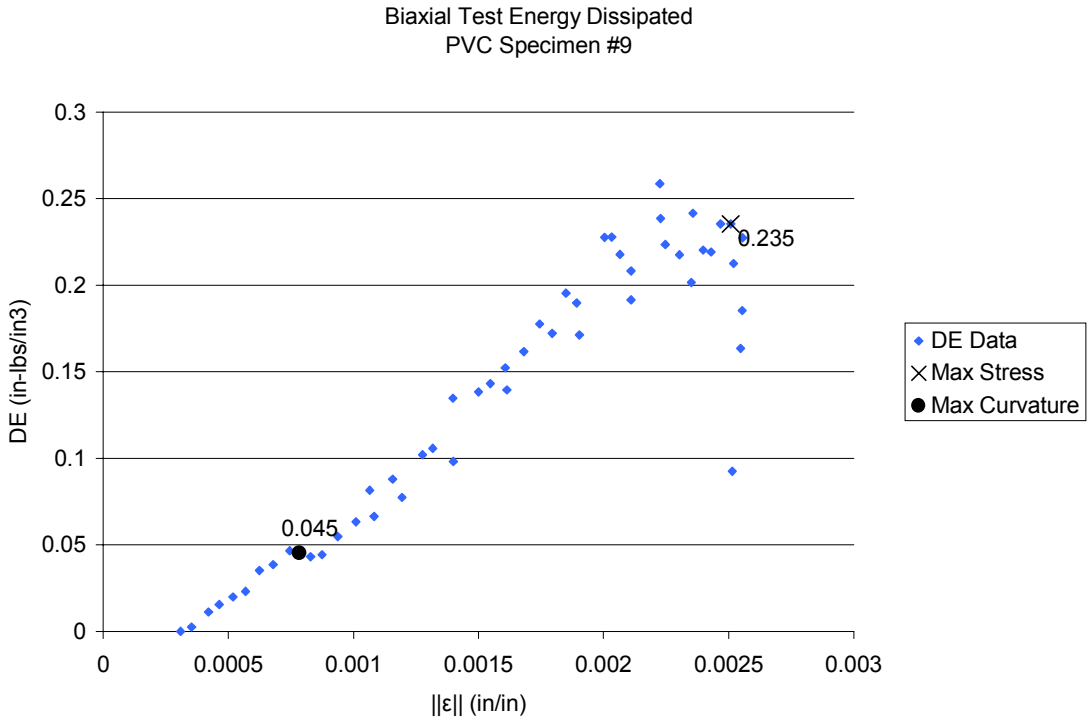
Biaxial Test Energy Dissipated
PVC Specimen #9
DE (in-lbs/in3)
||ε|| (in/in)
0.235
0.045
DE Data
Max Stress
Max Curvature

APPENDIX D: BENDING TEST RESULTS

Included in this appendix is a summary of the 3-Point bending tests performed in this research. Load-Displacement plots are shown for all three material formulations. Plots of dissipated energy density vs. strain are also shown.

The plots labeled HDPE show test data from the 67.5/32.5 Maple/HDPE formulation. Plots labeled HDPE w/ MAPE show test data from the 67.5/31 Maple/HDPE with 1.5% MAPE formulation. Plots labeled PVC show test data from the 50/50 Pine/PVC formulation.

Noted in all the plots are the average value for maximum stress (denoted with X), the average value of maximum curvature in the dissipated energy function (denoted with 0) and the value of the 5% parametric tolerance limit stress (denoted by □).

3-Point Bending Test Results
Load-Displacement of 67.5/32.5 Maple/HDPE

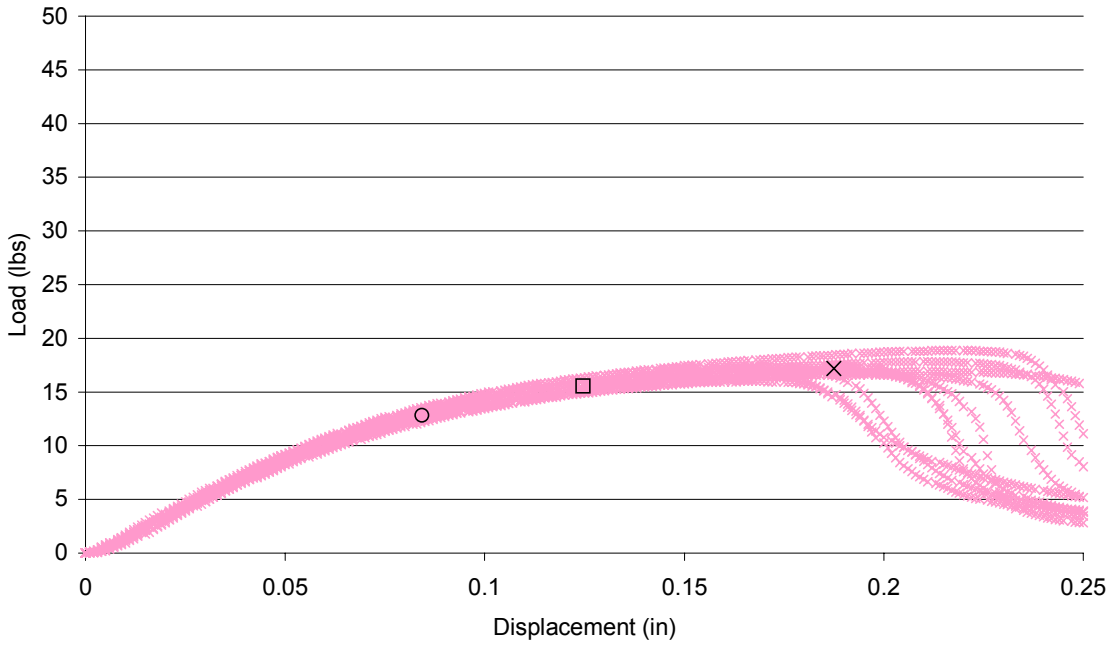

3-Point Bending Test Results
Dissipated Energy of 67.5/32.5 Maple/HDPE

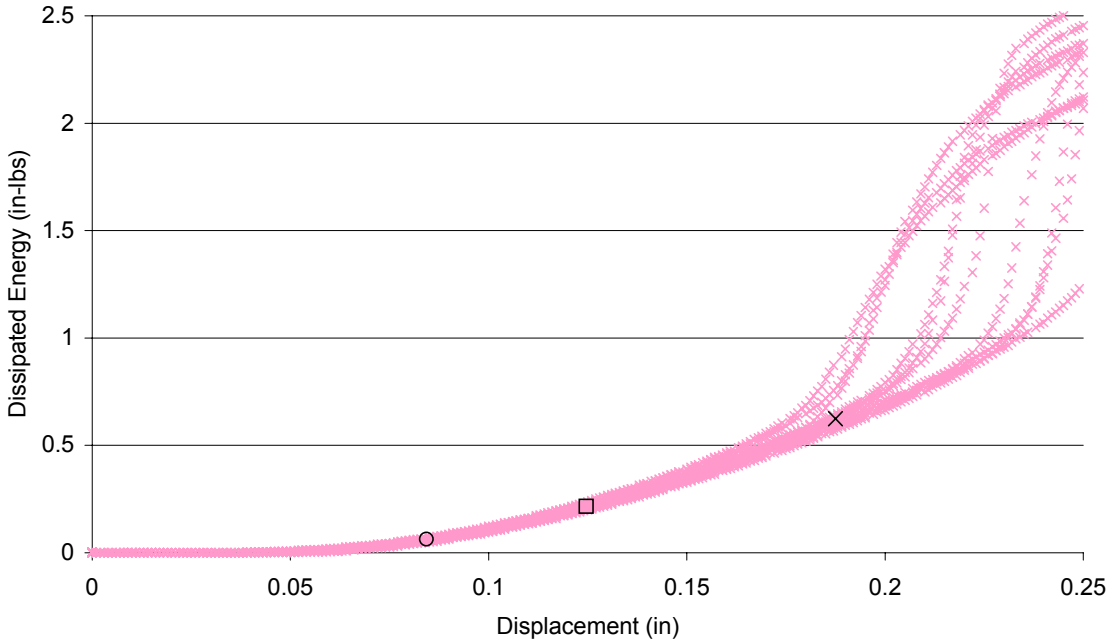

3-Point Bending Test Results
Load-Displacement of 67.5/31 Maple/HDPE with 1.5 MAPE

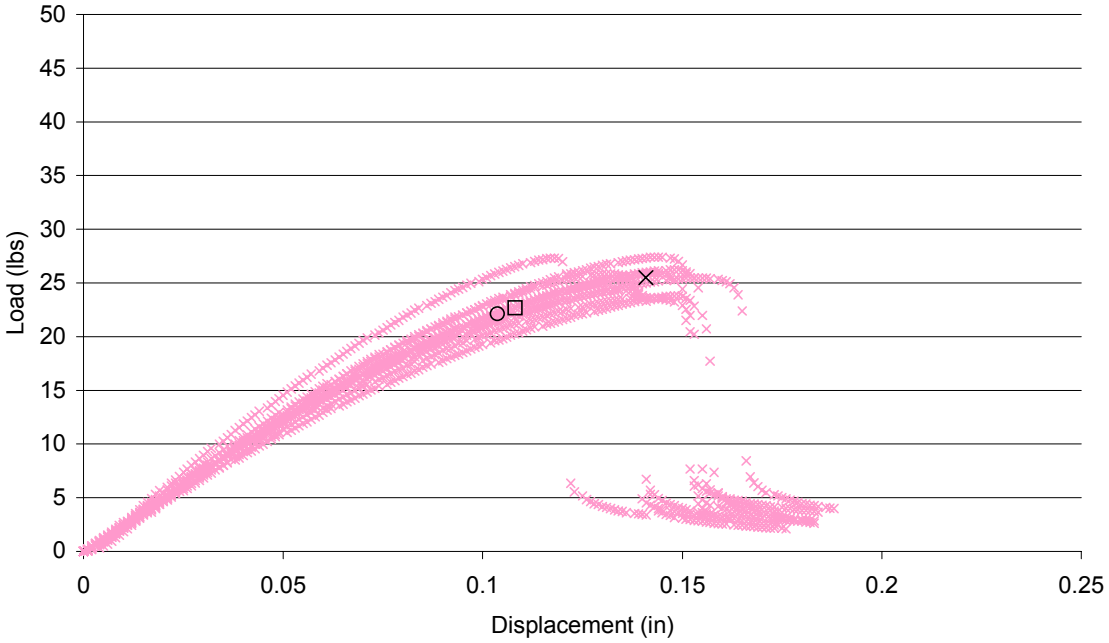

3-Point Bending Test Results
Dissipated Energy of 67.5/31 Maple/HDPE with 1.5 MAPE

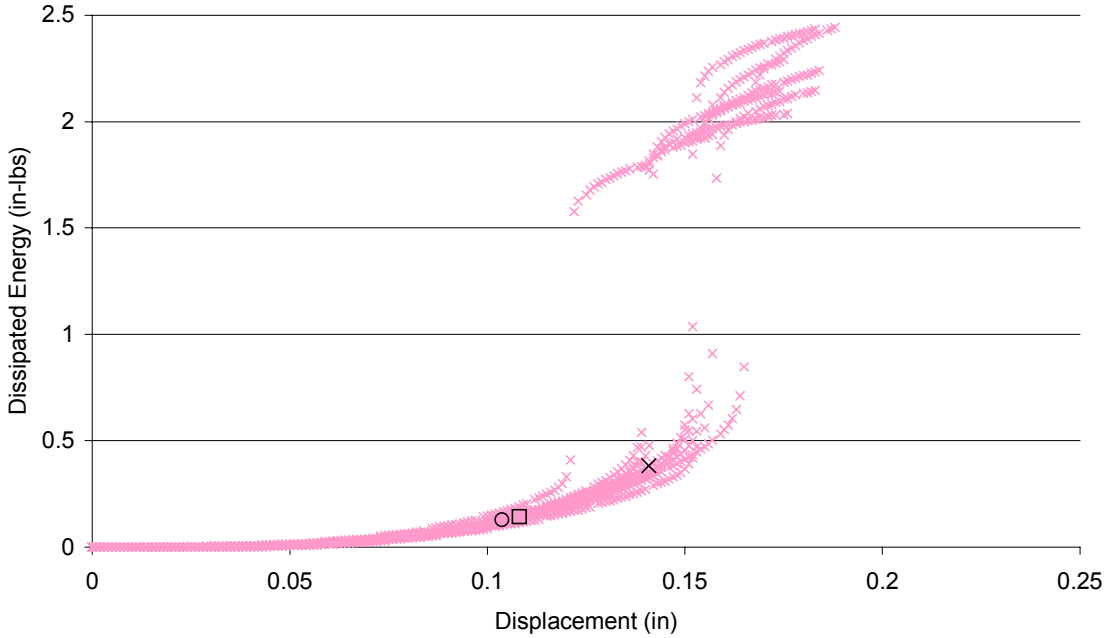

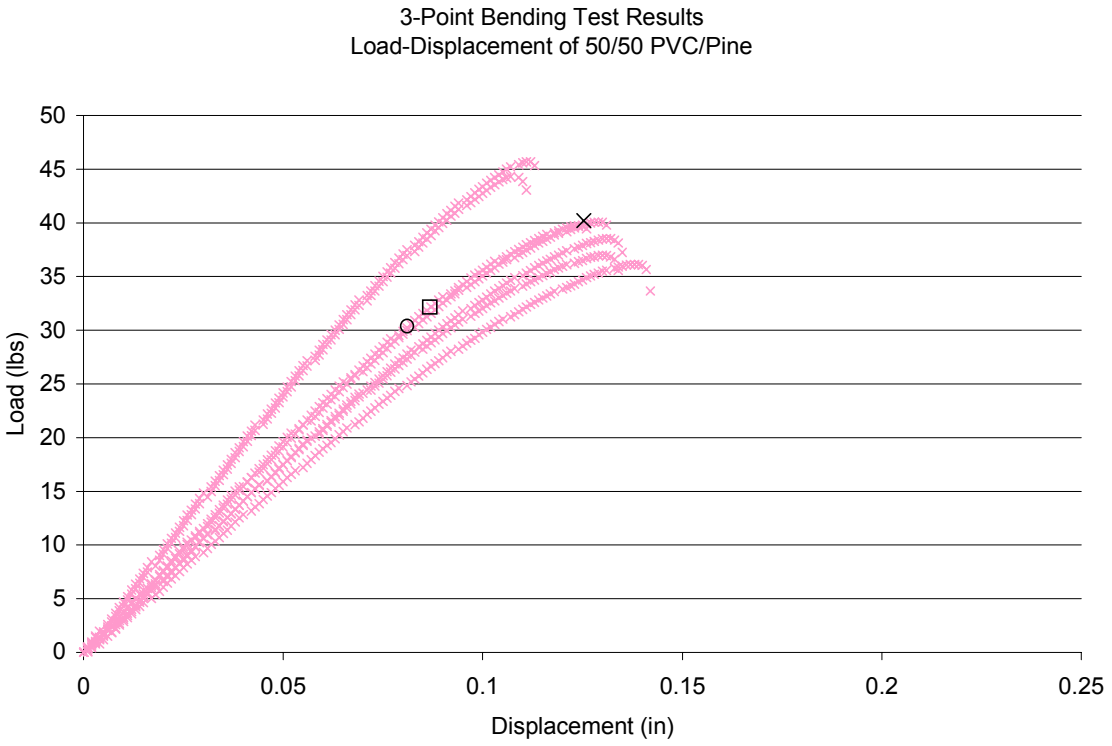
3-Point Bending Test Results
Load-Displacement of 50/50 PVC/Pine
Load (lbs)
50
45
40
35
30
25
20
15
10
5
0
0
0.05
0.1
0.15
0.2
0.25
Displacement (in)

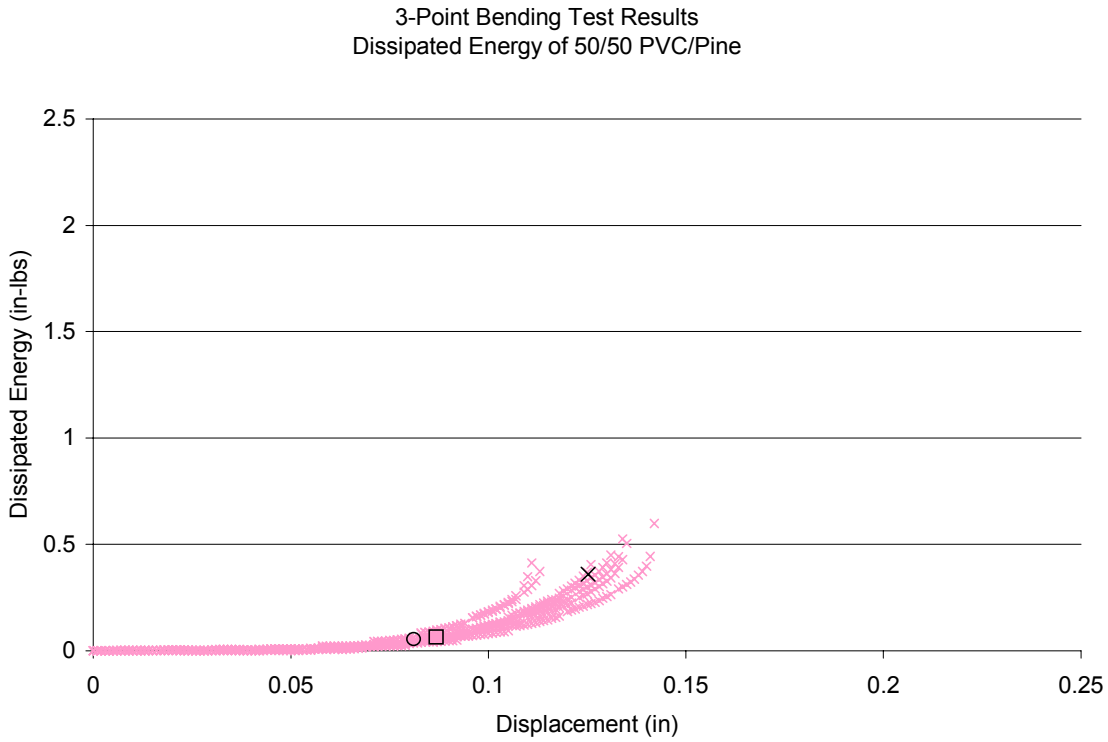
3-Point Bending Test Results
Dissipated Energy of 50/50 PVC/Pine
Dissipated Energy (in-lbs)
2.5
2
1.5
1
0.5
0
0
0.05
0.1
0.15
0.2
0.25
Displacement (in)